The Covariant-Evolution-Operator Method in Bound-State QED

Ingvar Lindgren, Sten Salomonson, Björn Åsén

Department of Physics, Chalmers University of Technology and Göteborg University, SE-41296 Göteborg, Sweden

Abstract

The methods of quantum-electrodynamical (QED) calculations on bound atomic systems are reviewed with emphasis on the newly developed covariant-evolution-operator method. The aim is to compare that method with other available methods and also to point out possibilities to combine that with standard many-body perturbation theory (MBPT) in order to perform accurate numerical QED calculations, including quasi-degeneracy, also for light elements, where the electron correlation is relatively strong.

As a background, the time-independent many-body perturbation theory (MBPT) is briefly reviewed, particularly the method with extended model space. Time-dependent perturbation theory is discussed in some detail, introducing the time-evolution operator and the Gell-Mann–Low relation, generalized to an arbitrary model space. Three methods of treating the bound-state QED problem are discussed. The standard S-matrix formulation, which is restricted to a degenerate model space, is discussed only briefly. Two methods applicable also to the quasi-degenerate problem are treated in more detail, the two-times Green's-function and the covariant-evolution-operator techniques. The treatment is concentrated on the latter technique, which has been developed more recently and which has not been discussed in more detail before. A comparison of the two-times Green's-function and the covariant-evolution-operator techniques, which have great similarities, is performed. In the Appendix a simple procedure is derived for expressing the evolution-operator diagrams of arbitrary order.

The possibilities of merging QED in the covariant evolution-operator formulation with MBPT in a systematic way is indicated. With such a technique it might be feasible to perform accurate QED calculations also on light elements, which is presently not possible with the techniques available.

Key words: Quantum electrodynamics, many-body perturbation theory, time-evolution operator, Gell-Mann–Low formula, S-matrix, electron self-energy, vacuum polarization, screened self-energy, two-photon exchange, quasi-degeneracy, two-times Green's function, covariant time-evolution operator.
PACS: 12.20-m, 31.10+z, 31.15.Ar, 31.25-v, 31.30.Jv, 32.10.Fn

Contents

sec:intro

1 Introduction

The theory of quantum electrodynamics (QED), i.e., the theory of interactions between electrons and electromagnetic radiation, was developed largely in the 1940's, but it is only during the last two decades or so that it has been possible to test the theory to a high degree of accuracy. The theory has been extremely successful for the simplest systems that are free from strong interaction, like the free electron and the exotic systems positronium and muonium. For the g-factor of the free electron the QED contribution has been experimentally verified with the amazing accuracy of a few ppb (parts per billion), and for positronium and muonium the agreement between theory and experiment is of the order of ppm (parts per million). The same order of agreement is also obtained for the fine structure of neutral helium. In these cases the *analytical approach* is used in the theoretical evaluation, i.e., a double power expansion in α and $Z\alpha$, starting from free particles.

The QED theory is less well tested in *strong fields*, for instance, in the neighborhood of a highly charged nucleus. During the last decade particularly interesting information has been accumulated concerning very highly charged few-electron systems – up to hydrogenlike uranium – mainly from the SIS/ESR facility at GSI in Darmstadt and the SuperEBIT ion trap at the Lawrence Livermore Nat. Lab. This has stimulated further development of the *numerical QED approach*, which starts from electrons generated in the field of the nucleus (Furry picture), thereby eliminating the $Z\alpha$ part of the expansion. This technique has now reached a high degree of sophistication, and good agreement with experimental data have been attained in a number of cases [Mo82,MPS98] (??). Since the QED effects increase rapidly with the nuclear charge, the heavy few-electron systems are of particular interest in testing the theory. One big difficulty in the theoretical treatment is here the *nuclear effect*, which in many cases is at least comparable to the QED effect. This effect can to some extent be eliminated by comparing, for instance, hydrogenlike and lithiumlike systems with the same nucleus. In the heaviest systems also new physical phenomena may occur, when the field reaches the 'supercritical' level [SBH96] (?).

Also the *intermediate region*, with nuclear charges in the range Z=5-30, say, is of great interest. Here, very accurate data is now appearing from laser and X-ray experiments, but so far there has been only limited comparison with QED theory. The most accurate test has been performed for the atomic g-factor of hydrogenlike carbon, where the bound-QED contribution is verified to the order of one part in 1000. Accurate experimental information is available also for heliumlike ions, but a major problem here is to treat the *electron correlation* properly within the QED formalism. This problem will be of major concern in the present article.

For atomic and molecular problems in general the *many-body perturbation theory* (MBPT) has proven to be quite successful, particularly in the form known as the *linked-diagram expansion* [LM86]. By means of various iterative techniques, such as the *coupled-cluster approach* (CCA), the electron correlation can be treated essentially to all orders of perturbation theory, and this is widely used in quantum chemistry. This scheme can be used also in the relativistic case, using the so-called *no-virtual-pair approximation* [Su80]. However, as higher accuracy is required, it is necessary to take also QED effects more properly into account.

According to present knowledge, iterative procedures used in MBPT cannot be used in QED calculations, and therefore correlation effects have to be treated perturbatively order by order. Since the complication of a QED calculation increases very rapidly with the order of perturbation, a strict QED treatment of strong electron correlation is presently not feasible. Mainly two techniques have so far been applied to QED calculations of few-electron systems in the intermediate Z region. One technique is the application of (relativistic) MBPT with the QED corrections added in the lowest order, i.e., lowest order in α as well as $Z\alpha$ [PJS94]. The other technique, which is limited to two-electron systems, is the use of correlated, nonrelativistic wavefunctions of Hylleraas type with low-order relativity as well as QED corrections from the power expansion [Dr88]. These techniques work relatively well in the intermediate region, but the restriction to low-order corrections limits the accuracy.

Particularly in the low-intermediate region, Z=5-10, say, it will be necessary to develop new numerical techniques in order to match the accuracy of the experimental data that is presently becoming available. Here, the new experimental techniques can determine, for instance, fine-structure splittings to ppm accuracy – an accuracy that seems out of reach for the presently available numerical as well as analytical techniques. An approach to improve the situation might be to 'merge' the MBPT and numerical QED techniques in some systematic fashion, as will be discussed in the present article.

Another serious problem in bound-state QED is the treatment of the *quasi-degeneracy*, appearing, for instance, in evaluating the fine-structure separations of light elements in the relativistic formalism. In MBPT this problem can readily be handled by means of an *extended model space*, which is not possible with the standard S-matrix procedure. Two techniques for handling this problem in QED are available and will be discussed in the present work – *the two-times Green's function* and the more recently developed *covariant-evolution-operator method*. Particularly the latter has a structure which largely resembles MBPT, and for that reason it is likely that this new technique may form the ground for merging the MBPT and QED procedures in a more systematic way than what has previously been possible. The vision is that it would then be possible to combine the QED and MBPT effects in such a way

that – in addition to important MBPT effects to all orders of perturbation theory – also QED effects would be included and combined with MBPT effects to all orders. Some ideas in that direction will be presented.

The outline of this paper is as follows. In the first chapter we summarize the *time-independent MBPT* – including relativistic MBPT – as an introduction, emphasizing the method with extended model space. In the next chapter we treat *time-dependent MBPT* in some detail, since this forms a natural link between MBPT and QED. In that chapter we introduce the field-theoretical form of the interaction between electrons and photons, which makes it possible to work also with *time-dependent (retarded) interactions* between the electrons. We derive the Gell-Mann-Low theorem for the energy shift for an arbitrary model space, and show that it is valid also for interactions of field-theoretical type. In the following chapters we treat the current methods for bound-state QED calculations, starting with the standard $S-matrix\,formulation$. Next, we treat the recently developed *covariant-evolution-operator method* and the *two-times Green's-function method*, which are capable of treating also quasi-degenerate states. A comparison of these two methods is also made. A simple procedure for expressing the covariant-evolution diagrams of arbitrary order is derived in the Appendix. In the final chapter we sketch an extension of the covariant-evolution-operator method to include also instantaneous interactions to arbitrary order, thereby making it possible to evaluate QED effects with *correlated* wavefunctions. When developed, this may hopefully improve the accuracy of numerical QED calculations significantly, particularly in the low-intermediate Z region.

2 Time-independent Many-Body Perturbation Theory

TimeIndMBPT

2.1 General

sec:MBPTGen

As an introduction to the general bound-state problem, we shall briefly review the time-independent many-body perturbation theory. This is well documented in the literature, and we refer to the book of LM86 ?) for further details. [1]

The time-dependent Schrödinger wavefunction for an N-electron system satisfies the *time-dependent Schrödinger equation* [2]

$$\mathrm{i}\frac{\partial}{\partial t}\Psi_{\mathrm{S}}(x) = H\Psi_{\mathrm{S}}(x), \tag{1}$$

TDSE

[1] The book is now out of print, but a number of copies is available and can be obtained upon request from the senior author: *ingvar.lindgren@fy.chalmers.se*

[2] Throughout this article we use *relativistic units*: $\hbar = m = c = \epsilon_0 = 1$, $e^2 = 4\pi\alpha$.

where $x = (t, \boldsymbol{x}_1, \ldots \boldsymbol{x}_N)$ is the space-time coordinate, $\boldsymbol{x}_i$ being the space coordinate of the individual electron, and H is the Hamiltonian of the system. This representation is known as the *Schrödinger picture* (SP).

We assume here that the Hamiltonian is *time independent*, which means that there are *stationary solutions* of the form [3]

$$\Psi_{\rm S}(x) = \Psi(\boldsymbol{x}_, \ldots \boldsymbol{x}_N)\, e^{-{\rm i}Et}. \tag{2}$$

WFStat

The space part of the wavefunction then satisfies the *time-independent Schrödinger equation*

$$H\Psi(\boldsymbol{x}_, \ldots \boldsymbol{x}_N) = E\,\Psi(\boldsymbol{x}_, \ldots \boldsymbol{x}_N). \tag{3}$$

SEtind

The eigenfunctions of the Hamiltonian

$$H\Psi_i = E_i\Psi_i \tag{4}$$

Eigenf

define a *Hilbert space*, where the number of particles (electrons and photons) is a constant of the motion [4].

In nonrelativistic MBPT for atomic and molecular systems we start from the N-electron Hamiltonian

$$H = \sum_{i=1}^{N}\Big(-\tfrac{1}{2}\nabla_i^2 + v_{\rm ext}(\boldsymbol{r}_i)\Big) + \sum_{i<j}^{N}\frac{e^2}{4\pi\, r_{ij}}, \tag{5}$$

Hamiltonian

where $v_{\rm ext}(\boldsymbol{r})$ is the external (normally nuclear) potential. As usual, we partition the Hamiltonian into a *zeroth-order Hamiltonian* and a *perturbation*,

$$H = H_0 + H', \tag{6}$$

Partition

where we assume that the eigenfunctions and eigenvalues of H_0 are known. The modifications due to the perturbation are in standard perturbation theory treated order by order. We assume here that the operators (6) are of the form

$$\begin{aligned} H_0 &= \sum_{i=1}^{N} h_{\rm S}(i) = \sum_{i=1}^{N}\Big(-\tfrac{1}{2}\nabla_i^2 + v_{\rm ext}(\boldsymbol{r}_i) + u(\boldsymbol{r}_i)\Big) \\ H' &= -\sum_{i=1}^{N} u(\boldsymbol{r}_i) + \sum_{i<j}^{N}\frac{e^2}{4\pi\, r_{ij}}. \end{aligned} \tag{7}$$

HOH

The additional single-electron potential, $u(\boldsymbol{r})$, is hermitian but otherwise optional and can be chosen to improve the convergence rate. The perturbation

[3] We do not consider the spontaneous decay of excited states here.

[4] Later, in the field-theoretical approach we shall work in the more general space, where these numbers are not necessarily conserved (see e.g., (?)).

Sch61

H' may also contain other (time-independent) interactions, such as interaction with a static magnetic field.

The eigenstates of H_0 form our spectrum of basis functions,

$$H_0\,\Phi_M = E_0^M\,\Phi_M. \tag{8}$$

BasisFcns

Since H_0 is assumed to be of *single-particle type*, the basis functions can be expressed in the form of antisymmetrized products of single-electron functions – or *Slater determinants* –

$$\Phi_M = \frac{1}{\sqrt{N!}}\,\det\Big\{\,\phi_1(\boldsymbol{x}_1)\,\phi_2(\boldsymbol{x}_2)\cdots\phi_N(\boldsymbol{x}_N)\,\Big\}. \tag{9}$$

SlaterDet

The single-electron functions satisfy the single-electron Schrödinger equation

$$h_{\rm S}\,\phi_i(\boldsymbol{x}) = \varepsilon_i\,\phi_i(\boldsymbol{x}). \tag{10}$$

SingElEq

2.2 Perturbation theory. Extended model space

sec:pert

In MBPT we are interested in one or several eigenstates of the Hamiltonian H with the eigenfunctions Ψ^α,

$$H\,\Psi^\alpha = E^\alpha\,\Psi^\alpha \quad (\alpha = 1, 2, \cdots d), \tag{11}$$

SchrEq

which we refer to as *target functions*, representing *target states*. For each target function, Ψ^α, we assume that there exists a zeroth-order approximation – or *model function* – Ψ_0^α, which, for instance, can be a wavefunction of the independent-particle type. If there are no states with the same or nearly the same energy that can be mixed by the perturbation, then a perturbation expansion can easily be generated in the standard way. In the more general case, on the other hand, the situation can be more complicated. Closely lying – or *quasi-degenerate* – states can lead to serious convergence problems. This can be the case, for instance, when studying the atomic fine-structure of light elements in the relativistic formalism. This problem can usually be remedied by *extending the model space* and including closely lying states in that subspace. Also completely degenerate states that are mixed by the perturbation are conveniently treated with this formalism, which we shall briefly review. (For more details, we refer to the book by ?LM86?).

The model functions define a *model space*, which can contain an arbitrary number of eigenvalues of the unperturbed Hamiltonian. All unperturbed functions of the same energy must be either completely inside or completely outside the model space. In other words, no degeneracy is allowed between states in the model space and states in the complementary space.

In the general case, we cannot find directly an expansion for the wavefunction as in the nondegenerate case, since the zeroth-order or model function is not generally known from the start. Instead, it is convenient to introduce a *wave operator* or *Møller operator* (??), which transforms all model functions into the corresponding target functions

Mo45,Lo65

$$\Psi^\alpha = \Omega \Psi_0^\alpha \quad (\alpha = 1, 2, \cdots d). \tag{12}$$

WaveOp

The model functions are solutions of a *secular equation*

$$H_{\text{eff}} \Psi_0^\alpha = E^\alpha \Psi_0^\alpha, \tag{13}$$

EffHam

where H_{eff} is an *effective Hamiltonian*, operating within the model space. The eigenvalues of this operator are the exact energies (11) of the target states. Also this operator is in general unknown at the start of the calculation.

SchrEq

The wave operator satisfies the *generalized Bloch equation* (??????)

Bl58a,Bl58b,Li74,Kv77,LM86

$$\boxed{\Big[\Omega, H_0\Big] P = H'\Omega P - \Omega H'_{\text{eff}} P.} \tag{14}$$

Bloch

H'_{eff} is here the *effective interaction*, defined by

$$H_{\text{eff}} = P H_0 P + H'_{\text{eff}}, \tag{15}$$

Heff

and P is the projection operator for the model space. A condition for the theory to work is that *the model states are linearly independent* and, thus, *span the entire model space.*

We assume now that *the model functions are the projections of the target functions onto model space*,

$$\Psi_0^\alpha = P \Psi^\alpha, \tag{16}$$

Psi0

which we refer to as the *intermediate normalization (IN).* The wave operator then satisfies the condition

$$P \Omega P = P, \tag{17}$$

IN

and the effective Hamiltonian and the effective interaction have the forms

$$H_{\text{eff}} = P H \Omega P\,; \quad H'_{\text{eff}} = P H' \Omega P. \tag{18}$$

EffInt

Then the Bloch equation assumes the frequently used form

$$\boxed{\Big[\Omega, H_0\Big] P = Q\Big(H'\Omega - \Omega P H' \Omega\Big) P.} \tag{19}$$

Bloch2

Here,

$$Q = I - P \tag{20}$$

Qoper

is the projection operator for the complementary space and I is the identity operator for the Hilbert space we operate in.

By expanding the wave operator perturbatively

$$\Omega = 1 + \Omega^{(1)} + \Omega^{(2)} + \cdots , \tag{21}$$

OmegaExp

the Bloch equation can be solved order by order. This leads to the *generalized Rayleigh-Schrödinger expansion*, valid also in the quasi-degenerate case,

$$\begin{aligned}
\left[\Omega^{(1)}, H_0\right] P &= QH'P \\
\left[\Omega^{(2)}, H_0\right] P &= Q\left(H'\Omega^{(1)} - \Omega^{(1)}PH'\right)P \\
\left[\Omega^{(3)}, H_0\right] P &= Q\left(H'\Omega^{(2)} - \Omega^{(1)}PH'\Omega^{(1)} - \Omega^{(2)}PH'\right)P.
\end{aligned} \tag{22}$$

OmegaExp2

We note that with the intermediate normalization all components of the wave operator - beyond the trivial zeroth order - have their final state in the complementary space, which is also a consequence of the condition (IN 17).

The general procedure of MBPT with an extended model space can be summarized in the following rules:

- *Evaluate the wave operator to the desired accuracy, using the Bloch equation*;
- *Evaluate the matrix elements of the effective Hamiltonian*;
- *Diagonalize the matrix of the effective Hamiltonian to obtain the exact energies of the target states and the model functions*;
- *Evaluate the wavefunction of the target states if needed.*

2.3 Second quantization. The electron-field operators

sec:SQ

In many-body theory it is convenient to work in *second quantization* (see, for instance, Sch61 (?, Ch.5) or LM86 (?, Ch.11). A quantum-mechanical operator, $\hat{\mathcal{O}}$, can then be expanded as [5]

$$\hat{\mathcal{O}} = C + c_i^\dagger\, d_{i,j}\, c_j + \frac{1}{2!} c_i^\dagger c_j^\dagger\, d_{ij,kl}\, c_l c_k + \frac{1}{3!}\cdots = \hat{\mathcal{O}}_0 + \hat{\mathcal{O}}_1 + \hat{\mathcal{O}}_2 + \hat{\mathcal{O}}_3 + \cdots , \tag{23}$$

SecQuant

where the terms on the right-hand side represent the zero-, one-, two-,... body parts of the operator. c_j and $c_j^\dagger$ are electron *annihilation/creation operators*, which satisfy the usual *anti-commutation relations*

[5] We shall use a 'hat' to indicate operators in second quantization, apart from the creation/annihilation operators. We employ the summation convention with implicit summations over repeated indices that appear only on the r.h.s.

$$\{c_i^\dagger, c_j^\dagger\} = c_i^\dagger c_j^\dagger + c_j^\dagger c_i^\dagger = 0$$
$$\{c_i, c_j\} = c_i c_j + c_j c_i = 0$$
$$\{c_i^\dagger, c_j\} = c_i^\dagger c_j + c_j c_i^\dagger = \delta_{ij}, \tag{24}$$

AntiComm

where δ_{ij} is the Kronecker delta factor. The coefficients in the expansion (23) can be expressed as

SecQuant

$$d_{i,j} = \langle i|\hat{\mathcal{O}}_1|j\rangle = \int \mathrm{d}^3\boldsymbol{x}_1\, \phi_i^\dagger(x_1)\, \hat{\mathcal{O}}_1\, \phi_j(x_1)$$
$$d_{ij,kl} = \langle ij|\hat{\mathcal{O}}_2|kl\rangle = \iint \mathrm{d}^3\boldsymbol{x}_1\, \mathrm{d}^3\boldsymbol{x}_2\, \phi_i^\dagger(x_1)\phi_j^\dagger(x_2)\, \hat{\mathcal{O}}_2\, \phi_k(x_1)\phi_l(x_2)$$
$$\text{etc.} \tag{25}$$

MatrixEl

$\{\phi_j(\boldsymbol{x})\}$ is a set of single-electron functions, which are solutions to the Schrödinger equation (10) in the field of the nucleus and possibly other electrons. This is usually referred to as the *Furry picture* (**?**), although in his original work Furry only considered the potential from the (point) nucleus.

SingElEq

Fu51

It should be noted that we here let the *bras and kets represent straight products* of single-particle functions. [6] An antisymmetric product of single-particle functions (Slater determinant) (9) can be expressed

SlaterDet

$$\Phi_M = c_1^\dagger c_2^\dagger \cdots c_N^\dagger |0\rangle, \tag{26}$$

SlaterDetSQ

where $|0\rangle$ represents the vacuum state.

The nonrelativistic Hamiltonian (5) has one- and two-body parts and can be expressed in second quantization as

Hamiltonian

$$\hat{H} = c_i^\dagger\, \langle i|H_1|j\rangle\, c_j + \tfrac{1}{2} c_i^\dagger c_j^\dagger\, \langle ij|H_2|kl\rangle\, c_l c_k, \tag{27}$$

HamSecQuant

where
$$H_1 = -\tfrac{1}{2}\nabla^2 + v_{\mathrm{ext}}(\boldsymbol{r}) \quad \text{and} \quad H_2 = \frac{e^2}{4\pi\, r_{12}}\,.$$

We define the *electron field operators* in the Schrödinger representation by

$$\hat{\psi}_{\mathrm{S}}(\boldsymbol{x}) = c_j\, \phi_j(\boldsymbol{x}); \quad \hat{\psi}_{\mathrm{S}}^\dagger(\boldsymbol{x}) = c_j^\dagger\, \phi_j^\dagger(\boldsymbol{x}), \tag{28}$$

ElFieldOp

which are time independent in this representation. The Hamiltonian (27) can

HamSecQuant

[6] The true two-body matrix elements, using antisymmetric wavefunctions, then becomes
$$\langle\{ij\}|\hat{\mathcal{O}}_2|\{kl\}\rangle = \tfrac{1}{2}\langle 0|c_i c_j\, c_{i'}^\dagger c_{j'}^\dagger\, d_{i'j',k'l'}\, c_{l'} c_{k'}\, c_k^\dagger c_l^\dagger|0\rangle$$
$$= \tfrac{1}{2}\big(d_{ij,kl} + d_{ji,lk} - d_{ji,kl} - d_{ij,lk}\big) = d_{ij,kl} - d_{ij,lk},$$
assuming the operator to be symmetric with respect to interchange of the coordinates $1 \leftrightarrow 2$, etc.

then be expressed

$$\hat{H} = \int \mathrm{d}^3\boldsymbol{x}_1\, \hat{\psi}^\dagger_{\mathrm{S}}(\boldsymbol{x}_1)\, H_1\, \hat{\psi}_{\mathrm{S}}(\boldsymbol{x}_1) + \tfrac{1}{2} \iint \mathrm{d}^3\boldsymbol{x}_1\, \mathrm{d}^3\boldsymbol{x}_2\, \hat{\psi}^\dagger_{\mathrm{S}}(\boldsymbol{x}_1)\, \hat{\psi}^\dagger_{\mathrm{S}}(\boldsymbol{x}_2)\, H_2\, \hat{\psi}_{\mathrm{S}}(\boldsymbol{x}_2)\, \hat{\psi}_{\mathrm{S}}(\boldsymbol{x}_1). \tag{29}$$

HamFieldOp

In an alternative to the Schrödinger picture, the *Heisenberg picture* (HP), the wavefunctions are time independent and the time-dependence is transferred to the operators,

$$\Psi_{\mathrm{H}} = \Psi_{\mathrm{S}}(t=0) = e^{\mathrm{i}\hat{H}t}\Psi_{\mathrm{S}}(x); \qquad \hat{O}_H = e^{\mathrm{i}\hat{H}t}\hat{O}_{\mathrm{S}}\, e^{-\mathrm{i}\hat{H}t}. \tag{30}$$

HP

In perturbation theory it is often convenient to work in an intermediate picture, known as the *interaction picture* (IP). Here, the operators and wavefunctions are related to those in the Schrödinger picture by

$$\Psi_{\mathrm{I}}(t) = \mathrm{e}^{\mathrm{i}\hat{H}_0 t}\, \Psi_{\mathrm{S}}(t); \qquad \hat{O}_{\mathrm{I}}(t) = \mathrm{e}^{\mathrm{i}\hat{H}_0 t}\, \hat{O}_{\mathrm{S}}\, \mathrm{e}^{-\mathrm{i}\hat{H}_0 t}, \tag{31}$$

IP

partitioning the Hamiltonian in the same way as before (Partition 6). The relation between the Heisenberg and the interaction pictures is

$$\Psi_{\mathrm{H}} = \mathrm{e}^{\mathrm{i}\hat{H}' t}\Psi_{\mathrm{I}}(t); \qquad \hat{O}_{\mathrm{H}}(t) = \mathrm{e}^{\mathrm{i}\hat{H}' t}\, \hat{O}_{\mathrm{I}}\, \mathrm{e}^{-\mathrm{i}\hat{H}' t}. \tag{32}$$

HPIP

The wavefunction of time-independent MBPT corresponds in all pictures considered here to the time-dependent wavefunction with $t = 0$,

$$\Psi = \Psi_{\mathrm{H}} = \Psi_{\mathrm{S}}(0) = \Psi_{\mathrm{I}}(0). \tag{33}$$

TimeIndWF

In the *Heisenberg picture* (HP 30) the electron-field operators (ElFieldOp 28) become

$$\hat{\psi}_{\mathrm{H}}(x) = e^{\mathrm{i}\hat{H}t}\, \hat{\psi}_{\mathrm{S}}(\boldsymbol{x})\, e^{-\mathrm{i}\hat{H}t}\,; \qquad \hat{\psi}^\dagger_{\mathrm{H}}(x) = e^{\mathrm{i}\hat{H}t}\, \hat{\psi}^\dagger_{\mathrm{S}}(\boldsymbol{x})\, e^{-\mathrm{i}\hat{H}t}, \tag{34}$$

ElFieldHP

and in the *interaction picture* (IP) (IP 31)

$$\begin{aligned} \hat{\psi}_{\mathrm{I}}(x) &= e^{\mathrm{i}\hat{H}_0 t}\hat{\psi}_{\mathrm{S}}(\boldsymbol{x})\, e^{-\mathrm{i}\hat{H}_0 t} = e^{\mathrm{i}\hat{H}_0 t} c_j\, \phi_j(\boldsymbol{x})\, e^{-\mathrm{i}\hat{H}_0 t} = c_j\, \phi_j(\boldsymbol{x})\, e^{-\mathrm{i}\varepsilon_j t} = c_j\, \phi_j(x) \\ \hat{\psi}^\dagger_{\mathrm{I}}(x) &= c^\dagger_j\, \phi^\dagger_j(\boldsymbol{x})\, e^{\mathrm{i}\varepsilon_j t} = c^\dagger_j\, \phi^\dagger_j(x). \end{aligned} \tag{35}$$

ElFieldIP

We now introduce the *time-dependent* creation/annihilations operators in the IP by

$$c_j(t) = c_j\, e^{-\mathrm{i}\varepsilon_j t}\,; \qquad c^\dagger_j(t) = c^\dagger_j\, e^{\mathrm{i}\varepsilon_j t}, \tag{36}$$

TimeDepSQ

which gives

$$\hat{\psi}_{\mathrm{I}}(x) = c_j(t)\, \phi_j(\boldsymbol{x})\,; \qquad \hat{\psi}^\dagger_{\mathrm{I}}(x) = c^\dagger_j(t)\, \phi^\dagger_j(\boldsymbol{x}). \tag{37}$$

ElFieldTD

The creation/annihilation operators are said to be in *normal order*, *if all creation operators appear to the left of the annihilation operators*. A *contraction* of

the operators is defined as the *difference between the ordinary (time-ordered) product and the normal-ordered product*,

$$\overset{\sqcap}{x\,y} = x\,y - \{x\,y\}, \tag{38}$$

ContractDef

where we use the *curly brackets to denote the normal product*. From this definition it follows that

$$\overset{\sqcap}{c_i^\dagger}\,\overset{\sqcap}{c_j^\dagger} = \overset{\sqcap}{c_i}\,\overset{\sqcap}{c_j} = \overset{\sqcap}{c_i^\dagger}\,\overset{\sqcap}{c_j} = 0 \quad \text{and} \quad \overset{\sqcap}{c_i}\,\overset{\sqcap}{c_j^\dagger} = \delta_{ij}. \tag{39}$$

Contraction

Normal order and Wick's theorem

The handling of operators in second quantization is greatly simplified by *Wick's theorem* [Wi50] (?), which states that a product of creation and annihilation operators $\hat{A}$ can be written as the normal product plus all single, double ... contractions with the uncontracted operators in normal form, or symbolically

$$\hat{A} = \{\hat{A}\} + \{\hat{A}\}. \tag{40}$$

Wick

A particularly useful form of Wick's theorem is the following. *If $\hat{A}$ and $\hat{B}$ are operators in normal form, then the product is equal to the normal product plus all normal-ordered contractions between $\hat{A}$ and $\hat{B}$*, or formally

$$\hat{A}\,\hat{B} = \{\hat{A}\,\hat{B}\} + \{\hat{A}\,\hat{B}\}. \tag{41}$$

GenWick

This forms the basic rule for constructing the MBPT diagrams.

2.4 The linked-diagram expansion

sec:LDE

By using second quantization and Wick's theorem, the perturbation expansion can conveniently be expressed in terms of *diagrams* – see, for instance [LM86] (?, Ch.12). By means of the theorem in the form (41), the Rayleigh-Schrödinger expansion can easily be transformed into normal-ordered products. Each such product is represented by a (Goldstone) diagram, and this leads to the diagrammatic expansion of the many-body wavefunction. The corresponding energy diagrams are obtained by 'closing' the wavefunction diagram by a final perturbation, so that the final state lies in the model space. It is then found that such an expansion can contain diagrams that are referred to as *unlinked*, i.e., contain one or several *disconnected, closed parts* (with the initial and the final state in the model space). The remaining diagrams are known as *linked*. It can be shown that all unlinked terms cancel in the Rayleigh-Schrödinger perturbation expansion, provided the model space is *complete*, i.e., contains all configurations that can be formed from the valence electrons. This is the

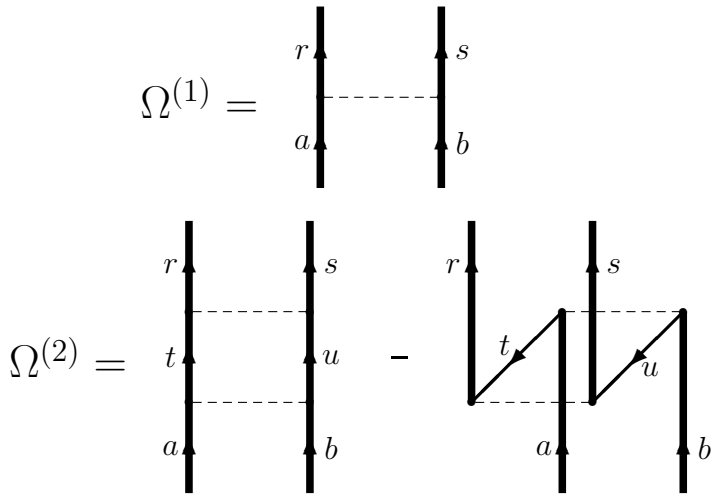

Fig. 1. Diagrammatic representation of the two lowest orders of the wave operator for a two-electron system. The heavy vertical lines represent electron states in the nuclear potential (10) and the dotted horizontal lines the Coulomb interaction. The last diagram, originating from the second term in the Bloch equation (42), is a type of model-space contribution (MSC) with the intermediate state in the model space. This is also referred to as *folded* and often drawn in a folded way.

Fig:Omega12

linked-diagram theorem, first shown for closed-shell systems by (?) and (?) and later extended to open-shell systems (?) as well as to quasi-degenerate model space (??). The Bloch equation (14) can then be written

$$\boxed{\left[\Omega, H_0\right] P = \left(H'\Omega - \Omega H'_{\rm eff}\right)_{\rm linked} P,} \qquad (42)$$

BlochLink

where $H'_{\rm eff} = PH'\Omega P$ in the intermediate normalization (17). The second term on the r.h.s. is referred to as *folded* and is usually interpreted in a special way. The denominators of the two parts, Ω and $H'_{\rm eff}$, are *independent*. For that reason the corresponding time-ordered (Goldstone) diagrams are often drawn as 'folded' with all possible time orderings between the interactions of the two parts. By using the standard Goldstone evaluation rules and the 'factorization theorem', the denominators of the two parts can then be factorized (?), (?, Ch.13).

In the formalism we shall develop, the 'folded' diagrams need not be drawn in a folded way. The factorization of the denominators follows directly from the Bloch equation. If drawn in a 'stretched' way, the folded diagrams have an intermediate state in the model space, and we shall refer to such contributions as *Model-Space Contributions* (MSC). Later, in dealing with time-dependent interactions, we shall find that there is an additional type of MSC.

In second order, the linked-diagram form of the Bloch equation (42) leads

instead of the Rayleigh-Schrödinger expression (22) to

$$\Big[\Omega^{(2)}, H_0\Big]\, P = Q\Big(H'\Omega^{(1)} - \Omega^{(1)} P H'\Big)_{\rm linked} P. \tag{43}$$

As an illustration we consider a two-electron system, where the electron orbitals are solutions of the Schrödinger equation in an external (nuclear) field (10). The solution to the equations for $\Omega^{(1)}$ and $\Omega^{(2)}$ can then be expressed

$$\begin{aligned}
\Big\langle rs\Big|\Omega^{(1)}\Big|ab\Big\rangle &= \frac{\langle rs|H'|ab\rangle}{\varepsilon_a + \varepsilon_b - \varepsilon_r - \varepsilon_s} \\
\Big\langle rs\Big|\Omega^{(2)}\Big|ab\Big\rangle &= \Bigg(\sum_{|tu\rangle \in Q} \frac{\langle rs|H'|tu\rangle\langle tu|H'|ab\rangle}{(\varepsilon_a + \varepsilon_b - \varepsilon_r - \varepsilon_s)(\varepsilon_a + \varepsilon_b - \varepsilon_t - \varepsilon_u)} \\
&\quad - \sum_{|tu\rangle \in P} \frac{\langle rs|H'|tu\rangle\langle tu|H'|ab\rangle}{(\varepsilon_a + \varepsilon_b - \varepsilon_r - \varepsilon_s)(\varepsilon_t + \varepsilon_u - \varepsilon_r - \varepsilon_s)} \Bigg)_{\rm linked} .
\end{aligned} \tag{44}$$

This is illustrated in Fig.1. The first diagram of $\Omega^{(2)}P$ represents $QH'\Omega^{(1)}P$. It follows from Wick's theorem (41) that only the fully contracted term can contribute in this case. Here, the intermediate state (tu) lies in the complementary space, Q. The second diagram represents the term $\Omega^{(1)}PH'P$, and this is a model-space contribution with the intermediate state in the model space, P. This diagram is here drawn in the conventional way as *folded*, so that the Goldstone evaluation rules can be used.

2.5 All-order procedures. The coupled-cluster approach

A great advantage of the many-body procedure of the type presented here is that important perturbative effects – i.e., most of the electron correlation – can be treated iteratively to essentially *all orders of perturbation theory*. This can be achieved by separating the wave operator in second quantization into one-, two-, ... body effects (23),

$$\Omega = 1 + \Omega_1 + \Omega_2 + \cdots \tag{45}$$

– which should not be confused with the perturbative expansion (21). Here, the n-body effects can be expanded as (see, for instance, (?, Ch.15))

$$\begin{aligned}
\Omega_1 &= c_i^\dagger\, x_j^i\, c_j \\
\Omega_2 &= \tfrac{1}{2}\, c_i^\dagger c_j^\dagger\, x_{kl}^{ij}\, c_l c_k \\
&\quad \text{etc.}
\end{aligned} \tag{46}$$

where x_j^i, $x_{kl}^{ij} \ldots$ are the expansion coefficients or 'amplitudes' for the particular 'excitation'. The Bloch equation in the linked-diagram form (42) can then

be separated into a set of equations for $n = 1, 2, \cdots$

$$\Big[\Omega_n, H_0\Big]\, P = Q\Big(H'\Omega - \Omega H'_{\rm eff}\Big)_{n,\,\rm linked} P. \tag{47}$$

ClusterEq

The equations for different orders n are *coupled* and have to be solved *iteratively*. The most important component is normally $n = 2$, which corresponds to *pair correlation* (??). For open-shell systems also $n = 1$ can be quite important, but less so for closed-shell systems. The latter contributions represent one-body effects that can be included in the single-electron orbitals. With such orbitals there are no single excitations in a configuration-interaction (CI) expansion, and the zeroth-order wavefunction has maximum overlap with the exact one. These orbitals are known as *Brueckner orbitals* or *maximum overlap orbitals* (????), (?, p.260).

sec:CCA

2.5.1 Coupled-cluster approach

An improved iterative technique can be obtained by expressing the wave operator in *exponential form*,

$$\Omega = \exp S = 1 + S + \tfrac{1}{2}S^2 + \cdots, \tag{48}$$

ExpOmega

a technique first developed in nuclear physics in the late 1950's (????) and later further developed and extensively applied in quantum chemistry (????). For open-shell systems the form (48) leads to 'spurious' terms, which are eliminated by choosing the *normal-ordered* form of the exponential (???)

$$\Omega = \{\exp S\} = 1 + S + \tfrac{1}{2}\{S^2\} + \cdots. \tag{49}$$

ExpOmegaNO

The normal-ordering, denoted by curly brackets, implies that there are no 'contractions' between the cluster operators, which eliminates the spurious terms of the straight exponential (48). It can be shown that with a complete model space the cluster terms are *connected*, which is a stronger condition than *linked* [7].

In analogy with the wave-operator expansion (45), we expand the cluster operator S in terms of one-, two, ... body clusters

$$S = S_1 + S_2 + \cdots \tag{50}$$

SExp

with

[7] A disconnected diagram is still termed 'linked', if all the separate pieces are *open*. If the model space is *incomplete*, then disconnected cluster diagrams may appear with the formalism described here. By modifying the procedure, it is possible to maintain the connectivity also for incomplete model space, as discussed particularly by (?), (?).

$$S_1 = c_i^\dagger \, s_j^i \, c_j$$
$$S_2 = \tfrac{1}{2} \, c_i^\dagger c_j^\dagger \, s_{kl}^{ij} \, c_l c_k$$
etc.

Inserted in the Bloch equation (14), this leads to the *coupled-cluster equations*

$$\Big[S_n, H_0\Big] \, P = Q\Big(H'\Omega - \Omega H'_{\rm eff}\Big)_{n,\,\rm conn} P, \tag{51}$$

CCA

where '*conn*' stands for terms/diagrams that are connected. As before, this leads to a set of coupled equations for $n = 1, 2, \cdots$, which are solved iteratively. One essential advantage of this approach over the simpler approach of the previous section (47) is that important *four-body effects* are automatically included in the pair-correlation approach via the $\{S^2\}$ term. For quantum-chemistry applications the approach furthermore has the advantage of satisfying the *separability condition* (?), which implies that the wavefunction of the system separates correctly upon fragmentation.

sec:PairCorr

2.5.2 Pair correlation

As before, the pair term, S_2, in the cluster expansion (50) is the most important, followed by the S_1 term. A frequently used approximation is the 'coupled-cluster-singles-and-doubles approximation' (CCSD), where the coupled equations for S_1 and S_2 are solved to self-consistency (?). Here, the wave operator is approximated by (?, Ch.15)

$$\Omega = 1 + S_1 + S_2 + \tfrac{1}{2}\{S_1\}^2 + \{S_1 S_2\} + \tfrac{1}{2}\{S_2\}^2 + \tfrac{1}{2}\{S_1^2 S_2\} + \frac{1}{3!}\{S_1\}^3 + \frac{1}{4!}\{S_1\}^4. \tag{52}$$

CCSD

(The effect of the last three terms with three or more disconnected clusters is usually quite small and often omitted.) Inserted into the cluster equation (51), the pair approximation yields the equations

$$\begin{aligned} \Big[S_1, H_0\Big] \, P &= \Big(H'\Omega - \Omega H'_{\rm eff}\Big)_{1,\,\rm conn} P \\ \Big[S_2, H_0\Big] \, P &= \Big(H'\Omega - \Omega H'_{\rm eff}\Big)_{2,\,\rm conn} P \end{aligned} \tag{53}$$

S1S2

with $H'_{\rm eff} = PH'\Omega P$ in the intermediate normalization. The CCSD approximation normally represents 95-98% of the electron correlation. In more elaborate calculations also connected triple and quadruple excitations are (partially) included (see, for instance, (?) for a review).

As a simple illustration of the pair equation we shall consider a two-electron system (He-like system) with the zeroth-order Hamiltonian and the perturba-

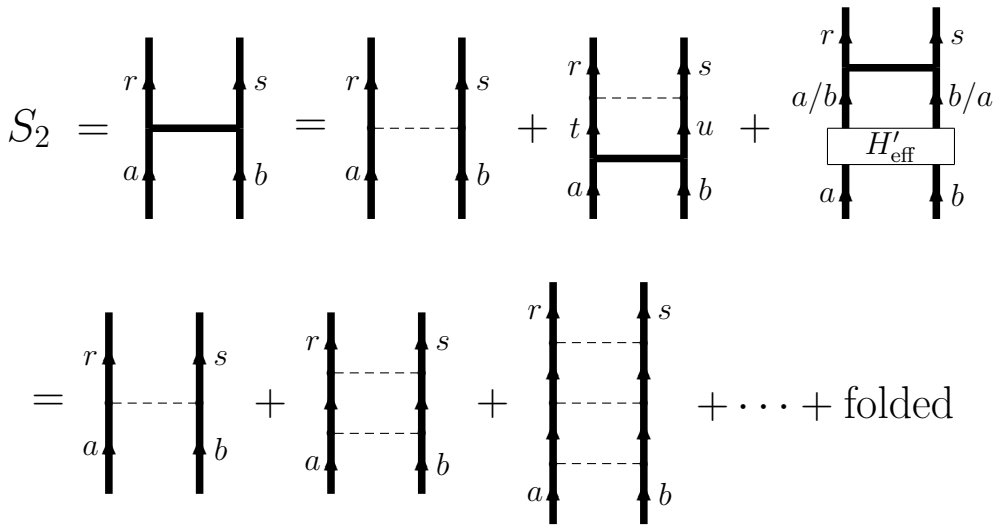

Fig. 2. The pair function for a two-electron system (with no core electrons) is equivalent to an infinite sequence of ladder diagrams (including the folded diagrams).

Fig:PairEq

tion (7)

H0H

$$H_0 = \sum_{i=1}^{2} \Big(-\tfrac{1}{2}\nabla_i^2 + \frac{Ze^2}{4\pi\, r_i} \Big); \quad H' = \frac{e^2}{4\pi\, r_{12}}\,. \tag{54}$$

H0H2

The pair equation (53) then becomes

S1S2

$$\Big[S_2, H_0\Big]\, P = Q\Big(H'(1+S_2) - S_2 H'_{\rm eff}\Big)_{2,\,\rm conn} P. \tag{55}$$

PairEq

Since there are no core electrons in this case, there are no S_1 clusters. With the expansion (50) this becomes

SExp

$$\Big(\varepsilon_a + \varepsilon_b - \varepsilon_r - \varepsilon_s\Big)\, s_{ab}^{rs} = \langle rs|H'|ab\rangle + \langle rs|H'|tu\rangle\, s_{ab}^{tu} - s_{ab}^{rs}\, \langle ab|H'_{\rm eff}|ab\rangle\,, \tag{56}$$

PairEq2

where the last folded term should also include an exchange contribution. The pair (r,s) is here different from the pair (a,b). This equation is graphically illustrated in Fig. 2. By introducing the *pair function*

Fig:PairEq

$$|\rho_{ab}\rangle = s_{ab}^{rs}|rs\rangle\,, \tag{57}$$

PairFcn

we obtain the following *pair equation*

$$\begin{aligned}&\Big(\varepsilon_a + \varepsilon_b - h_0(1) - h_0(2)\Big)|\rho_{ab}\rangle = \\ &|rs\rangle\langle rs|H'|ab\rangle + |rs\rangle\langle rs|H'|\rho_{ab}\rangle - |\rho_{ab}\rangle\, \langle ab|H'_{\rm eff}|ab\rangle.\end{aligned} \tag{58}$$

PairEq3

Solving this equation self-consistently, is equivalent to generating an infinite sequence of ladder diagrams – in addition to the folded diagrams – as indicated in the second row of the figure. This corresponds to *solving the two-particle equation exactly.*

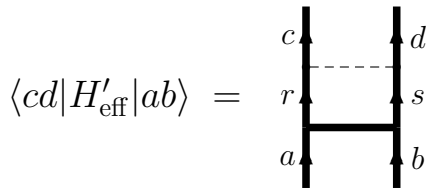

Fig. 3. Closing the pair function by a final interaction yields the contribution to the energy – or generally the effective interaction. The final state (c, d) lies here in the model space.

Fig:ClosPf

The corresponding contribution to the energy – or generally the effective interaction (18) – is then obtained by 'closing' the pair function by a final interaction

$$\langle cd|H'_{\rm eff}|ab\rangle = \langle cd|H'_{\rm eff}|rs\rangle\, s^{rs}_{ab} = \langle cd|H'_{\rm eff}|\rho_{ab}\rangle \qquad (59)$$

ClosPf

depicted in Fig. 3. Here, the final state (cd) lies in the model space.

sec:Num

2.5.3 Numerical evaluation

For atomic problems we primarily consider here, it is convenient to separate the MBPT diagrams into spin-angular and radial parts. This is based upon the standard expansion of the perturbation (54) in spherical waves, using the relation

$$\frac{1}{r_{12}} = \sum_{l=0}^{\infty} \frac{r_<^l}{r_>^{l+1}}\, \boldsymbol{C}^l(1)\cdot\boldsymbol{C}^l(2), \qquad (60)$$

SphW

where $\boldsymbol{C}^l$ is a spherical tensor, closely related to the spherical harmonics (**?**). The spin-angular part can be evaluated using angular-momentum diagrams, and only the radial part has to be evaluated numerically. For the numerical evaluation essentially two schemes have been developed. One scheme is based upon the use of *B splines* and used particularly by the Notre Dame group (**?**). The other scheme is based upon a *discretization* of the radial space and matrix inversion. This is developed by (**??**) and used mainly by the Göteborg group. (See also the review by (**?**).)

2.6 Relativistic MBPT

sec:RMBPT

2.6.1 The Dirac equation

sec:Dirac

According to Dirac's relativistic electron theory, the equation for a single electron in an external (nuclear) potential $v_{\rm ext}$ is

$$\mathrm{i}\frac{\partial}{\partial t}\,\phi(x) = \Big(\boldsymbol{\alpha}\cdot\mathbf{p} + \beta + v_{\rm ext}\Big)\,\phi(x). \tag{61}$$

DiracTD

Here, $\phi(x)$ represents a four-component wavefunction, $\mathbf{p} = -\mathrm{i}\boldsymbol{\nabla}$ is the momentum operator and $\boldsymbol{\alpha}$, β are the 4×4 Dirac matrices. The stationary states are of the form $\phi_i(x) = \phi_i(\boldsymbol{x})\,e^{-\mathrm{i}\varepsilon_i t}$, where the space part satisfies the corresponding time-independent equation

$$h_{\rm D}\,\phi_i(\boldsymbol{x}) = \varepsilon_i\,\phi_i(\boldsymbol{x})\,; \qquad h_{\rm D} = \boldsymbol{\alpha}\cdot\boldsymbol{p} + \beta + v_{\rm ext}. \tag{62}$$

Dirac

2.6.2 No-Virtual-Pair Approximation

sec:NVPA

Formally, relativistic many-body problems have to be treated in the framework of QED. There exists no relativistic Hamiltonian corresponding to the nonrelativistic one (5). However, various approximations can be constructed, which have been found to work quite well.

Hamiltonian

The first natural choice for a relativistic many-body Hamiltonian might be to replace the Schrödinger single-electron operator of the nonrelativistic Hamiltonian (5) by the Dirac operator (62), which leads to the Hamiltonian

Hamiltonian Dirac

$$H_{\rm DC} = \sum_{i=1}^{N} h_{\rm D}(i) + \sum_{i<j}^{N} \frac{e^2}{4\pi\, r_{ij}}\,, \tag{63}$$

DirCoul

known as the *Dirac-Coulomb Hamiltonian*. Due to the negative-energy continuum of the Dirac equation, the eigenvalues of this Hamiltonian are not bound from below, and it is therefore, as it stands, not suitable for many-body calculations. This is known as the *Brown-Ravenhall disease* (?). Nevertheless, the Hamiltonian has been used for a long time in practical works, particularly in self-consistent Dirac-Fock and multi-configurational Dirac-Fock calculations (?). It turns out that by choosing appropriate boundary conditions, the appearance of negative energy states can be strongly suppressed. Formally, this can be expressed as a *projected Dirac-Coulomb Hamiltonian* (?)

BR51 De75 Su80

$$H_{\rm ProjDC} = \Lambda_+\Big(\sum_{i=1}^{N} h_{\rm D}(i) + \sum_{i<j}^{N} \frac{e^2}{4\pi\, r_{ij}}\Big)\,\Lambda_+\,, \tag{64}$$

CoulHamProj

where Λ_+ is the projection operator for the positive energy spectrum of the Dirac equation.

When relativity is considered, there is, in addition to the electrostatic interaction between the electrons, a *magnetic interaction* of order α^2, where α is the fine-structure constant ($\alpha \approx 1/137,0600$). This leads to an additional term in the Hamiltonian, first formulated by [Gaunt29] (?), and the so-called *Coulomb-Gaunt interaction*,

$$H_{\rm CG} = \sum_{i<j}^{N} \frac{e^2}{4\pi\, r_{ij}} \Big(1 - \boldsymbol{\alpha}_i \cdot \boldsymbol{\alpha}_j\Big). \tag{65}$$

CoulGaunt

The Coulomb and the Gaunt interactions above are *instantaneous*. It was first shown by [Breit30,Breit32] (??) that also the *retardation* of the Coulomb interaction gives rise to effects of the same order. This leads together with the magnetic interaction to the so-called *Breit interaction* and the *Coulomb-Breit interaction*

$$H_{\rm CB} = \sum_{i<j}^{N} \frac{e^2}{4\pi\, r_{ij}} \left(1 - \tfrac{1}{2}\boldsymbol{\alpha}_i \cdot \boldsymbol{\alpha}_j - \frac{(\boldsymbol{\alpha_i} \cdot \boldsymbol{r_{ij}})\,(\boldsymbol{\alpha_j} \cdot \boldsymbol{r_{ij}})}{2r_{ij}^2}\right). \tag{66}$$

Breit

Replacing the instantaneous Coulomb interaction in the projected Hamiltonian by this operator, leads to

$$H_{\rm NVPA} = \Lambda_+\Big(\sum_{i=1}^{N} h_D(i) + H_{\rm CB}\Big)\,\Lambda_+, \tag{67}$$

NVPA

known as the *No-Virtual-Pair Approximation (NVPA)* [Su80] (?).

The Breit interaction is instantaneous, although it compensates for the leading effect of the retardation of the Coulomb interaction. In a proper QED treatment, there is an additional retardation effect of the Breit interaction of order α^3. The Coulomb interaction, on the other hand, is strictly instantaneous in this model, which is the *Coulomb gauge*. In an alternative gauge, frequently used in QED, the *Feynman gauge*, the instantaneous interaction is identical to the Coulomb-Gaunt interaction. This interaction does not contain any retardation, and therefore the retardation correction to this interaction is of the order α^2, i.e., an order of $1/\alpha$ larger than in the Coulomb gauge. This implies that when the Feynman-gauge is used in the NVPA for heavy elements, considerable errors may be introduced [GI88,LM89,Su88,Li90] (????). In QED calculations, on the other hand, when the retardation is properly taken care of, this error is eliminated, and the Feynman gauge is often used due to its simplicity.

The NVPA in the Coulomb gauge is normally a very good starting point for relativistic MBPT. The Hamiltonian is partitioned as before [Partition] (6) with

$$H_0 = \sum_{i=1}^{N} \Big(h_{\rm D}(i) + u(\boldsymbol{r}_i)\Big) \qquad H' = -\sum_{i=1}^{N} u(\boldsymbol{r}_i) + H_{\rm CB}.$$

Then the linked-diagram expansion and the coupled-cluster approach can be generated in a straightforward manner (S089 ?). This yields very good results also for quite heavy elements.

3 Time-dependent MBPT

TimeDepMBPT

3.1 General

sec:TDGen

In this section we shall consider the *time-dependent* form of MBPT, which will form a link between time-independent MBPT and quantum electrodynamics (QED) for bound states to be discussed in the following chapters. In QED the interaction of electrons/positrons with the photon field is in the interaction picture (IP) (IP 31) represented by

$$\hat{H}'_{\rm I}(t) = \int {\rm d}^3\boldsymbol{x}\, \hat{\mathcal{H}}'_{\rm I}(x), \tag{68}$$

IntHam

where

$$\hat{\mathcal{H}}'_{\rm I}(x) = -e\hat{\psi}^\dagger(x)\,\alpha^\mu \hat{A}_\mu(x)\hat{\psi}(x)$$

is the *interaction Hamiltonian density* (Sch61 ?). Here, $\hat{\psi}^\dagger(x)$, $\hat{\psi}(x)$ are the electron-field operators in the IP (ElFieldTD 37), and α^μ represents the four-component Dirac matrices, related to the standard Dirac $\boldsymbol{\alpha}$ matrices (DiracTD 61) by

$$\alpha^\mu = (1, \boldsymbol{\alpha}).$$

(These are related to the Dirac γ matrices by $\alpha^\mu = \gamma^0\gamma^\mu$.) $\hat{A}_\mu$ are the electromagnetic field operators

$$\hat{A}_\mu \propto \varepsilon_{\mu j}(\boldsymbol{k})\left(a_j^\dagger(\boldsymbol{k})\, e^{i\kappa x} + a_j(\boldsymbol{k})\, e^{-i\kappa x}\right), \tag{69}$$

ElmagnField

where $\varepsilon_{\mu j}(\boldsymbol{k})$ are the four-component polarization vectors, $a_j^\dagger(\boldsymbol{k})$ and $a_j(\boldsymbol{k})$ the photon creation and annihilation operators, respectively, and $x = (t, \boldsymbol{x})$ and $\kappa = (\omega, \boldsymbol{k})$ the four-component k vector. With the metric we use, the four-component scalar product is $\kappa x = \omega t - \boldsymbol{k}\cdot\boldsymbol{x}$. The only nonvanishing commutation relation for the photon operators is (MS84 ?, Eq. 5.28)

$$[a_i, a_j^\dagger] = a_i\, a_j^\dagger - a_j^\dagger\, a_i = \pm\delta_{i,j}, \tag{70}$$

Comm

where the upper (lower) sign is for the space (time) part of the operators.

The perturbation (IntHam 68) commutes with the number operator for the *electrons*,

$$N = \sum_i c_i^\dagger c_i, \tag{71}$$

NumberOp

which means that the electronic charge (number of electrons minus positrons) is conserved. The electromagnetic-field operator, on the other hand, contains unpaired creation and annihilation *photon* operators, which implies that *the number of photons in not conserved by the perturbation*. Therefore, this perturbation operates in a more general space (see, e.g., [?, Ch.6]), which we can write as

$$\boldsymbol{\mathcal{H}} = \mathcal{H}_0 \otimes \mathcal{H}_{+1} \otimes \mathcal{H}_{-1}. \tag{72}$$

Fock

$\mathcal{H}_x$ represents here a 'restricted' Hilbert space, where the number of photons is conserved. $\mathcal{H}_0$ is the 'central' space, where the model functions are located, while $\mathcal{H}_{+1}$ and $\mathcal{H}_{-1}$ represent the corresponding spaces with one photon more and less, respectively. This will be further discussed in chapter 8.

With a perturbation of the type (68), the *interaction* between the electrons is formed by *two* perturbations with contracted photon operators. This contraction (38) defines a *photon propagator*, $D_{\mathrm{F}\nu\mu}$, by

$$\mathrm{i}D_{\mathrm{F}\nu\mu}(x_2 - x_1) = \overbrace{A_\nu(x_2)A_\mu(x_1)} = \Big\langle 0\Big|T_{\mathrm{D}}[A_\nu(x_2)A_\mu(x_1)]\Big|0\Big\rangle\,. \tag{73}$$

PhotProp

T_{D} is here the *Dyson time-ordering operator*,

$$T_{\mathrm{D}}[A(x_1)B(x_2)] = \begin{cases} A(x_1)B(x_2) & (t_1 > t_2) \\ B(x_2)A(x_1) & (t_1 < t_2), \end{cases} \tag{74}$$

TimeOrdering2

and $|0\rangle$ represents the vacuum state. Since the vacuum-expectation value of the normal-ordered product vanishes, the contraction is given by the time-ordered product.

The *Fourier transform* of the photon propagator is defined by

$$D_{\mathrm{F}\nu\mu}(x_2 - x_1) = \int \frac{\mathrm{d}z}{2\pi}\, D_{\mathrm{F}\nu\mu}(\boldsymbol{x}_2 - \boldsymbol{x}_1, z)\, \mathrm{e}^{-\mathrm{i}z(t_2 - t_1)}, \tag{75}$$

FourierProp

which in the *Feynman gauge* becomes

$$D_{\mathrm{F}\nu\mu}(\boldsymbol{x}_2 - \boldsymbol{x}_1, z) = -g_{\nu\mu} \int \frac{\mathrm{d}^3\boldsymbol{k}}{(2\pi)^3}\, \frac{\mathrm{e}^{\mathrm{i}\mathbf{k}\cdot(\boldsymbol{x}_2 - \boldsymbol{x}_1)}}{z^2 - k^2 + \mathrm{i}\eta} = -\frac{g_{\nu\mu}}{2\pi^2 r_{12}} \int_0^\infty \frac{k\,\mathrm{d}k\, \sin(kr_{12})}{z^2 - k^2 + \mathrm{i}\eta}, \tag{76}$$

PhotPropF

where $k = |\mathbf{k}|$. The interaction between the electrons then becomes

$$I(\boldsymbol{x}_2, \boldsymbol{x}_1, z) = e^2 \alpha_1^\mu \alpha_2^\nu\, D_{F\nu\mu}(\boldsymbol{x}_2 - \boldsymbol{x}_1, z) = \int_0^\infty \frac{2k\,\mathrm{d}k\, f(k)}{z^2 - k^2 + \mathrm{i}\eta}, \tag{77}$$

Interact

where

$$f(k) = -\frac{e^2}{4\pi^2\, r_{12}}\, (1 - \boldsymbol{\alpha}_1 \cdot \boldsymbol{\alpha}_2)\, \sin(kr_{12}).$$

Performing the k integration yields

$$I(\boldsymbol{x}_2, \boldsymbol{x}_1, z) = \frac{e^2}{4\pi\, r_{12}}\, (1 - \boldsymbol{\alpha}_1 \cdot \boldsymbol{\alpha}_2)\, \mathrm{e}^{\mathrm{i}|z|r_{12}}. \tag{78}$$

RetCoulGaunt

This is the *retarded Gaunt interaction*. When $z = 0$, this becomes the corresponding instantaneous interaction (65). In the *Coulomb gauge* the corresponding interaction becomes

$$I_{\rm C}(\boldsymbol{x}_2, \boldsymbol{x}_1, z) = \frac{e^2}{4\pi}\left\{\frac{1}{r_{12}} - \boldsymbol{\alpha}_1 \cdot \boldsymbol{\alpha}_2 \, \frac{e^{{\rm i}|z|r_{12}}}{r_{12}} + \left[\boldsymbol{\alpha}_1 \cdot \boldsymbol{\nabla}_1, \left[\boldsymbol{\alpha}_2 \cdot \boldsymbol{\nabla}_2, \; \frac{e^{{\rm i}|z|r_{12}} - 1}{z^2 r_{12}}\right]\right]\right\}, \tag{79}$$

IntCoul

which is the *retarded form of the Coulomb-Breit interaction* (66).

For numerical work it is often convenient to expand the interaction (77) in spherical waves, in analogy with the expansion (60),

$$\frac{\sin kr_{12}}{kr_{12}} = \sum_{l=0}^{\infty}(2l+1) j_l(kr_1) j_l(kr_2) \, \boldsymbol{C}^l(1) \cdot \boldsymbol{C}^l(2), \tag{80}$$

SphW2

where $j_l(kr)$ are spherical Bessel functions, and to perform the radial integrations *before* the k integrations.

3.2 The time-evolution operator

c:TimeEvolOp

We consider now a general time-dependent perturbation, of which the QED perturbation (68) is one example. We assume further that the operators involved are expressed in second quantization and that the states are represented by *state vectors* in the generalized Fock space (72). A state represented by the *function* $\Psi(x)$ will then be represented by the *vector* $|\Psi(t)\rangle$. The time-dependent Schrödinger equation (1) then takes the form

$${\rm i}\frac{\partial}{\partial t}\Big|\Psi(t)\Big\rangle = \hat{H}(t)\,\Big|\Psi(t)\Big\rangle \tag{81}$$

SchrTD

and in the interaction picture (31)

$${\rm i}\frac{\partial}{\partial t}\Big|\Psi_{\rm I}(t)\Big\rangle = \hat{H}'_{\rm I}(t)\,\Big|\Psi_{\rm I}(t)\Big\rangle\,. \tag{82}$$

SchrInt

The Schrödinger equation (82) has the solution

$$\Big|\Psi_{\rm I}(t)\Big\rangle = \Big|\Psi_{\rm I}(t_0)\Big\rangle - {\rm i}\int_{t_0}^{t} {\rm d}t' \; \hat{H}'_{\rm I}(t')\,\Big|\Psi_{\rm I}(t')\Big\rangle, \tag{83}$$

and we introduce the *time-evolution operator* in the IP, defined by [8]

$$\Big|\Psi_{\rm I}(t)\Big\rangle = \hat{U}(t, t_0)\,\Big|\Psi_{\rm I}(t_0)\Big\rangle, \tag{84}$$

UDef

[8] This operator does not preserve the intermediate normalization (17).

which satisfies the equation

$$\boxed{\mathrm{i}\frac{\partial}{\partial t}\hat{U}(t,t_0) = \hat{H}'_{\mathrm{I}}(t)\,\hat{U}(t,t_0).} \tag{85}$$

UEq

This leads to the expansion (FW71 (?, Eq. 6.23), IZ80 (?, Eq. 4-56)

$$\hat{U}(t,t_0) = 1 + \sum_{n=1}^{\infty}(-\mathrm{i})^n \int_{t_0}^{t}\mathrm{d}t_n \int_{t_0}^{t_n}\mathrm{d}t_{n-1}\ldots\int_{t_0}^{t_2}\mathrm{d}t_1 \hat{H}'_{\mathrm{I}}(t_n)\ldots\hat{H}'_{\mathrm{I}}(t_1) = 1 +$$
$$\sum_{n=1}^{\infty}\frac{(-\mathrm{i})^n}{n!}\int_{t_0}^{t}\mathrm{d}t_n\ldots\int_{t_0}^{t}\mathrm{d}t_1\, T_{\mathrm{D}}\Big[\hat{H}'_{\mathrm{I}}(t_n)\ldots\hat{H}'_{\mathrm{I}}(t_1)\Big] = T_{\mathrm{D}}\exp\Big[-\mathrm{i}\int_{t_0}^{t}\mathrm{d}t\,\hat{H}'_{\mathrm{I}}(t)\Big], \tag{86}$$

UExp

where T_{D} is the time-ordering operator (TimeOrdering2 74). Using the interaction density (IntHam 68), the evolution operator can then be expressed

$$\begin{aligned}\hat{U}(t,t_0) &= 1 + \sum_{n=1}^{\infty}\frac{(-\mathrm{i})^n}{n!}\int_{t_0}^{t}\mathrm{d}^4x_n\ldots\int_{t_0}^{t}\mathrm{d}^4x_1\, T_{\mathrm{D}}\Big[\hat{\mathcal{H}}'_{\mathrm{I}}(x_n)\ldots\hat{\mathcal{H}}'_{\mathrm{I}}(x_1)\Big] \\ &= T_{\mathrm{D}}\,\exp\Big[-\mathrm{i}\int_{t_0}^{t}\mathrm{d}^4x\,\hat{\mathcal{H}}'_{\mathrm{I}}(x)\Big],\end{aligned} \tag{87}$$

EvolOpExp

where the space integration is performed over all space and the time integration as indicated.

3.3 Adiabatic damping. The Gell-Mann–Low relation

sec:GML

3.3.1 Nondegenerate case

sec:GMLND

In time-dependent perturbation theory for bound-state problems an '*adiabatic damping factor*' is normally added to the perturbation,

$$\hat{H}'_{\mathrm{I}}(t) \to \hat{H}'_{\mathrm{I}}(t,\gamma) = \hat{H}'_{\mathrm{I}}(t)\,\mathrm{e}^{-\gamma|t|}, \tag{88}$$

Damping

where γ is a small, positive number. We assume that the damping is the only time dependence of the perturbation in the Schrödinger picture. With the damping, the time-dependent Schrödinger equation (SchrTD 81) is still valid, but there are no stationary solutions for finite γ. In order to return to the original problem, the damping factor is adiabatically 'switched off' at the end of the calculation, and we shall now study this limiting process.

We consider first the case with a single target function, which in the IP evolves according to (UDef 84)

$$\Big|\Psi_{\mathrm{I}\gamma}(t)\Big\rangle = \hat{U}_\gamma(t,t_0)\,\Big|\Psi_{\mathrm{I}\gamma}(t_0)\Big\rangle. \tag{89}$$

EvolvDamp

The evolution operator satisfies now the equation (85) with the damped perturbation,

$$\mathrm{i}\frac{\partial}{\partial t}\hat{U}_\gamma(t,t_0) = \hat{H}'_{\mathrm{I}}(t)\,\mathrm{e}^{-\mathrm{i}\gamma|t|}\,\hat{U}_\gamma(t,t_0), \tag{90}$$

UEqDamp

which leads to the expansion (86)

$$\hat{U}_\gamma(t,t_0) = 1 + \sum_{n=1}^{\infty}\frac{(-\mathrm{i})^n}{n!}\int_{t_0}^{t}\mathrm{d}t_n\ldots\int_{t_0}^{t}\mathrm{d}t_1\,T_{\mathrm{D}}\Big[\hat{H}'_{\mathrm{I}}(t_n)\ldots\hat{H}'_{\mathrm{I}}(t_1)\Big]\mathrm{e}^{-\gamma(|t_1|+|t_2|\ldots+|t_n|)}. \tag{91}$$

UDamp

The damped perturbation (88) vanishes, when $\gamma t \to \pm\infty$, and the perturbed (target) wavefunction approaches in these limits an eigenfunction of $\hat{H}_0$,

$$\Big|\Psi_{\mathrm{I}\gamma}(t)\Big\rangle \Rightarrow \Big|\Psi_0\Big\rangle. \tag{92}$$

UnpertWF

We can expect this function to be identical to the unperturbed model function of time-independent MBPT,

$$\hat{H}_0\Big|\Psi_0\Big\rangle = E_0\Big|\Psi_0\Big\rangle. \tag{93}$$

E0

The target function in the IP at arbitrary time for finite γ is then according to (89)

$$\Big|\Psi_{\mathrm{I}\gamma}(t)\Big\rangle = \frac{\hat{U}_\gamma(t,-\infty)\Big|\Psi_0\Big\rangle}{\langle\Psi_0|\hat{U}_\gamma(t,-\infty)\,|\Psi_0\rangle}, \tag{94}$$

WavefIN

using intermediate normalization (17). This function will depend on the parameter γ, but we shall show that $|\Psi_{\mathrm{I}\gamma}(0)\rangle$ satisfies the time-independent Schrödinger equation in the limit $\gamma \to 0$. Note that it is not possible to let $\gamma \to 0$ in the unnormalized form (89), since the evolution operator will then be singular. In order to study the limit $\gamma \to 0$, we shall follow essentially the treatment of [?] (see also (?, p. 61), (?, p. 336)).

We consider one term in the expansion (91)

$$\hat{U}^{(n)}_\gamma(t,-\infty) = \frac{(-\mathrm{i})^n}{n!}\int_{-\infty}^{t}\mathrm{d}t_n\int_{-\infty}^{t}\mathrm{d}t_{n-1}\cdots T_{\mathrm{D}}\Big[\hat{H}'_{\mathrm{I}}(t_n)\hat{H}'_{\mathrm{I}}(t_{n-1})\cdots\Big]\,\mathrm{e}^{\gamma(t_1+t_2\ldots+t_n)}. \tag{95}$$

Un

(As long as t does not approach $+\infty$, we can leave out the absolute signs in the damping factor.) Using the identity

$$[H_0, ABC\cdots] = [H_0,A]\,BC\cdots + A[H_0,B]\,C\cdots + \cdots$$

we obtain

$$\Big[\hat{H}_0, \hat{H}'_{\mathrm{I}}(t_n)\hat{H}'_{\mathrm{I}}(t_{n-1})\cdots\Big] = -\mathrm{i}\Big(\frac{\partial}{\partial t_n} + \frac{\partial}{\partial t_{n-1}} + \cdots\Big)\,\hat{H}'_{\mathrm{I}}(t_n)\hat{H}'_{\mathrm{I}}(t_{n-1})\cdots. \tag{96}$$

HOComm

(We note that $\hat{H}'$ is assumed to be time independent in the SP.) This gives

$$\Big[\hat{H}_0, \hat{U}_\gamma^{(n)}(t,-\infty)\Big] = \frac{(-\mathrm{i})^{n+1}}{n!}\int_{-\infty}^{t}\mathrm{d}t_n\int_{-\infty}^{t}\mathrm{d}t_{n-1}\cdots$$
$$\times\, T_D\Big[\Big(\frac{\partial}{\partial t_n}+\frac{\partial}{\partial t_{n-1}}+\cdots\Big)\hat{H}'_{\mathrm{I}}(t_n)\hat{H}'_{\mathrm{I}}(t_{n-1})\cdots\Big]\,\mathrm{e}^{\gamma(t_1+t_2\ldots+t_n)}.$$

When integrating by parts, each term yields the same contribution, and the result can be expressed

$$\Big[\hat{H}_0, \hat{U}_\gamma^{(n)}(t,-\infty)\Big] = -\hat{H}'_{\mathrm{I}}(t)\,\hat{U}_\gamma^{(n-1)}(t,-\infty) + \mathrm{i}n\gamma\,\hat{U}_\gamma^{(n)}(t,-\infty). \tag{97}$$ UComm2

Introducing an order parameter, λ,

$$\hat{H} = \hat{H}_0 + \lambda\,\hat{H}'_{\mathrm{I}}(t), \tag{98}$$ HLambda

the result can be expressed

$$\boxed{\Big[\hat{H}_0, \hat{U}_\gamma(t,-\infty)\Big] = -\hat{H}'_{\mathrm{I}}(t)\,\hat{U}_\gamma(t,-\infty) + \mathrm{i}\gamma\lambda\,\frac{\partial}{\partial\lambda}\hat{U}_\gamma(t,-\infty).} \tag{99}$$ UComm3

By operating with this commutator on the unperturbed function (92), we obtain for $t=0$

$$\Big(\hat{H}_0 - E_0 + \hat{H}'\Big)\,\hat{U}_\gamma(0,-\infty)\,\Big|\Psi_0\Big\rangle = \mathrm{i}\gamma\lambda\,\frac{\partial}{\partial\lambda}\hat{U}_\gamma(0,-\infty)\,\Big|\Psi_0\Big\rangle, \tag{100}$$ UComm4

where $\hat{H}' = \hat{H}'_{\mathrm{I}}(0)$, and using (94) this yields

$$\Big(\hat{H}_0 + \hat{H}' - E_0\Big)\,\Big|\Psi_\gamma\Big\rangle = \mathrm{i}\gamma\lambda\,\frac{\frac{\partial}{\partial\lambda}\hat{U}_\gamma(0,-\infty)|\Psi_0\rangle}{\langle\Psi_0|\hat{U}_\gamma(0,-\infty)|\Psi_0\rangle}, \tag{101}$$ EigenvEq

where $\Big|\Psi_\gamma\Big\rangle = \Big|\Psi_{\mathrm{I}\gamma}(0)\Big\rangle$. The r.h.s. is here

$$\mathrm{i}\gamma\lambda\,\frac{\frac{\partial}{\partial\lambda}\hat{U}_\gamma(0,-\infty)|\Psi_0\rangle}{\langle\Psi_0|\hat{U}_\gamma(0,-\infty)|\Psi_0\rangle} = \Delta E_\gamma\,\Big|\Psi_\gamma\Big\rangle + \mathrm{i}\gamma\lambda\,\frac{\partial}{\partial\lambda}\Big|\Psi_\gamma\Big\rangle$$

with

$$\Delta E_\gamma = \mathrm{i}\gamma\lambda\,\frac{\langle\Psi_0|\frac{\partial}{\partial\lambda}\hat{U}_\gamma(0,-\infty)|\Psi_0\rangle}{\langle\Psi_0|\hat{U}_\gamma(0,-\infty)|\Psi_0\rangle}, \tag{102}$$ DeltaE

which yields

$$\Big(\hat{H}_0 + \hat{H}' - E_0 - \Delta E_\gamma\Big)\,\Big|\Psi_\gamma\Big\rangle = \mathrm{i}\gamma\lambda\,\frac{\partial}{\partial\lambda}\Big|\Psi_\gamma\Big\rangle. \tag{103}$$ EigenvEq2

Provided that the perturbation expansion of $|\Psi_\gamma\rangle$ converges, the r.h.s. will

vanish as $\gamma \to 0$. Then

$$\boxed{\Big|\Psi\Big\rangle = \lim_{\gamma\to 0}\Big|\Psi_\gamma\Big\rangle = \lim_{\gamma\to 0}\frac{\hat{U}_\gamma(0,-\infty)\Big|\Psi_0\Big\rangle}{\langle\Psi_0|\hat{U}_\gamma(0,-\infty)\,|\Psi_0\rangle}} \qquad (104)$$ GML

will be an *eigenfunction of the original, undamped Hamiltonian* of the system and satisfy the time-independent Schrödinger equation (3)

$$\Big(\hat{H}_0+\hat{H}'\Big)\Big|\Psi\Big\rangle = E\Big|\Psi\Big\rangle \qquad (105)$$ SchrEqn

with the energy eigenvalue $E = E_0 + \Delta E$. The *energy shift* due to the perturbation is given by

$$\boxed{\Delta E = \lim_{\gamma\to 0}\mathrm{i}\gamma\lambda\,\frac{\langle\Psi_0|\frac{\partial}{\partial\lambda}\hat{U}_\gamma(0,-\infty)|\Psi_0\rangle}{\langle\Psi_0|\hat{U}_\gamma(0,-\infty)|\Psi_0\rangle}.} \qquad (106)$$ GMLShift

The relations (104) and (106) represent the *Gell-Mann–Low theorem*, which is the basis for time-dependent perturbation theory.

Generally, the evolution operator contains *singularities*, due to *unlinked terms* – in the graphical representation corresponding to *unlinked diagrams*. These terms do not appear in the *ratios* (104) and (106), which are *regular*. This is the *linked-diagram theorem*, mentioned in section 2.4, and first shown by [?], using time-dependent perturbation theory. Goldstone thereby showed that the limits (104) and (106) do exist and are represented by linked diagrams only. In its original formulation the relation is valid only for a single reference function, Ψ_0, i.e., for a one-dimensional model space, but it can be extended to more general cases, as we shall demonstrate below.

We have assumed here that the perturbation is of general time-dependent form. If it is of the form (68), then the photon number is not a constant of the motion. This implies that the eigenfunctions are superpositions of functions with different photon numbers. This is necessary in order to be able to handle time-dependent interactions between the electrons, which are formed by contracting the field-theoretical perturbation at different times. We shall discuss that further in the following chapters.

In the nondegenerate case, singularities of the evolution operator appear when the initial or reference state appears as an intermediate state. The singularities are eliminated in the Gell-Mann–Low expressions, such as (106). When the perturbation is *time or energy dependent*, the elimination of such a contribution is incomplete, and there is a *residual contribution*, usually known as the *reference-state contribution*. In the more general situation we shall consider below, we shall refer to this contribution as the *Model-Space Contribution*

(MSC). To determine this contribution, the limiting process $\gamma \to 0$ has to be carried out.

GenGellMann

3.3.2 Extended model space. The generalized Gell-Mann–Low relation

The time-dependent MBPT was in the 1960's and 1970's further developed by several groups [Mo63,KB66,BK67,To69,JM70,DOR70,KLR71] (????????), mainly in connection with nuclear calculations. We shall summarize and extend this treatment here. In particular, we shall prove a generalization of the Gell-Mann–Low theorem for an arbitrary model space.

Following [To69] (?), we choose the parent states to be the limits of the target states (89) for finite γ as $t \to -\infty$,

$$\Big|\Psi^\alpha\Big\rangle_{\mathrm{I}\gamma} \Rightarrow \Big|\Phi^\alpha\Big\rangle \qquad (\alpha = 1, 2 \cdots d). \tag{107}$$

ParentTolm

The parent functions are then eigenfunctions of H_0,

$$\hat{H}_0 \Big|\Phi^\alpha\Big\rangle = E_0^\alpha \Big|\Phi^\alpha\Big\rangle, \tag{108}$$

ParentEigenv

but we cannot say which eigenvalue a specific target state will converge to in the general case.

In analogy with (94) we construct the states

$$\Big|\Psi_\gamma^\alpha\Big\rangle = \frac{N^\alpha \hat{U}_\gamma(0,-\infty)\Big|\Phi^\alpha\Big\rangle}{\langle\Phi^\alpha|\hat{U}_\gamma(0,-\infty)|\Phi^\alpha\rangle} = N^\alpha \Big|\widetilde{\Psi}_\gamma^\alpha\Big\rangle. \tag{109}$$

WavefIN2

The states $\Big|\widetilde{\Psi}_\gamma^\alpha\Big\rangle$ are normalized to the parent states, $\langle\Phi^\alpha|\widetilde{\Psi}_\gamma^\alpha\rangle = 1$, and hence regular as $\gamma \to 0$. In the intermediate normalization (16) we normalize against the projection of the target functions on the model space, $\Big|\Psi_0^\alpha\Big\rangle = P\Big|\Psi^\alpha\Big\rangle$, and then an additional normalization constant, N^α, is generally needed. Below we shall show that

$$\boxed{\Big|\Psi^\alpha\Big\rangle = \lim_{\gamma\to 0} \frac{N^\alpha\, \hat{U}_\gamma(0,-\infty)\Big|\Phi^\alpha\Big\rangle}{\langle\Phi^\alpha|\hat{U}_\gamma(0,-\infty)|\Phi^\alpha\rangle}} \tag{110}$$

GenGML

is an eigenfunction of the original Hamiltonian of the system for all values of α,

$$\Big(\hat{H}_0 + \hat{H}'\Big)\Big|\Psi^\alpha\Big\rangle = E^\alpha\Big|\Psi^\alpha\Big\rangle \qquad (\alpha = 1, 2, \cdots d). \tag{111}$$

SEGML2

This is a *generalization of the Gell-Mann–Low relation* (104), and it holds for an arbitrary model space, i.e., also when this is quasi-degenerate with several energy levels.

In the one-dimensional model space, singularities appear in $\hat{U}$ for unlinked terms. In the general multi-dimensional case, singularities can appear also

for linked diagrams, which have an *intermediate state in the model space*. We refer to such diagrams as *reducible* [9] . The remaining *irreducible* diagrams are regular. In addition, so-called *quasi-singularities* can appear – i.e., very large, but finite, contributions – when an intermediate state is *quasi-degenerate* with the initial state. All singularities and quasi-singularities are eliminated in the ratio (110) – in analogy with the original Gell-Mann–Low theorem. The elimination of these quasi-singularities represent the major advantage of the procedure using an extended model space. In the next section we shall see that this procedure can be applied also in QED, thus eliminating a major shortcoming of the standard S-matrix formulation.

In order to show that the functions (110) are eigenfunctions of the original Hamiltonian, we shall mainly follow the procedure used in the previous case. We start from the identity (99) at $t = 0$

$$\left(\hat{H}_0+\hat{H}'\right)\frac{\hat{U}_\gamma(0,-\infty)\left|\Phi^\alpha\right\rangle}{\langle\Phi^\alpha|\hat{U}_\gamma(0,-\infty)|\Phi^\alpha\rangle}=\frac{\hat{U}_\gamma(0,-\infty)\hat{H}_0\left|\Phi^\alpha\right\rangle}{\langle\Phi^\alpha|\hat{U}_\gamma(0,-\infty)|\Phi^\alpha\rangle}+\mathrm{i}\gamma\lambda\,\frac{\frac{\partial}{\partial\lambda}\hat{U}_\gamma(0,-\infty)\left|\Phi^\alpha\right\rangle}{\langle\Phi^\alpha|\hat{U}_\gamma(0,-\infty)|\Phi^\alpha\rangle}, \tag{112}$$

UComm5

and in analogy with (103), using (109), we obtain

$$\left(\hat{H}_0+\hat{H}'-\mathrm{i}\gamma\lambda\,\frac{\langle\Phi^\alpha|\frac{\partial}{\partial\lambda}\hat{U}_\gamma(0,-\infty)|\Phi^\alpha\rangle}{\langle\Phi^\alpha|\hat{U}_\gamma(0,-\infty)|\Phi^\alpha\rangle}\right)\left|\Psi^\alpha_\gamma\right\rangle=\frac{N^\alpha\,\hat{U}_\gamma(0,-\infty)\hat{H}_0\left|\Phi^\alpha\right\rangle}{\langle\Phi^\alpha|\hat{U}_\gamma(0,-\infty)|\Phi^\alpha\rangle}+\mathrm{i}\gamma\lambda\frac{\partial}{\partial\lambda}\left|\Psi^\alpha_\gamma\right\rangle. \tag{113}$$

Since the parent functions are assumed to be eigenfunctions of $\hat{H}_0$ (108), we see that the first term on the r.h.s. becomes $E_0^\alpha\left|\Psi^\alpha_\gamma\right\rangle$, and we retrieve the relation (103) for a general model space,

$$\left(\hat{H}_0+\hat{H}'-E_0^\alpha-\Delta E_\gamma^\alpha\right)\left|\Psi^\alpha_\gamma\right\rangle=\mathrm{i}\gamma\lambda\frac{\partial}{\partial\lambda}\left|\Psi^\alpha_\gamma\right\rangle. \tag{114}$$

EigenvEqalpha

As before, we can assume that the second term on the r.h.s. vanishes as $\gamma\to 0$, which demonstrates that the functions (110) are eigenfunctions of the original Hamiltonian. An important observation is here that *a necessary condition* for the wavefunction (110) to satisfy the time-independent Schrödinger equation is that *the parent state is an eigenfunction of* H_0 [10] .

The energy of the target states are given by

$$E^\alpha=\lim_{\gamma\to 0}\left[E_0^\alpha+\mathrm{i}\gamma\lambda\frac{\langle\Phi^\alpha|\frac{\partial}{\partial\lambda}\hat{U}_\gamma(0,-\infty)|\Phi^\alpha\rangle}{\langle\Phi^\alpha|\hat{U}_\gamma(0,-\infty)|\Phi^\alpha\rangle}\right]. \tag{115}$$

Ealpha

[9] See footnote in section 3.4.3.

[10] This observation is in conflict with the assumption of [?], who state that – for the ground state – the parent state can be any state in the model space with nonzero overlap with the final wave function. If the model space contains several energies, the results are conflicting.

This expression is not very useful for evaluating the energy, since the eigenvalue E_0^α of the parent state is generally not known. The procedure is here used mainly to demonstrate that the functions satisfy the Schrödinger equation. Instead we shall derive an expression for the effective Hamiltonian (13), which is the natural tool for a multi-level model space.

3.4 The reduced time-evolution operator

sec:RedEvOp

In order to find more useful expressions for actual evaluations, we introduce a new operator, the *reduced evolution operator*, $\widetilde{U}_\gamma$, by the relation (**?**)

$$\boxed{U_\gamma(t,-\infty)P = P + \widetilde{U}_\gamma(t,-\infty)PU_\gamma(0,-\infty)P.} \qquad (116)$$

Utildet

(We leave out the 'hat' on the evolution operator.) This leads to the expansion

$$U(t)P = P + \widetilde{U}(t)P + \widetilde{U}(t)P\widetilde{U}P + \widetilde{U}(t)P\widetilde{U}P\widetilde{U}P + \cdots,$$

where we temporarily leave out the initial time $t_0 = -\infty$ and the final time $t' = 0$ in the factors $P\widetilde{U}P$ as well as the subscript γ. This can also be expressed

$$\boxed{\widetilde{U}(t)P = U(t)P - P - \widetilde{U}(t)P\widetilde{U}P - \widetilde{U}(t)P\widetilde{U}P\widetilde{U}P - \cdots,} \qquad (117)$$

UtildeExp

which is a very useful expression that we shall use frequently in the following. Expanding this operator perturbatively

$$\widetilde{U}(t) = \widetilde{U}^{(1)}(t) + \widetilde{U}^{(2)}(t) + \widetilde{U}^{(3)}(t) + \cdots,$$

we obtain in the lowest orders

$$\begin{aligned}
&\widetilde{U}^{(1)}(t)P = U^{(1)}P \\
&\widetilde{U}^{(2)}(t)P = U^{(2)}(t)P - U^{(1)}(t)PU^{(1)}P \\
&\widetilde{U}^{(3)}(t)P = U^{(3)}(t)P - \widetilde{U}^{(2)}(t)PU^{(1)}P - U^{(1)}(t)P\widetilde{U}^{(2)}P - U^{(1)}(t)PU^{(1)}PU^{(1)}P.
\end{aligned} \qquad (118)$$

UtildeExp2

These relations will be used below (section 3.4.4) to show that *the 'open' part of the reduced evolution operator is regular* – or, in other words – that *the counterterms* $\widetilde{U}P\widetilde{U}P$, $\widetilde{U}P\widetilde{U}P\widetilde{U}P\cdots$, *eliminate the single, double*$\cdots$ *(quasi)-singularities.*

sec:All orders

We recall that with the field-theoretical perturbation (68), the evolution operator does not conserve the number of photons and therefore operates in the extended Fock space, $\boldsymbol{\mathcal{H}}$ (72). The P operator is the projection operator for the model space, which is a part of the Hilbert space $\mathcal{H}_0$, where the photon

number is conserved. The Q operator is the projection operator for the complementary part of this space (20). We now introduce a *generalized projection operator* $\boldsymbol{Q}$

$$\boldsymbol{Q} = I - P \tag{119}$$

GenQ

for the extended space $\boldsymbol{\mathcal{H}}$, where the number of photons is not necessarily conserved. The general evolution operator can now be expressed

$$\hat{U}_\gamma(0,-\infty)P = P\hat{U}_\gamma(0,-\infty)P + \boldsymbol{Q}\hat{U}_\gamma(0,-\infty)P, \tag{120}$$

Identity

which with (116) leads to the *generalized factorization theorem*,

$$\boxed{\hat{U}_\gamma(0,-\infty)P = \left[1 + \boldsymbol{Q}\tilde{U}(0,-\infty)\right] P\hat{U}_\gamma(0,-\infty)P.} \tag{121}$$

FactTh

We shall demonstrate below that the first factor on the r.h.s. is *regular* in the limit $\gamma \to 0$, and consequently all (quasi)singularities are contained in the second factor. This is a generalization to the more general Fock space (72) of the *factorization theorem*, demonstrated in nuclear theory (????).

The fact that the reduced evolution operator is regular has important implications. This implies that in that part each adiabatic-damping factor γ can be turned off individually, in contrast to the situation with the original Gell-Mann–Low relation, as discussed above. The *sign* of the γ term, though, is normally important, since that determines the position of the pole in the integration process. The model-space contribution is obtained by means of the expansion (118) without the need of any limiting process.

WOEH

3.4.1 Wave operator and effective Hamiltonian

The model states corresponding to the target states (110) are in intermediate normalization given by the projection onto the model space (16),

$$\left|\Psi_0^\alpha\right\rangle = P\left|\Psi^\alpha\right\rangle = \lim_{\gamma\to 0} \frac{N^\alpha P\, U_\gamma(0,-\infty)\left|\Phi^\alpha\right\rangle}{\langle\Phi^\alpha|U_\gamma(0,-\infty)|\Phi^\alpha\rangle}, \tag{122}$$

Psi03

and the wavefunction (110) can then be expressed, using the factorization theorem (121),

$$\boxed{\left|\Psi^\alpha\right\rangle = \left[1 + \boldsymbol{Q}\tilde{U}(0,-\infty)\right]\left|\Psi_0^\alpha\right\rangle.} \tag{123}$$

WavefTD

This leads to a *generalized wave operator* (12)

$$\boxed{\boldsymbol{\Omega} = 1 + \boldsymbol{Q}\tilde{U}(0,-\infty),} \tag{124}$$

WaveOpTD

operating in the extended space $\boldsymbol{\mathcal{H}}$. In a 'restricted' Hilbert space $\mathcal{H}_0$, where the number of photons is conserved, this operator is identical to the standard MBPT wave operator (12). WaveUp

The *effective Hamiltonian* is defined by (13) EffHam

$$\hat{H}_{\text{eff}} \left|\Psi_0^\alpha\right\rangle = E^\alpha \left|\Psi_0^\alpha\right\rangle, \tag{125}$$ EffHam0

which in the extended space leads to

$$\hat{H}_{\text{eff}} = P\hat{H}\boldsymbol{\Omega}P = P\hat{H}\Big[1 + \boldsymbol{Q}\widetilde{U}(0,-\infty)\Big]P \tag{126}$$ EffHam1

and to the effective interaction (18) EffInt

$$\hat{H}'_{\text{eff}} = PH'\boldsymbol{\Omega}P = P\hat{H}'\Big[1 + \boldsymbol{Q}\widetilde{U}(0,-\infty)\Big]P. \tag{127}$$ EffInt1

$\hat{H}$ and $\hat{H}'$ are the Hamiltonian and the perturbation, respectively, at $t = 0$.

An alternative form of the effective interaction can be obtained in the following way. From (85) UEq we have

$$\mathrm{i}\frac{\partial}{\partial t}U_\gamma(t,-\infty)P = \hat{H}'(t)\,U_\gamma(t,-\infty)P, \tag{128}$$ ddtU

and using the definition (116) Utildet and the factorization theorem (121) FactTh this yields for $t = 0$

$$\left[\mathrm{i}\frac{\partial}{\partial t}\widetilde{U}_\gamma(t,-\infty)\right]_{t=0} PU_\gamma(0,-\infty)P = \hat{H}'\left[1+\boldsymbol{Q}\widetilde{U}(0,-\infty)\right]PU_\gamma(0,-\infty)P \tag{129}$$

or

$$\boxed{\hat{H}'_{\text{eff}} = P\left[\mathrm{i}\frac{\partial}{\partial t}\widetilde{U}(t,-\infty)\right]_{t=0} P.} \tag{130}$$ EffInt2

This is a generalization of the energy-shift formula given by Jones and Mohling (?), JM70 and it is the form we shall mainly use in the following.

The form (130) EffInt2 of the effective interaction can also be derived in an alternative way. We start now from the time-dependent Schrödinger equation (1) TDSE at $t = 0$,

$$\left[\mathrm{i}\frac{\partial}{\partial t}\left|\Psi_{\text{S}}^\alpha(x)\right\rangle\right]_{t=0} = \hat{H}\left|\Psi^\alpha\right\rangle. \tag{131}$$ TDSE0

The eigenfunctions of the system at $t = 0$, $\left|\Psi^\alpha\right\rangle$, are given by the generalized Gell-Mann–Low relation (110) GenGML and satisfy the time-independent Schrödinger equation (111). SEGML2 This gives

$$\left[\mathrm{i}\frac{\partial}{\partial t}\left|\Psi_{\text{S}}^\alpha(x)\right\rangle\right]_{t=0} = E^\alpha\left|\Psi^\alpha\right\rangle \tag{132}$$ TDSE1

and
$$P\Big[\mathrm{i}\frac{\partial}{\partial t}\Big|\Psi_{\rm S}^{\alpha}(x)\Big\rangle\Big]_{t=0} = E^{\alpha}\Big|\Psi_0^{\alpha}\Big\rangle, \tag{133}$$
PTDSE1

where $P\Big|\Psi^{\alpha}\Big\rangle = \Big|\Psi_0^{\alpha}\Big\rangle$ is the model function (122). With the relation (31) this leads to

$$P\hat{H}_0\Big|\Psi^{\alpha}\Big\rangle + P\Big[\mathrm{i}\frac{\partial}{\partial t}\Big|\Psi^{\alpha}\Big\rangle\Big]_{t=0} = E^{\alpha}\Big|\Psi_0^{\alpha}\Big\rangle, \tag{134}$$
TDSE3

where $\Big|\Psi^{\alpha}\Big\rangle$ is the wavefunction in the IP.

From the Gell-Mann–Low relation (110) we can also obtain the wave function in the interaction picture at arbitrary (finite) time

$$\Big|\Psi^{\alpha}(t)\Big\rangle = \lim_{\gamma\to 0}\frac{N^{\alpha}U_{\gamma}(t,-\infty)\Big|\Phi^{\alpha}\Big\rangle}{\langle\Phi^{\alpha}|U_{\gamma}(0,-\infty)|\Phi^{\alpha}\rangle}, \tag{135}$$
Psit

and using the relations (122) and (116) we find that

$$\Big[\mathrm{i}\frac{\partial}{\partial t}\Big|\Psi^{\alpha}(t)\Big\rangle\Big]_{t=0} = \Big[\mathrm{i}\frac{\partial}{\partial t}\widetilde{U}(t,-\infty)\Big]_{t=0}\Big|\Psi_0^{\alpha}\Big\rangle. \tag{136}$$

This leads with the relation (134) to the secular equation

$$\hat{H}_{\rm eff}\Big|\Psi_0^{\alpha}\Big\rangle = E^{\alpha}\Big|\Psi_0^{\alpha}\Big\rangle,$$

where the operator

$$\hat{H}_{\rm eff} = P\hat{H}_0P + P\Big[\mathrm{i}\frac{\partial}{\partial t}\widetilde{U}(t,-\infty)\Big]_{t=0}P \tag{137}$$
EffHamTD

is the *effective Hamiltonian* (13) and the second term is the effective interaction (130).

We recall that we have assumed here that the perturbations can be of general time-dependent form. All forms of the effective Hamiltonian/interaction given here are therefore valid for interaction between the electrons that are time- or energy dependent, including the field-theoretical perturbation (68).

c:TimeIndInt

3.4.2 Time-independent interactions

We shall now apply the formalism presented here to atomic systems with interactions that are *time independent* in the Schödinger picture, like the instantaneous Coulomb interaction. Time- or energy dependent interactions will be treated in the following section.

When using the field-theoretical perturbation, the time-independent interactions between the electrons correspond to *contractions at equal time*. Therefore, only perturbations of even order of the evolution operator will appear.

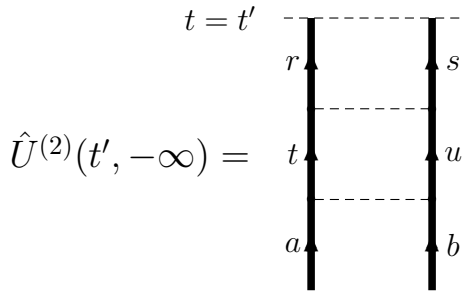

Fig. 4. The second-order evolution-operator diagram for the Coulomb interaction between two electrons. Fig:ElSecOrd

We can now work in the restricted Hilbert space $\mathcal{H}_0$ (72) and replace the general projection operator $\boldsymbol{Q}$ by the traditional operator Q. The wave operator then becomes

$$\Omega = 1 + Q\widetilde{U}(0, -\infty) \tag{138}$$ WaveOpTind

and the effective interaction

$$\hat{H}'_{\text{eff}} = P\hat{H}'\,\Omega P = P\hat{H}'\left[1 + Q\widetilde{U}(0, -\infty)\right]P. \tag{139}$$ EffIntTind

As a first illustration of the evolution-operator technique, we consider the second-order Coulomb interaction between two electrons illustrated in Fig. 4. The evolution operator (87) can then be expressed

$$U^{(2)}(t', -\infty) = -\int_{-\infty}^{t'} \mathrm{d}t_2 \int_{-\infty}^{t_2} \mathrm{d}t_1\, V_{\mathrm{I}}(t_2)\, V_{\mathrm{I}}(t_1)\, e^{\gamma(t_1+t_2)}, \tag{140}$$ U2El

where V_{I} is the Coulomb interaction in the interaction picture,

$$V_{\mathrm{I}}(t) = e^{\mathrm{i}H_0 t} V e^{-\mathrm{i}H_0 t}, \tag{141}$$ VI

and $V = \frac{e^2}{4\pi\, r_{12}}$ is the time-independent interaction in the Schrödinger picture. This gives

$$\langle rs|U^{(2)}(t', -\infty)|ab\rangle = -\int_{-\infty}^{t'} \mathrm{d}t_2 \int_{-\infty}^{t_2} \mathrm{d}t_1\, \langle rs|V_{\mathrm{I}}(t_2)|tu\rangle\, \langle tu|V_{\mathrm{I}}(t_1)|ab\rangle\, e^{\gamma(t_1+t_2)} \tag{142}$$ U2El2

after inserting a complete set of intermediate states [11], which leads to the time integral

[11] As before, we employ the *summation convention* with implicit summation over repeated indices that do not appear on the l.h.s.

$$\int_{-\infty}^{t'} \mathrm{d}t_2\, e^{-\mathrm{i}t_2(\varepsilon_t+\varepsilon_u-\varepsilon_r-\varepsilon_s+\mathrm{i}\gamma)} \int_{-\infty}^{t_2} \mathrm{d}t_1\, e^{-\mathrm{i}t_1(\varepsilon_a+\varepsilon_b-\varepsilon_t-\varepsilon_u+\mathrm{i}\gamma)}$$
$$= -\frac{e^{-\mathrm{i}t'(\varepsilon_a+\varepsilon_b-\varepsilon_r-\varepsilon_s+2\mathrm{i}\gamma)}}{(\varepsilon_a+\varepsilon_b-\varepsilon_r-\varepsilon_s+2\mathrm{i}\gamma)(\varepsilon_a+\varepsilon_b-\varepsilon_t-\varepsilon_u+\mathrm{i}\gamma)}.$$

The result then becomes

$$\langle rs|U^{(2)}(t',-\infty)|ab\rangle = \frac{\langle rs|V|tu\rangle\langle tu|V|ab\rangle}{(E_{\mathrm{in}}-E_{\mathrm{out}}+2\mathrm{i}\gamma)(E_{\mathrm{in}}-E_{\mathrm{int}}+\mathrm{i}\gamma)}\, e^{-\mathrm{i}t'(E_{\mathrm{in}}-E_{\mathrm{out}}+2\mathrm{i}\gamma)}, \tag{143}$$

U2El3

using the notations $E_{\mathrm{in}} = \varepsilon_a + \varepsilon_b$, $E_{\mathrm{out}} = \varepsilon_r + \varepsilon_s$ and $E_{\mathrm{int}} = \varepsilon_t + \varepsilon_u$. In the limit $\gamma \to 0$, this becomes (quasi)singular, when $E_{\mathrm{int}} \approx E_{\mathrm{in}}$ or $E_{\mathrm{out}} \approx E_{\mathrm{in}}$. In the former case we include the quasi-degenerate state(s) in the model space. From the expansion (118) we then have

UtildeExp2

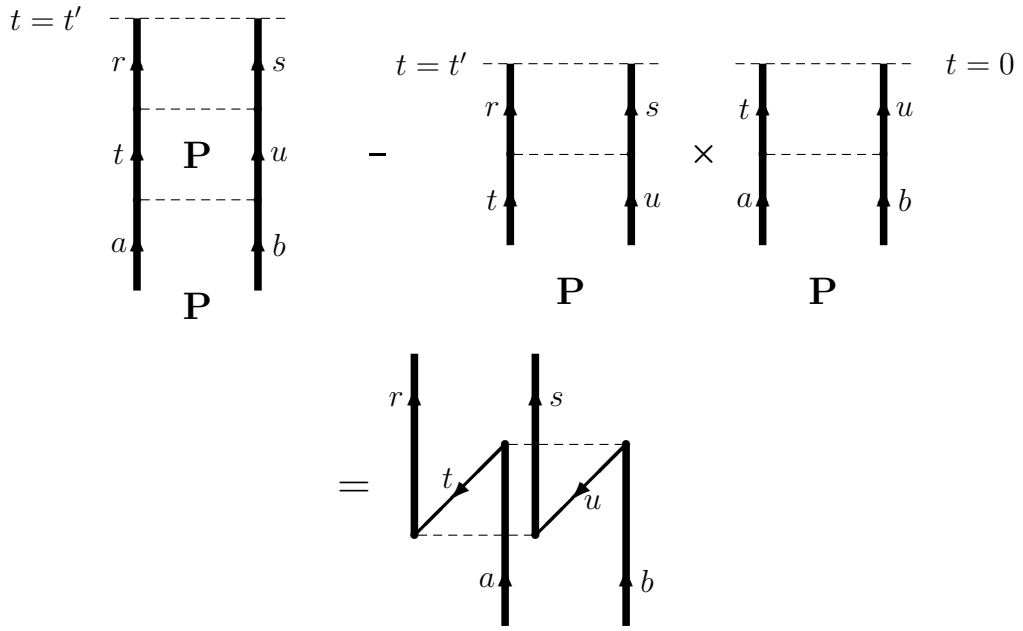

Fig. 5. For time-independent interactions the open, reducible two-photon-photon ladder diagram with the corresponding counterterm corresponds to a *folded* diagram (147) in standard MBPT, c.f. Fig. 1. The intermediate state $|tu\rangle$ lies in the model space.

Folded

Fig:Omega12

Fig:FoldDiag

$$\widetilde{U}^{(2)}P = U^{(2)}P - U^{(1)}PU^{(1)}P, \tag{144}$$

Utilde4

where the second term is the counterterm. This case is illustrated in Fig. 5. This is a model-space contribution with the intermediate state in the model space, and such a diagram is also referred to as *reducible*.

Fig:FoldDiag

In the same way as before we obtain for the counterterm

$$\langle rs|U^{(1)}PU^{(1)}|ab\rangle = -\int_{-\infty}^{t'} \mathrm{d}t_2 \int_{-\infty}^{0} \mathrm{d}t_1 \, \langle rs|V_{\mathrm{I}}(t_2)\,|tu\rangle \, \langle tu|V_{\mathrm{I}}(t_1)|ab\rangle \, e^{\gamma(t_1+t_2)}, \tag{145}$$

ElCounter

which yields

$$\langle rs|U^{(1)}PU^{(1)}|ab\rangle = \frac{\langle rs|V|tu\rangle\langle tu|V|ab\rangle}{(E_{\mathrm{int}} - E_{\mathrm{out}} + \mathrm{i}\gamma)(E_{\mathrm{in}} - E_{\mathrm{int}} + \mathrm{i}\gamma)} \, e^{-\mathrm{i}t'(E_{\mathrm{int}} - E_{\mathrm{out}} + \mathrm{i}\gamma)}. \tag{146}$$

ElCounter2

Subtracting this from the main term (143), gives for the reducible or MSC part of evolution operator $\widetilde{U}^{(2)}$ at time $t' = 0$

$$\langle rs|\widetilde{U}^{(2)}(0,-\infty)|ab\rangle_{\mathrm{Red}} = -\frac{\langle rs|V|tu\rangle\langle tu|V|ab\rangle}{(E_{\mathrm{in}} - E_{\mathrm{out}} + 2\mathrm{i}\gamma)(E_{\mathrm{int}} - E_{\mathrm{out}} + \mathrm{i}\gamma)}. \tag{147}$$

Folded

When the outgoing state lies in the Q space, this is according to the definition (123) a contribution to the wave operator. We see that the (quasi)singularity for $E_{\mathrm{int}} \approx E_{\mathrm{in}}$ is here eliminated. This model-space contribution is identical to the *folded* diagram obtained in time-independent MBPT (Fig. 1, Eq. (44)).

The effective interaction (139) is in second order

$$H'^{(2)}_{\mathrm{eff}} = P\hat{H}'_{\mathrm{I}}(0)\, QU^{(1)}(0,-\infty)P, \tag{148}$$

Heff2

and this yields for the example considered here

$$\langle rs|H'^{(2)}_{\mathrm{eff}}|ab\rangle = \frac{\langle rs|V|tu\rangle\langle tu|V|ab\rangle}{E_{\mathrm{in}} - E_{\mathrm{int}}}. \tag{149}$$

Heff2a

The intermediate state is here confined to the Q space, and there is no (quasi)singularity and no MSC or folded diagram in the second-order effective Hamiltonian. In third order we have

$$H'^{(3)}_{\mathrm{eff}} = PH'\, Q\widetilde{U}^{(2)}(0,-\infty)P, \tag{150}$$

Heff3

and here there is a contribution from the folded diagram (147) in $\widetilde{U}^{(2)}$.

We have now shown that the reducible part of $Q\widetilde{U}^{(2)}$ is regular, and since the irreducible part is always regular, it follows that $Q\widetilde{U}^{(2)}$ is *completely regular for time-independent interactions*. We shall generalize this proof to higher orders in the next section in connection with time-dependent interactions.

c:TimeDepInt

3.4.3 Time-dependent interactions

We have seen that when the interactions between the electrons are time independent, there is a model-space contribution to the effective interaction and

the wave operator, normally represented by so-called folded diagrams, which appear in the energy and effective interaction of third and higher orders. We shall now consider *time or energy dependent* interactions and show that this leads to an additional form of MSC, appearing also in the second-order energy or effective interaction.

As an illustration we consider the second-order diagram shown in Fig. 6. We assume that the interaction is of the form Fig:SecOrdTD

$$V(t_2 - t_1) = \int \frac{\mathrm{d}z}{2\pi}\, V(z)\, e^{-\mathrm{i}z(t_2-t_1)}, \tag{151}$$ VTD

where $V(z)$ is the Fourier transform and z is the energy parameter. In the interaction picture this becomes

$$V_{\mathrm{I}}(t_2 - t_1) = \int \frac{\mathrm{d}z}{2\pi}\, V(z)\Big(e^{\mathrm{i}H_0 t_2}\, e^{-\mathrm{i}zt_2}\, e^{-\mathrm{i}H_0 t_2}\Big)\Big(e^{\mathrm{i}H_0 t_1}\, e^{\mathrm{i}zt_1}\, e^{-\mathrm{i}H_0 t_1}\Big). \tag{152}$$ VTDIP

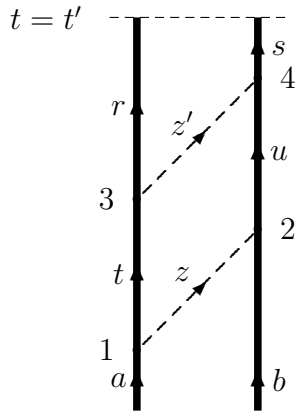

Fig. 6. Second-order diagram with time-dependent interactions Fig:SecOrdTD

We assume the time orderings to be $t' > t_3 > t_1$ and $t' > t_4 > t_2$, and the matrix element of the evolution operator, corresponding to the time-independent result (142), is then U2EI2

$$\langle rs|U^{(2)}(t', -\infty)|ab\rangle = \int_{-\infty}^{t'} \mathrm{d}t_4 \int_{-\infty}^{t_4} \mathrm{d}t_2 \int_{-\infty}^{t'} \mathrm{d}t_3 \int_{-\infty}^{t_3} \mathrm{d}t_1\, \langle rs|V_{\mathrm{I}}(t_4 - t_3)|tu\rangle\, \langle tu|V_{\mathrm{I}}(t_2 - t_1)|ab\rangle. \tag{153}$$ U2TD

The time dependence is here (in the limit $\gamma \to 0$)

$$e^{\mathrm{i}t_4(\varepsilon_s - \varepsilon_u - z')}\, e^{\mathrm{i}t_3(\varepsilon_r - \varepsilon_t + z')}\, e^{\mathrm{i}t_2(\varepsilon_u - \varepsilon_b - z)}\, e^{\mathrm{i}t_1(\varepsilon_u - \varepsilon_a + z)}$$

or

$$e^{-\mathrm{i}t_4(q' - p' + z')}\, e^{-\mathrm{i}t_3(q - p - z')}\, e^{-\mathrm{i}t_2(p' + z)}\, e^{-\mathrm{i}t_1(p - z)},$$

using the notations $p = \varepsilon_a - \varepsilon_t$, $p' = \varepsilon_b - \varepsilon_u$, $q = \varepsilon_a - \varepsilon_r$, $q' = \varepsilon_b - \varepsilon_s$. The time integrations then yield

$$\frac{e^{-\mathrm{i}t'(q+q')}}{(q'+z+z')(p'+z)(q-z-z')(p-z)}. \tag{154}$$

U2TD2

If the *interactions do not overlap in time*, as in Fig. 6, the diagram is said to be *separable*.[12] We can then have the time orderings $t_4 > t_3 > t_1,\ t_2$, which leads to the integration ordering

$$\int_{-\infty}^{t'} \mathrm{d}t_4 \int_{-\infty}^{t_4} \mathrm{d}t_3 \Big(\int_{-\infty}^{t_3} \mathrm{d}t_2 \int_{-\infty}^{t_2} \mathrm{d}t_1 + \int_{-\infty}^{t_3} \mathrm{d}t_1 \int_{-\infty}^{t_1} \mathrm{d}t_2 \Big). \tag{155}$$

Considering also the time ordering $t_3 > t_4 > t_1,\ t_2$, the integral becomes

$$\frac{e^{-\mathrm{i}t'(q+q')}}{q+q'} \Big(\frac{1}{q+p'-z'} + \frac{1}{q'+p+z'} \Big) \frac{1}{p+p'} \Big(\frac{1}{p-z} + \frac{1}{p'+z} \Big).$$

The matrix element (153) can then be expressed

$$\langle rs|U^{(2)}(t',-\infty)|ab\rangle_{\mathrm{Sep}} = \frac{\langle rs|V(q+p',q'+p)|tu\rangle \, \langle tu|V(p,p')|ab\rangle}{(q+q')(p+p')} \, e^{-\mathrm{i}t'(q+q')}, \tag{156}$$

U2TDSep

where
$$V(A,B) = \int \frac{\mathrm{d}z}{2\pi} V(z) \Big(\frac{1}{A-z} + \frac{1}{B+z} \Big).$$

Using the previous notations (143), this becomes

$$\langle rs|U^{(2)}(t',-\infty)|ab\rangle_{\mathrm{Sep}} = \frac{\langle rs|V(q+p',q'+p)|tu\rangle \, \langle tu|V(p,p')|ab\rangle}{(E_{\mathrm{in}}-E_{\mathrm{out}})(E_{\mathrm{in}}-E_{\mathrm{int}})} e^{-\mathrm{i}t'(E_{\mathrm{in}}-E_{\mathrm{out}})}. \tag{157}$$

U2TDSep2

When $E_{\mathrm{in}} - E_{\mathrm{int}} \approx 0$ we have a (quasi)singularity and a corresponding counterterm in analogy with the previous result (146)

$$\langle rs|U^{(1)}PU^{(1)}|ab\rangle = \frac{\langle rs|V(q-p,q'-p')|tu\rangle \, \langle tu|V(p,p')|ab\rangle}{(E_{\mathrm{int}}-E_{\mathrm{out}})(E_{\mathrm{in}}-E_{\mathrm{int}})} \, e^{-\mathrm{i}t'(E_{\mathrm{int}}-E_{\mathrm{out}})}. \tag{158}$$

ElTDCounter

With the notations

$$V(q+p',q'+p) = V(E_{\mathrm{in}}-\varepsilon_r-\varepsilon_u, E_{\mathrm{in}}-\varepsilon_t-\varepsilon_s) = V_2(E_{\mathrm{in}})$$
$$V(q-p,q'-p') = V(E_{\mathrm{int}}-\varepsilon_r-\varepsilon_u, E_{\mathrm{int}}-\varepsilon_t-\varepsilon_s) = V_2(E_{\mathrm{int}}),$$

[12] A diagram is here said to be *separable*, if it can be separated into two legitimate diagrams by cutting all orbital lines at a certain time. In the older literature (see, for instance, (?)) the term *reducible* was normally used for this type of diagram. We have, however, adopted the terminology developed mainly in recent years, where the term 'reducible' is used for separable diagrams with the intermediate state is in the model space. We have therefore introduced the term *separable* for the wider group in order to avoid confusion (?). *Note that a reducible diagram must always be separable.*

the main 'ladder' term (156) becomes

$$\langle rs|U^{(2)}(t',-\infty)|ab\rangle_{\rm Lad} = \frac{\langle rs|V_2(E_{\rm in})|tu\rangle\,\langle tu|V(p,p')|ab\rangle}{(E_{\rm in}-E_{\rm out})(E_{\rm in}-E_{\rm int})}\,e^{-{\rm i}t'(E_{\rm in}-E_{\rm out})} \quad (159)$$

ElTDSep2

and the counterterm (158)

$$\langle rs|U^{(1)}PU^{(1)}|ab\rangle_{\rm Counter} = \frac{\langle rs|V_2(E_{\rm int})|tu\rangle\,\langle tu|V(p,p')|ab\rangle}{(E_{\rm int}-E_{\rm out})(E_{\rm in}-E_{\rm int})}\,e^{-{\rm i}t'(E_{\rm int}-E_{\rm out})}. \quad (160)$$

ElTDCounter2

Applying the relation (130), the time derivative eliminates the last (leftmost) denominator, and the corresponding *reducible* contribution to the effective interaction becomes

$$\langle rs|H'^{(2)}_{\rm eff}|ab\rangle_{\rm Red} = \frac{\langle rs|V_2(E_{\rm in})-V_2(E_{\rm int})|tu\rangle\,\langle tu|V(p,p')|ab\rangle}{E_{\rm in}-E_{\rm int}}\,. \quad (161)$$

HeffRed

With $\Delta E = E_{\rm in} - E_{\rm int}$ this becomes in the limit $\Delta E \to 0$

$$\boxed{\langle rs|H'^{(2)}_{\rm eff}|ab\rangle_{\rm Red} = \Big\langle rs\Big|\frac{\partial}{\partial E}\big(V_2(E)\big)_{E=E_{\rm in}}\Big|tu\Big\rangle\,\Big\langle tu\Big|V(p,p')\Big|ab\Big\rangle.} \quad (162)$$

MSCdegen

This shows that the (quasi)singularity is eliminated also when the interactions are time dependent, but that *there is an additional finite Model-Space Contribution* also in second order due to the time dependence.

In order to obtain the corresponding contribution to the wave operator (123), ElTDSep2 ElTDCounter2 we set the time $t' = 0$, and the expressions (159) and (160) yield the contribution

$$\frac{\langle rs|V_2(E_{\rm in})|tu\rangle\langle tu|V(p,p')|ab\rangle}{(E_{\rm in}-E_{\rm out})\,\Delta E} - \frac{\langle rs|V_2(E_{\rm in}-\Delta E)|tu\rangle\langle tu|V(p,p')|ab\rangle}{(E_{\rm in}-\Delta E-E_{\rm out})\,\Delta E},$$

which we can write as

$$\begin{aligned}&\frac{1}{\Delta E}\Big[\langle rs|\Omega_2(E_{\rm in})|tu\rangle - \langle rs|\Omega_2(E_{\rm in}-\Delta E)|tu\rangle\Big]\,\langle tu|V(p,p')|ab\rangle\\ &= \Big[\Big\langle rs\Big|\frac{\partial}{\partial E}\big(\Omega_2(E)\big)_{E=E_{\rm in}}\Big|tu\Big\rangle + \cdots\Big]\Big\langle tu\Big|V(p,p')\Big|ab\Big\rangle \quad (163)\end{aligned}$$

MSC2

by including the last denominator in Ω_2. This shows that the (quasi)singularity is eliminated also in the second-order wave operator. The remaining part is the model-space contribution, which in this case contains a folded part, present also for time-independent interactions, as well as an additional part due to the time dependence.

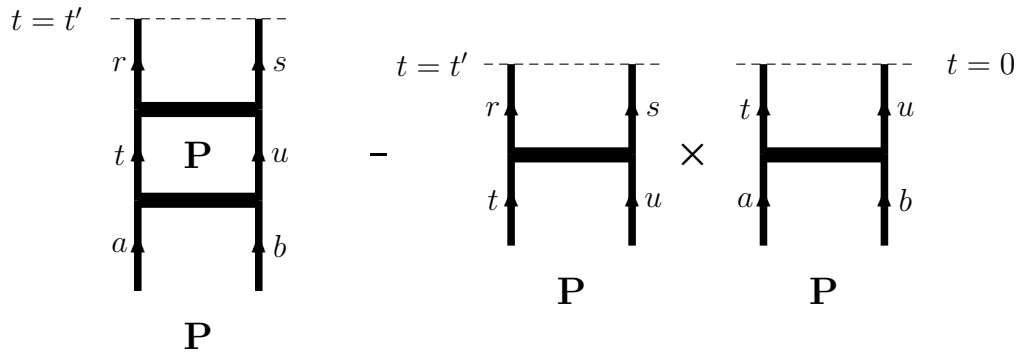

Fig. 7. Reducible diagram of higher order and the corresponding counterterm.

FoldDiag2

c:All orders

3.4.4 Generalization to all orders

The previous treatment can be generalized to higher orders. Let us consider a reducible U diagram of the form $U^{(m)}PU^{(n)}$, as indicated in the left diagram in Fig. 7, where the two parts represent irreducible m- and n-fold interactions, respectively, and the intermediate state lies in the model space. This is regarded as a single diagram of 'ladder' type, which implies that all denominators are evaluated from the bottom. All energies are then functions of the initial energy, $E_{\rm in} = \varepsilon_a + \varepsilon_b$, and we can represent the contribution to the wave operator by

$$\frac{\langle rs|W_2(E_{\rm in})|tu\rangle\langle tu|W_1(E_{\rm in})|ab\rangle}{(E_{\rm in} - E_{\rm out})\,\Delta E} = \frac{\langle rs|\Omega_2(E_{\rm in})|tu\rangle\langle tu|W_1(E_{\rm in})|ab\rangle}{\Delta E}.$$

Here, $E_{\rm out} = \varepsilon_r + \varepsilon_s$ and $\Delta E = \varepsilon_a + \varepsilon_b - \varepsilon_t - \varepsilon_u$, and W_1/W_2 represent the m/n-fold interactions. This diagram is (quasi)singular, due to the denominator ΔE. From the expansion (117) it follows that there is a counterterm of similar form, represented by the second term in the figure. This differs from the leading term only in the fact that the denominators of the left part are evaluated from the intermediate state (t,u) and that the time of the right part is set to zero. The denominators of the left part are the same as in the ladder with $E_{\rm in}$ replaced by $E_{\rm in} - \Delta E$. Assuming as before that the interactions depend on the initial energy, the counterterm can be expressed

$$\frac{\langle rs|W_2(E_{\rm in} - \Delta E)|tu\rangle\langle tu|W_1(E_{\rm in})|ab\rangle}{(E_{\rm in} - \Delta E - E_{\rm out})\,\Delta E} = \frac{\langle rs|\Omega_2(E_{\rm in} - \Delta E)|tu\rangle\langle tu|W_1(E_{\rm in})|ab\rangle}{\Delta E},$$

and the sum of the reducible ladder and the counterterm can be expanded in analogy with the second-order case (163)

$$\left\langle rs\middle|\frac{\partial}{\partial E}\big(\Omega_2(E)\big)_{E=E_{\rm in}}\middle|tu\right\rangle\left\langle tu\middle|W_1(E_{\rm in})\middle|ab\right\rangle + \cdots.$$

This shows that the (quasi)singularity is eliminated also in this higher-order case.

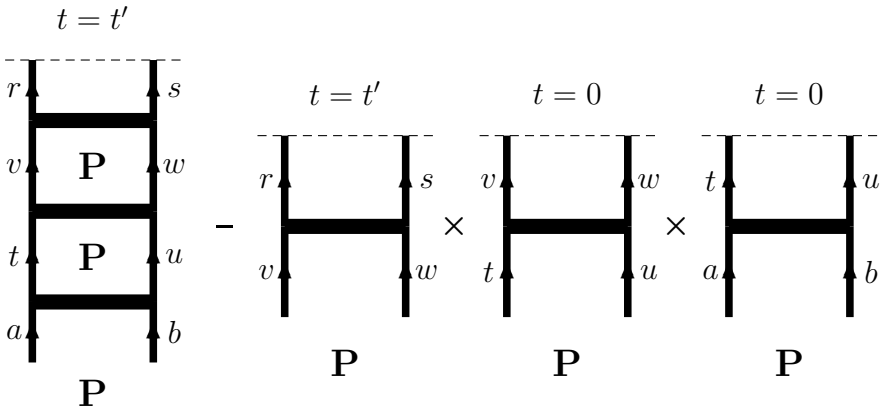

Fig. 8. Doubly reducible diagram with the corresponding counterterm.

FoldDiag3

Next we consider in a similar way a diagram that is *doubly reducible*, i.e., with *two* intermediate model-space states, as illustrated in Fig. 8. With obvious notations we can then express the ladder diagram, representing the wave operator, as

$$\langle rs|\Omega_3(E_{\rm in})|vw\rangle\frac{1}{\Delta E_2}\,\langle vw|W_2(E_{\rm in})|tu\rangle\,\frac{1}{\Delta E_1}\,\langle tu|W_1(E_{\rm in})|ab\rangle$$

and the counterterm as

$$\langle rs|\Omega_3(E_{\rm in}-\Delta E_2)|vw\rangle\frac{1}{\Delta E_2}\,\langle vw|W_2(E_{\rm in}-\Delta E_1)|tu\rangle\,\frac{1}{\Delta E_1}\,\langle tu|W_1(E_{\rm in})|ab\rangle.$$

In the limit when the $\Delta E's \to 0$, the latter becomes

$$\begin{aligned}&\Big\langle rs\Big|\Omega_3(E_{\rm in})-\Delta E_2\Big(\frac{\partial}{\partial E}\Omega_3(E)\Big)_{E=E_{\rm in}}\Big|vw\Big\rangle\\ &\times\frac{1}{\Delta E_2}\Big\langle vw\Big|W_2(E_{\rm in})-\Delta E_1\Big(\frac{\partial}{\partial E}W_2(E)\Big)_{E=E_{\rm in}}\Big|tu\Big\rangle\,\frac{1}{\Delta E_1}\Big\langle tu\Big|V_1(E_{\rm in})\Big|ab\Big\rangle.\end{aligned}$$

The double singularity is eliminated by the counterterm, and the difference becomes

$$-\Big\langle rs\Big|\Big(\frac{\partial}{\partial E}\Omega_3(E)\Big)_{E=E_{\rm in}}\Big|vw\Big\rangle\Big\langle vw\Big|\Big(\frac{\partial}{\partial E}W_2(E)\Big)_{E=E_{\rm in}}\Big|tu\Big\rangle\Big\langle tu\Big|V_1(E_{\rm in})\Big|ab\Big\rangle,$$

in addition to the *single* singularities, introduced by the counterterm,

$$\Big\langle rs\Big|\Omega_3(E_{\rm in})\Big|vw\Big\rangle\frac{1}{\Delta E_2}\Big\langle vw\Big|\Big(\frac{\partial}{\partial E}W_2(E)\Big)_{E=E_{\rm in}}\Big|tu\Big\rangle\Big\langle tu\Big|V_1(E_{\rm in})\Big|ab\Big\rangle$$

$$\Big\langle rs\Big|\Big(\frac{\partial}{\partial E}\Omega_3(E)\Big)_{E=E_{\rm in}}\Big|vw\Big\rangle\Big\langle vw\Big|W_2(E_{\rm in})\Big|tu\Big\rangle\frac{1}{\Delta E_1}\Big\langle tu\Big|V_1(E_{\rm in})\Big|ab\Big\rangle.$$

These single singularities are eliminated by the terms $-\tilde{U}^{(m)}P\tilde{U}^{(n)}P-\tilde{U}^{(n)}P\tilde{U}^{(m)}P$ of the expansion (118). In a similar way the cancellation of (quasi)singularities for triply ... reducible diagrams can be shown.

UtildeExp2

This verifies that the wave operator (124) and the effective interaction (127) are regular in all orders for a two-electron system.

3.5 Comparison with time-independent MBPT

sec:Comp

We shall now summarize our observations regarding the relation between the time-dependent and time-independent forms of MBPT. In *time-independent MBPT* generated by means of the Bloch equation in the linked-diagram form (42), there are two types of contributions to the wave operator. The first type originates from the first term on the r.h.s., and in the case of a two-electron system this gives rise to diagrams of *'ladder'* type. The second term on the r.h.s. of the Bloch equation gives rise to *'folded'* diagrams. *In the ladder type of diagrams all intermediate states lie in the Q space and in the folded diagrams one or several intermediate states lie in the P space.* The folded diagrams are therefore a type of *Model-Space Contribution* (MSC).

In *time-dependent MBPT* with time-independent interactions the wave operator can be expressed by means of the reduced evolution operator (138). Here, states of the model space can appear as intermediate states, which leads to a (quasi)singularity – so-called reducible contributions – and then there is a corresponding counterterm, which eliminates the singularity (117). The combination of the singular ladder diagram and the corresponding counterterm leads to a MSC that exactly corresponds folded to the diagram of time-independent MBPT.

In time-dependent MBPT with time- or energy-dependent interactions there is an additional MSC, which in the case of complete degeneracy leads to a contribution involving the energy derivative of the interaction (162).

4 S-matrix formulation

sec:S-matrix

In the present and the following two chapters we shall consider different schemes for bound-state QED calculations. We shall begin with a brief review of the standard S-matrix formulation, which is well documented in the literature. (For further details we refer to the recent extensive review by Mohr, Plunien and Soff (?)). Then we shall consider two more general methods, which have been developed more recently and which can be applied also to the quasi-degenerate situation. First we shall describe in some detail the *covariant-evolution-operator* method, developed by us (??), and the present report represents – together with the thesis of (?) – the first more detailed account of this new method. Next we shall more briefly describe the *two-times*

Green's-function method, developed by Shabaev et al., which has recently been extensively reviewed (Shab02 (?)), and we refer to this article for further details concerning this method. The two methods will be intercompared, and the possibility of combining the former with MBPT in a systematic fashion will be indicated.

We assume now that the perturbation is of the field-theoretical form (IntHam (68))

$$\hat{\mathcal{H}}'_{\rm I}(x) = -e\hat{\psi}^\dagger(x)\,\alpha^\mu A_\mu(x)\hat{\psi}(x). \tag{164}$$

IntHam1

The electron-field operators are in the IP given by (ElFieldTD (37)), and we assume that the orbitals are solutions of the Dirac equation (Dirac (62)) in the field of the nucleus (nuclei). We have in the previous chapter discussed this type of perturbation and derived the corresponding Gell-Mann–Low relations in the non-relativistic case. This theory, however, is not *covariant* in the relativistic sense, and the relativistic problem with negative energy states cannot be handled. The simplest way to remedy the situation is to let the time integrations run over all times, which leads to the *S-matrix formulation*. This we shall consider in this chapter. Another way is to modify the standard time evolution operator to make it covariant, which we shall consider in the next chapter.

The Sucher energy formula

Su57 (?) has shown that the energy shift can as an alternative to the Gell-Mann–Low formula (GMLShift (106)) be expressed

$$\Delta E = \lim_{\gamma\to 0}\frac{\rm i}{2}\gamma\lambda\,\frac{\langle\Psi_0|\frac{\partial}{\partial\lambda}U_\gamma(\infty,-\infty)|\Psi_0\rangle}{\langle\Psi_0|U_\gamma(\infty,-\infty)|\Psi_0\rangle}. \tag{165}$$

Sucher

$U_\gamma(\infty,-\infty)$ is the *scattering matrix* or *S-matrix*, primarily used in scattering theory. Like the Gell-Mann–Low formula, the Sucher formula is valid also when the interaction between the electrons is time- or energy dependent, but in contrast to the former it is also valid in the relativistic case. The Gell-Mann–Low–Sucher procedure has been the standard approach in bound-state QED for a long time (see, for instance MPS98 (?)) and will be discussed briefly in the next section.

4.1 Single-photon exchange. The photon propagator

sec:SingPhot

The field-theoretical form of the evolution operator, representing multi-photon exchange between the electrons, is given by the expansion (UExp (86))

$$U(t,t_0) =$$
$$1 - \tfrac{1}{2}\iint_{t_0}^{t} \mathrm{d}^4x_1\,\mathrm{d}^4x_2\,T_\mathrm{D}\Big[\Big(\hat\psi^\dagger(x)\,e\alpha^\mu A_\mu(x)\hat\psi(x)\Big)_1\Big(\hat\psi^\dagger(x)\,e\alpha^\nu \hat A_\nu(x)\hat\psi(x)\Big)_2\Big] + \cdots, \quad (166)$$

UQED

where, as before, the space integration is performed over all space and the time integration as indicated. We consider first the exchange of a single photon between the electrons, as indicated in Fig. 9. As in the previous chapter we consider the limit, where the initial time $t_0 \to -\infty$, which implies that we start from an eigenstate of the unperturbed Hamiltonian $\hat H_0$. The evolution operator, including the adiabatic damping (88), is then given by

Fig:SingPhot

Damping

$$\hat U^{(2)}(t',-\infty) =$$
$$-\tfrac{1}{2}\iint_{-\infty}^{t'} \mathrm{d}^4x_1\,\mathrm{d}^4x_2\,T_\mathrm{D}\Big[\Big(\hat\psi^\dagger(x)e\alpha^\mu \hat A_\mu(x)\hat\psi(x)\Big)_1\Big(\hat\psi^\dagger(x)e\alpha^\nu \hat A_\nu(x)\hat\psi(x)\Big)_2\Big]\,\mathrm{e}^{-\gamma(|t_1|+|t_2|)}. \quad (167)$$

USingP

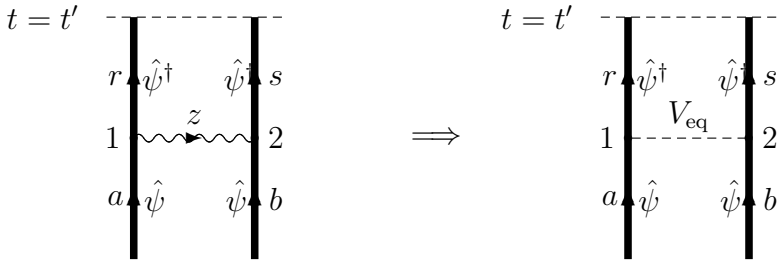

Fig. 9. The single-photon exchange between the electrons, compared with potential scattering.

Fig:SingPhot

The contraction between the electromagnetic field operators leads to the *photon propagator* (73), and disregarding for the moment other possible contractions, this yields

PhotProp

$$\hat U^{(2)}(t',-\infty) = -\tfrac{1}{2}\iint_{-\infty}^{t'} \mathrm{d}^4x_1\,\mathrm{d}^4x_2\,\hat\psi^\dagger(x_1)\hat\psi^\dagger(x_2)\;\mathrm{i}I(x_2,x_1)\,\hat\psi(x_2)\hat\psi(x_1)\,\mathrm{e}^{-\gamma(|t_1|+|t_2|)} \quad (168)$$

U2

with [13]

$$I(x_2,x_1) = e\alpha_1^\mu D_{\mathrm{F}\nu\mu}(x_2-x_1)\,e\alpha_2^\nu\,. \quad (169)$$

I

The Fourier transforms of $I(x_2,x_1)$ is defined by

$$I(x_2,x_1) = \int \frac{\mathrm{d}z}{2\pi}\,I(\boldsymbol{x}_2,\boldsymbol{x}_1,z)\,\mathrm{e}^{-\mathrm{i}z(t_2-t_1)},$$

where $I(\boldsymbol{x}_2,\boldsymbol{x}_1,z)$ is given by the definition (77).

Interact

[13] $I(x_2,x_1)$ corresponds to $\mathrm{i}I_{21}$ of ref. (??).

Li00,LAS01

c:S-SingPhot

4.1.1 S-matrix for single-photon exchange

The *scattering matrix* (S-matrix) is defined by $S = U(\infty, -\infty)$, and as a first illustration we shall study the S-matrix for a single-photon exchange. Eq. (168) then yields

U2

$$\hat{S}^{(2)} = -\tfrac{1}{2} \iint \mathrm{d}^4x_1 \mathrm{d}^4x_2 \, \hat{\psi}^\dagger(x_1)\hat{\psi}^\dagger(x_2)\, \mathrm{i}I(x_2,x_1)\, \hat{\psi}(x_2)\hat{\psi}(x_1)\, \mathrm{e}^{-\gamma(|t_1|+|t_2|)}$$
$$= -\tfrac{1}{2} \iint \mathrm{d}^4x_1 \mathrm{d}^4x_2 \, c_i^\dagger \phi_i^\dagger(x_1) c_j^\dagger \phi_j(x_2)\, \mathrm{i}I(x_2,x_1)\, c_l\phi_l(x_2) c_k\phi_k(x_1)\, \mathrm{e}^{-\gamma(|t_1|+|t_2|)}, \quad (170)$$ S2

where the integration is performed over the entire space-time volume. This is a two-body operator and becomes according to the second-quantization expression (23)

SecQuant

$$S^{(2)} = \tfrac{1}{2} \sum_{i,j,k,l} c_i^\dagger c_j^\dagger \left\langle ij \middle| S^{(2)} \middle| kl \right\rangle c_l c_k. \quad (171)$$ SecQuantS2

Identification then yields the expansion coefficients

$$\left\langle rs \left| S^{(2)} \right| ab \right\rangle = -\iint \mathrm{d}^4x_1\, \mathrm{d}^4x_2\, \phi_r^\dagger(x_1)\phi_s^\dagger(x_2)\, \mathrm{i}I(x_2,x_1)\,)\phi_b(x_2)\phi_a(x_1)\, \mathrm{e}^{-\gamma(|t_1|+|t_2|)}$$
$$= -\iint \mathrm{d}^4x_1\, \mathrm{d}^4x_2 \int \frac{\mathrm{d}z}{2\pi}\, \phi_r^\dagger(\boldsymbol{x}_1)\phi_s^\dagger(\boldsymbol{x}_2)\, \mathrm{i}I(\boldsymbol{x}_2,\boldsymbol{x}_1,z)\,)\phi_b(\boldsymbol{x}_2)\phi_a(\boldsymbol{x}_1)$$
$$\times \mathrm{e}^{-\mathrm{i}t_1(\varepsilon_a-\varepsilon_r-z)} \mathrm{e}^{-\mathrm{i}t_2(\varepsilon_b-\varepsilon_s+z)}\, \mathrm{e}^{-\gamma(|t_1|+|t_2|)}. \quad (172)$$ S22

After the time integrations this becomes

$$\left\langle rs \left| \hat{S}^{(2)} \right| ab \right\rangle = -\mathrm{i} \int \frac{\mathrm{d}z}{2\pi}\, 2\pi\, \Delta_\gamma(q-z)\, 2\pi\, \Delta_\gamma(q'+z) \left\langle rs \middle| I(\boldsymbol{x}_2,\boldsymbol{x}_1,z) \middle| ab \right\rangle, \quad (173)$$ S2SingPhot

where $q = \varepsilon_a - \varepsilon_r$ and $q' = \varepsilon_b - \varepsilon_s$. The Δ function is here defined

$$\int_{-\infty}^{\infty} \mathrm{d}t\, e^{\mathrm{i}qt}\, e^{-\gamma|t|} = \frac{2\gamma}{q^2+\gamma^2} = 2\pi\, \Delta_\gamma(q), \quad (174)$$ Delta

which has the following properties

$$\lim_{\gamma\to 0} \Delta_\gamma(q) = \delta(q)$$
$$\lim_{\gamma\to 0} \pi\gamma\, \Delta_\gamma(q) = \delta_{q,0}$$
$$\int_{-\infty}^{\infty} \mathrm{d}z\, \Delta_\gamma(z-a)\, \Delta_\kappa(z-b) = \Delta_{\gamma+\kappa}(a-b).$$

Here, $\delta(q)$ is the *Dirac delta function* and $\delta_{q,r}$ is the *Kronecker delta factor* (=1 for $q = r$ and zero otherwise). [14]

[14] The first two relations are obvious, and the third can easily be shown by means of the identity

$$\Delta_\gamma(z-a)\, \Delta_\kappa(z-b) \equiv \frac{1}{(2\pi\mathrm{i})^2} \Big(\frac{1}{z-a-\mathrm{i}\gamma} - \frac{1}{z-a+\mathrm{i}\gamma}\Big)\Big(\frac{1}{z-b-\mathrm{i}\kappa} - \frac{1}{z-b+\mathrm{i}\kappa}\Big).$$

Using the last relation above we can for small γ approximate the expression (173) by

$$\left\langle rs \left| \hat{S}^{(2)} \right| ab \right\rangle = -2\pi \mathrm{i}\, \Delta_{2\gamma}(q+q')\, \langle rs|I(\boldsymbol{x}_2, \boldsymbol{x}_1, q)|ab\rangle.$$

The single-photon exchange can be compared with the S matrix for the *potential scattering* from a time- or energy-dependent potential, $V_{\rm eq}(x_2 - x_1)$ with the Fourier transform $V_{\rm eq}(\boldsymbol{x}_1, \boldsymbol{x}_2, z)$, as indicated by the rightmost diagram in Fig. 9. Since two times are involved also in this process, it has to be regarded as a *second-order process*, yielding

$$\hat{S}^{(2)}_{\rm pot} = -\tfrac{1}{2} \iint \mathrm{d}^4x_1 \mathrm{d}^4x_2\, \hat{\psi}^\dagger(x_1)\hat{\psi}^\dagger(x_2)\, V_{\rm eq}(x_2 - x_1)\, \hat{\psi}(x_2)\hat{\psi}(x_1)\, \mathrm{e}^{-\gamma(|t_1|+|t_2|)}. \quad (175)$$

PotScatt

After time integration, the matrix element becomes as in the previous case

$$\left\langle rs \left| \hat{S}^{(1)}_{\rm pot} \right| ab \right\rangle = -2\pi \mathrm{i}\, \Delta_{2\gamma}(q+q') \left\langle rs \middle| V_{\rm eq}(q) \middle| ab \right\rangle. \quad (176)$$

SmatrixEl

This implies that the single-photon exchange is equivalent to potential scattering by an *equivalent potential* given by

$$\boxed{V_{\rm eq}(q) = I(\boldsymbol{x}_2, \boldsymbol{x}_1, q) = e^2 \alpha_1^\mu \alpha_2^\nu\, D_{{\rm F}\nu\mu}(\boldsymbol{x}_2 - \boldsymbol{x}_1, q).} \quad (177)$$

EqPot

In the *Feynman gauge* the equivalent potential becomes, using the definition (77),

$$V^{\rm F}_{\rm eq}(q) = \int_0^\infty \frac{2k\, \mathrm{d}k\, f(k)}{q^2 - k^2 + \mathrm{i}\eta}; \qquad f(k) = -\frac{e^2}{4\pi^2\, r_{12}} (1 - \boldsymbol{\alpha}_1 \cdot \boldsymbol{\alpha}_2)\, \sin(k r_{12}) \quad (178)$$

EqPotF

or after integrating over the k space

$$V^{\rm F}_{\rm eq}(q) = \frac{e^2}{4\pi\, r_{12}} (1 - \boldsymbol{\alpha}_1 \cdot \boldsymbol{\alpha}_2)\, \mathrm{e}^{\mathrm{i}|q|r_{12}}, \quad (179)$$

EqPotF2

which is the *retarded Coulomb-Gaunt interaction* (78).

The energy shift is given by the Sucher formula (165), which in the lowest order ($n = 2$) yields

$$\Delta E = \lim_{\gamma \to 0} \mathrm{i}\gamma\, \langle rs|\hat{S}^{(2)}|ab\rangle. \quad (180)$$

Sucher1

In the present case this gives, using (173),

$$\Delta E = \delta_{q,-q'} \left\langle rs \middle| V_{\rm eq}(q) \middle| ab \right\rangle. \quad (181)$$

EnergyShift

Here, only the cross products, which have one pole on each side of the axis, contribute to the integral.

The Kronecker delta factor implies here that the result is nonvanishing only for $q + q' = 0$ or $\varepsilon_a + \varepsilon_b = \varepsilon_r + \varepsilon_s$, which means that *in the S-matrix formalism energy must be conserved between the initial and final states*. This has the disadvantage that those elements of the effective Hamiltonian that are nondiagonal in energy cannot be evaluated. Therefore, the procedure is not applicable to the procedure of an extended model space, discussed above for the treatment of quasi-degeneracy. In the following two chapters we shall discuss two methods that do not have this serious shortcoming, but first we shall develop the S-matrix formulation a little further.

4.2 The electron propagator

sec:ElProp

In relativistic problems we must also allow for time running backwards, which represents antiparticle creation. For that purpose the so-called *Feynman electron propagator*, $S_{\mathrm{F}}(x, x_0)$, is introduced, defined by

$$\begin{aligned} &\mathrm{i}S_{\mathrm{F}}(x, x_0) = \langle 0|T[\hat{\psi}(x)\,\hat{\psi}^\dagger(x_0)]|0\rangle \\ &= \langle 0|\Theta(t - t_0)\,\hat{\psi}(x)\,\hat{\psi}^\dagger(x_0) - \Theta(t_0 - t)\,\hat{\psi}^\dagger(x_0)\,\hat{\psi}(x)|0\rangle. \end{aligned} \tag{182}$$

ElProp1

Here, $\Theta(t)$ is the Heaviside step function (equal to unity for $t > 0$ and zero for $t < 0$) and T is the *Wick time-ordering operator*

$$T[A(x_1)B(x_2)] = \begin{cases} A(x_1)B(x_2) & (t_1 > t_2) \\ -B(x_2)A(x_1) & (t_1 < t_2), \end{cases} \tag{183}$$

TimeOrdering

not to be confused with the *Dyson* time-ordering operator (74). The expression (182) represents the *contraction* between the electron field operators (38). Separating the field operators (35) into *particle* ($\hat{\psi}_+$) and *hole* ($\hat{\psi}_-$) parts, corresponding to electrons with positive and negative energy, respectively, the electron propagator can be expressed

$$\begin{aligned} &\mathrm{i}S_{\mathrm{F}}(x, x_0) = \left\langle 0\middle|\Theta(t - t_0)\hat{\psi}_+(x)\,\hat{\psi}_+^\dagger(x_0) - \Theta(t_0 - t)\hat{\psi}_-^\dagger(x_0)\,\hat{\psi}_-(x)\middle|0\right\rangle \\ &= \Theta(t - t_0)\phi_p(\boldsymbol{x})\,\phi_p^\dagger(\boldsymbol{x}_0)\,e^{-\mathrm{i}\varepsilon_p(t-t_0)} - \Theta(t_0 - t)\phi_h^\dagger(\boldsymbol{x}_0)\,\phi_h(\boldsymbol{x})\,e^{-\mathrm{i}\varepsilon_h(t-t_0)}. \end{aligned} \tag{184}$$

ElProp2

Here, ϕ_p, ϕ_h represent the single-electron wavefunctions (10), with positive energy ('particle states') and negative energy ('hole states'), respectively. By analytical continuation the electron propagator can be expressed as an integral in the complex plane

$$\boxed{S_{\mathrm{F}}(x, x_0) = \int \frac{\mathrm{d}\omega}{2\pi} \frac{\phi_j(\boldsymbol{x})\,\phi_j^\dagger(\boldsymbol{x}_0)}{\omega - \varepsilon_j + \mathrm{i}\eta_j}\,e^{-\mathrm{i}\omega(t-t_0)},} \tag{185}$$

ElPropInt

where j runs over all states (with positive as well as negative energy), and η_j is an infinitesimally small quantity with the same sign as ε_j, indicating the position of the pole. The *Fourier transform* (with respect to time) of the electron propagator is

$$S_{\mathrm{F}}(\boldsymbol{x}, \boldsymbol{x}_0, \omega) = \frac{\phi_j(\boldsymbol{x})\, \phi_j^\dagger(\boldsymbol{x}_0)}{\omega - \varepsilon_j + \mathrm{i}\eta_j}. \tag{186}$$

ElPropFour

Regarding the space part of the single-electron functions as *coordinate representations* of the corresponding Dirac states,

$$\phi_j(\boldsymbol{x}) = \langle \boldsymbol{x}|j\rangle\,; \quad \phi_j^\dagger(\boldsymbol{x}_0) = \langle j|\boldsymbol{x}_0\rangle,$$

we can express the electron propagator (186) ElPropFour

$$S_{\mathrm{F}}(\boldsymbol{x}, \boldsymbol{x}_0, \omega) = \langle \boldsymbol{x}|\hat{S}_{\mathrm{F}}(\omega)|\boldsymbol{x}_0\rangle \tag{187}$$

ElPropCoord

or as the coordinate representation of the *electron-propagator operator*

$$\hat{S}_{\mathrm{F}}(\omega) = \frac{|j\rangle\langle j|}{\omega - \varepsilon_j + \mathrm{i}\eta_j}. \tag{188}$$

ElPropDiracFou

We also introduce the *four-dimensional* coordinate representations of the Dirac states,

$$\langle x|j\rangle = \phi_j(x) = \phi_j(\boldsymbol{x})\, e^{-\mathrm{i}\varepsilon_j t}\,; \quad \langle j|x\rangle = \phi_j^\dagger(x) = \phi_j^\dagger(\boldsymbol{x})\, e^{\mathrm{i}\varepsilon_j t}. \tag{189}$$

Then the field operators (35) ElFieldIP become

$$\hat{\psi}(x) = \langle x|j\rangle\, c_j; \qquad \hat{\psi}^\dagger(x) = c_j^\dagger\, \langle j|x\rangle, \tag{190}$$

FieldDirac

and the electron-propagator (184) ElProp2 can be expressed

$$\mathrm{i}S_{\mathrm{F}}(x, x_0) = \Theta(t - t_0)\langle x|p\rangle\langle p|x_0\rangle - \Theta(t_0 - t)\langle x|h\rangle\langle h|x_0\rangle, \tag{191}$$

ElPropDirac1

and the form (185) ElPropInt

$$S_{\mathrm{F}}(x, x_0) = \int \frac{\mathrm{d}\omega}{2\pi}\, \frac{\langle x|j\rangle\langle j|x_0\rangle}{\omega - \varepsilon_j + \mathrm{i}\eta_j}. \tag{192}$$

ElPropOp

Operating with the electron propagator (191) ElPropDirac1 on the field operator, $\hat{\psi}(x_0)$, and integration over the space coordinates, then yields

$$\begin{aligned} \int \mathrm{d}^3\boldsymbol{x}_0\, \mathrm{i}S_{\mathrm{F}}(x, x_0)\, \hat{\psi}(x_0) &= \Theta(t - t_0)\langle x|p\rangle\, c_p - \Theta(t_0 - t)\langle x|h\rangle\, c_h \\ &= \Theta(t - t_0)\hat{\psi}_+(x_0) - \Theta(t_0 - t)\hat{\psi}_-(x_0) \end{aligned} \tag{193}$$

ElPropFieldOp1

and similarly

$$\int \mathrm{d}^3\boldsymbol{x}\,\hat{\psi}^\dagger(x)\,\mathrm{i}S_\mathrm{F}(x,x_0) = \Theta(t-t_0)\hat{\psi}^\dagger_+(x) - \Theta(t_0-t)\hat{\psi}^\dagger_-(x). \tag{194}$$

ElPropFieldCoo

4.3 The Lamb shift

sec:LS

In the second-order evolution operator (USingPhot 167) we can also have contractions between the electron-field operators in various ways. Two equivalent contractions are indicated below,

$$\big(\hat{\psi}^\dagger(x)e\alpha^\mu A_\mu\hat{\psi}(x)\big)_1\big(\hat{\psi}^\dagger(x)e\alpha^\nu A_\nu\hat{\psi}(x)\big)_2 \qquad \big(\hat{\psi}^\dagger(x)e\alpha^\mu A_\mu\hat{\psi}(x)\big)_1\big(\hat{\psi}^\dagger(x)e\alpha^\nu A_\nu\hat{\psi}(x)\big)_2, \tag{195}$$

ElContr1

and together with the photon field contraction this represents the *electron self-energy*, depicted for the S-matrix in Fig. Fig:LS 10 (left). Contracting the electron field operators at the same vertex

$$\big(\hat{\psi}^\dagger(x)e\alpha^\mu A_\mu\hat{\psi}(x)\big)_1\big(\hat{\psi}^\dagger(x)e\alpha^\nu A_\nu\hat{\psi}(x)\big)_2 \quad \big(\hat{\psi}^\dagger(x)e\alpha^\mu A_\mu\hat{\psi}(x)\big)_1\big(\hat{\psi}^\dagger(x)e\alpha^\nu A_\nu\hat{\psi}(x)\big)_2 \tag{196}$$

ElCont2

represents the *vacuum polarization*, shown in the right diagram of the figure.

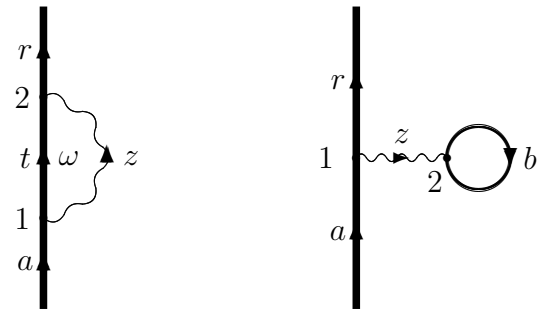

Fig. 10. The S-matrix diagrams representing the first-order electron self-energy and vacuum polarization.

Fig:LS

sec:SE

4.3.1 The electron self-energy

By considering only one of the electron-field contractions in (ElContr1 195), we can eliminate the factor of $\frac{1}{2}$, and the S-matrix for the electron self-energy becomes in analogy with the single-photon exchange (S2 170)

$$\begin{aligned} S^{(2)}_\mathrm{SE} &= -\iint \mathrm{d}^4x_2\mathrm{d}^4x_1\,\hat{\psi}^\dagger(x_2)\,\mathrm{i}S_\mathrm{F}(x_2,x_1)\,\mathrm{i}I(x_2,x_1)\,\hat{\psi}(x_1)\,\mathrm{e}^{-\gamma(|t_1|+|t_2|)} \\ &= -\iint \mathrm{d}^4x_2\mathrm{d}^4x_1\,c_i^\dagger\phi_i^\dagger(x_2)\,\mathrm{i}S_\mathrm{F}(x_2,x_1)\,\mathrm{i}I(x_2,x_1)\,c_j\phi_j(x_1)\,\mathrm{e}^{-\gamma(|t_1|+|t_2|)}. \end{aligned} \tag{197}$$

SSE1

This is a one-body operator, and identification with the expansion (23) then yields the 'matrix element'

$$\Big\langle r\Big|S_{\rm SE}^{(2)}\Big|a\Big\rangle = -\iint {\rm d}^4x_2\,{\rm d}^4x_1\,\phi_r^\dagger(x_2)\,{\rm i}S_{\rm F}(x_2,x_1)\,{\rm i}I(x_2,x_1)\,\phi_a(x_1)\,{\rm e}^{-\gamma(|t_1|+|t_2|)}. \quad (198)$$

SSE2

Using the Fourier transforms of the propagator and the interaction, this becomes

$$\Big\langle r\Big|S_{\rm SE}^{(2)}\Big|a\Big\rangle = \iint {\rm d}^4x_2\,{\rm d}^4x_1\int\frac{{\rm d}\omega}{2\pi}\int\frac{{\rm d}z}{2\pi}\,\phi_r^\dagger(\boldsymbol{x}_2)\,S_{\rm F}(\boldsymbol{x}_2,\boldsymbol{x}_1,\omega)\;I(\boldsymbol{x}_2,\boldsymbol{x}_1,z)\,\phi_a(\boldsymbol{x}_1)$$
$$\times\,{\rm e}^{-{\rm i}t_2(\omega+z-\varepsilon_r)}\,{\rm e}^{-{\rm i}t_1(\varepsilon_a-\omega-z)}\,{\rm e}^{-\gamma(|t_1|+|t_2|)}. \quad (199)$$

SSE3

The time integrations yield here in analogy with the single-photon exchange (173) the factors $2\pi\Delta_\gamma(\omega+z-\varepsilon_r)$ and $2\pi\Delta_\gamma(\varepsilon_a-\omega-z)$, and after integration over ω this becomes

$$\Big\langle r\Big|S_{\rm SE}^{(2)}\Big|a\Big\rangle = 2\pi\Delta_{2\gamma}(\varepsilon_a-\varepsilon_r)\iint {\rm d}^3\boldsymbol{x}_2\,{\rm d}^3\boldsymbol{x}_1$$
$$\times\int\frac{{\rm d}z}{2\pi}\,\phi_r^\dagger(\boldsymbol{x}_2)\,S_{\rm F}(\boldsymbol{x}_2,\boldsymbol{x}_1,\varepsilon_a-z)\;I(\boldsymbol{x}_2,\boldsymbol{x}_1,z)\,\phi_a(\boldsymbol{x}_1). \quad (200)$$

SSE4

This can be expressed

$$\Big\langle r\Big|S_{\rm SE}^{(2)}\Big|a\Big\rangle = -2\pi{\rm i}\Delta_{2\gamma}(\varepsilon_a-\varepsilon_r)\,\Big\langle r\Big|\Sigma(\varepsilon_a)\Big|a\Big\rangle, \quad (201)$$

SSE5

defining the *self-energy operator* by

$$\langle r|{\rm i}\Sigma(\varepsilon_a)|a\rangle = \iint {\rm d}^3\boldsymbol{x}_2\,{\rm d}^3\boldsymbol{x}_1\int\frac{{\rm d}z}{2\pi}\,\phi_r^\dagger(\boldsymbol{x}_2)\,{\rm i}S_{\rm F}(\boldsymbol{x}_2,\boldsymbol{x}_1,\varepsilon_a-z)\,{\rm i}I(\boldsymbol{x}_2,\boldsymbol{x}_1,z)\,\phi_a(\boldsymbol{x}_1)$$
$$= -\int\frac{{\rm d}z}{2\pi}\,\frac{\langle tr|I(z)|at\rangle}{\varepsilon_a-\varepsilon_t-z+{\rm i}\eta_t} \quad (202)$$

SelfEn

and using the form (187) of the electron propagator. With the photon interaction in the Feynman gauge (77) this becomes (see Appendix A.1)

$$\Big\langle r\Big|\Sigma(\varepsilon_a)\Big|a\Big\rangle = {\rm i}\int\frac{{\rm d}z}{2\pi}\int{\rm d}k\frac{\langle tr|2kf(k)|at\rangle}{(\varepsilon_a-\varepsilon_t-z+{\rm i}\gamma_t)(z^2-k^2+{\rm i}\eta)}$$
$$= \int{\rm d}k\,\frac{\langle tr|f(k)|at\rangle}{\varepsilon_a-\varepsilon_t-(k-{\rm i}\gamma)_t}, \quad (203)$$

SelfEnInt

where $(\cdot)_t$ has the same sign as ε_t.

The energy shift due to the electron self-energy is then given by the Sucher formula (180)

$$\delta E_{\rm SE} = \delta_{\varepsilon_a,\varepsilon_r}\,\Big\langle r\Big|\Sigma(\varepsilon_a)\Big|a\Big\rangle. \quad (204)$$

SEShift

As in the previous case, the energy must be preserved between the initial and final states in this procedure. A more general treatment is given in section 5.3.

sec:RenormSE

4.3.2 Self-energy renormalization

The electron self-energy, represented by the emission and absorption of the same photon, is a process that corresponds to an infinite energy or mass. For the free electron this is in analogy with the bound-state result (203) SelfEnInt

$$\delta E_{\rm SE}^{\rm free}(\varepsilon_{\boldsymbol{p}r}) = \langle \boldsymbol{p}r|\Sigma(\varepsilon_{\boldsymbol{p}r})|\boldsymbol{p}r\rangle = \int {\rm d}k\, \frac{\langle \boldsymbol{p}r, \boldsymbol{q}s|f(k)|\boldsymbol{q}s, \boldsymbol{p}r\rangle}{\varepsilon_{\boldsymbol{p}r} - \varepsilon_{\boldsymbol{q}s} - (k - {\rm i}\gamma)_q}, \qquad (205)$$

SEfree

illustrated in Fig. 11. We use here the *momentum representation* — $\boldsymbol{p}$, $\boldsymbol{q}$ denote the momentum and r, s components of the Dirac spinor. The factor $(k - {\rm i}\gamma)_q$ is positive for electrons and negative for positrons. Fig:SEfree

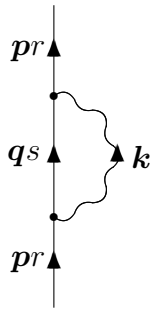

Fig. 11. The free-electron self-energy (205). SEfree

Fig:SEfree

The free-electron self-energy represents a part δm of the physical mass of the electron and should be subtracted from the self-energy of the bound electron. This *renormalization process* eliminates the singularity. For an electron in the bound state $|a\rangle$ the renormalized self-energy is then given by

$$\delta E_{\rm SE}^{\rm renorm} = \Big\langle a\Big|\Sigma(\varepsilon_a)\Big|a\Big\rangle - \Big\langle a\Big|\delta m\Big|a\Big\rangle. \qquad (206)$$

SEShift2

The renormalization term – also referred to as the *mass counterterm* – is the average of free-electron self-energy in the state $|a\rangle$, as illustrated in Fig. 12. Fig:SERen1

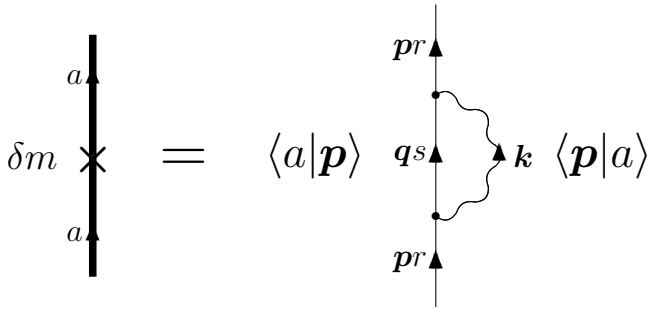

Fig. 12. The mass counterterm is the average of the free-electron self-energy in the bound state $|a\rangle$. The thick vertical line represents a bound-electron and the thin line a free-electron state.

Fig:SERen1

A bound-electron propagator can be expanded in a free-electron propagator with zero, one, two,... interactions of the external (nuclear) field. Applied to the

self-energy diagram this leads to the expansion in Fig. 13. Here, the first two terms are infinite, while the last 'many-potential term' is finite. In the method introduced by (?) and later modified by (?) the zero- and one-potential terms are combined with the mass counterterm, which leads to a finite quantity that can be evaluated analytically. The final result is then obtained by evaluating numerically the finite many-potential term.

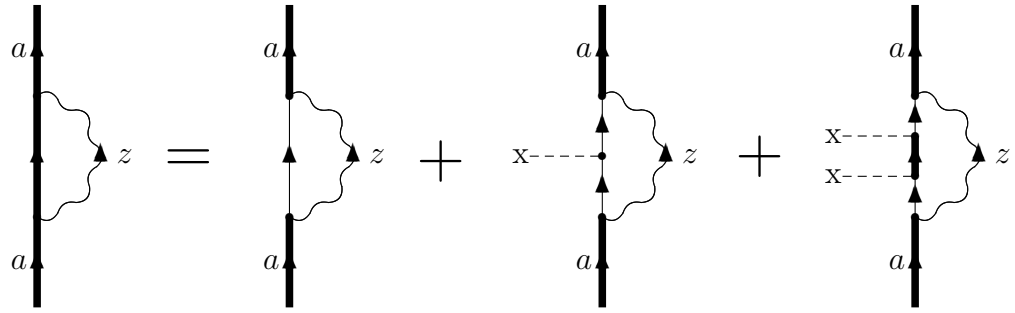

Fig. 13. The bound-electron self-energy can be expanded into a zero-, a one- and a many-potential term.

sec:VacPol

4.3.3 The vacuum polarization

The second part of the Lamb shift (Fig. 10), the vacuum polarization (VP), is also singular and has to be renormalized. The bound-state VP can be expanded into a zero-potential, a one-potential and a many-potential term, as in the self-energy case (Fig. 14). The zero-potential term is zero, due to the Furry theorem (?). The one-potential term is singular but can be renormalized analytically, as first shown by (?) and (?). The last term, known as the *Wichmann-Kroll term* (?), is finite and evaluated numerically.

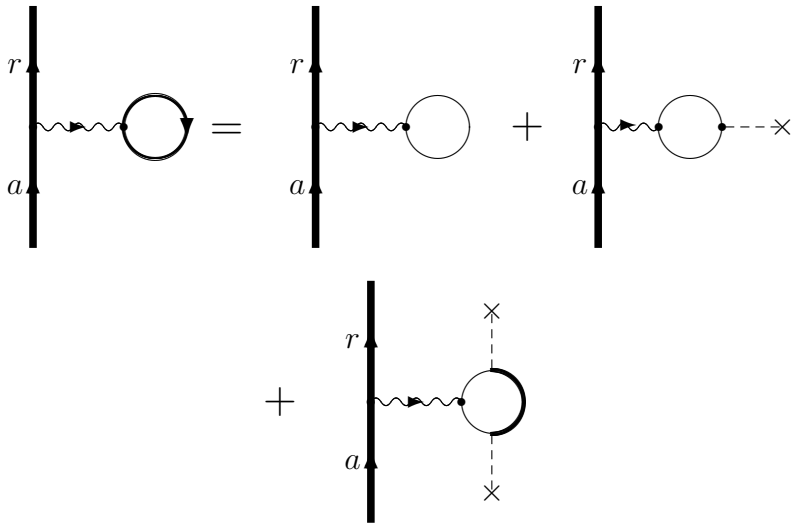

Fig. 14. The bound-state vacuum polarization can be expanded in a zero-, one-, and many-potential term as in the self-energy case (Fig. 13).

Some applications of the S-matrix formulation are briefly discussed in chapter 7. For further information the reader is referred to the review article by [?].

5 Covariant-evolution-operator formalism.

5.1 Single-photon exchange

As mentioned previously, the S-matrix formalism cannot handle the quasi-degeneracy problem, due to the energy-conservation condition (181), which is caused by the integration over all times. A possibility to circumvent this problem might therefore be to consider instead of the S-matrix the original evolution operator (86) with a limited time integration. As mentioned, however, the evolution operator in its original form is *not relativistically covariant*, implying that the relativistic problem can not be handled. By generalizing the operator, so that time can evolve *forwards as well as backwards*, it can be shown that the relativistic covariance can be restored. This method – which we refer to as the *covariant-evolution-operator method* – has recently been developed and successfully applied to the quasi-degenerate situation (**???**) and is illustrated in Fig. 15 for single-photon exchange.

In the covariant-evolution-operator method we use for the single-photon exchange between two electrons – instead of the standard time-evolution operator (168) – the expression

$$U^{(2)}_{\rm Cov}(t',-\infty) = -\tfrac{1}{2}\iint \mathrm{d}^4x_1\,\mathrm{d}^4x_2\,\Big[\Theta(t'-t_1)\,\hat\psi^\dagger_+(x_1) - \Theta(t_1-t')\,\hat\psi^\dagger_-(x_1)\Big]$$
$$\times\Big[\Theta(t'-t_2)\,\hat\psi^\dagger_+(x_2) - \Theta(t_2-t')\,\hat\psi^\dagger_-(x_2)\Big]\,\mathrm{i}I(x_2,x_1)\,\hat\psi(x_2)\,\hat\psi(x_1)\,\mathrm{e}^{-\gamma(|t_1|+|t_2|)}. \quad (207)$$

Here, we *integrate over all times*. For integration times smaller than the time t' of the evolution operator, which corresponds to positive-energy states, we integrate in the *positive* direction from the negative infinity, and correspondingly for integration times larger than t', which corresponds to negative-energy states, we integrate in the *negative* direction from the positive infinity. With this operator, positive- and negative-energy states can be handled in analogous ways.

Generally, the evolution operator (86) is a *two-times operator*, with an initial as well as a final time. However, in perturbation theory, using the adiabatic damping (91), it is convenient to set the initial time $t_0 = -\infty$, which directly leads to a perturbation expansion starting from an unperturbed state. We shall normally apply that in the following.

Using the relation (194), we can replace the square brackets in (207) by space

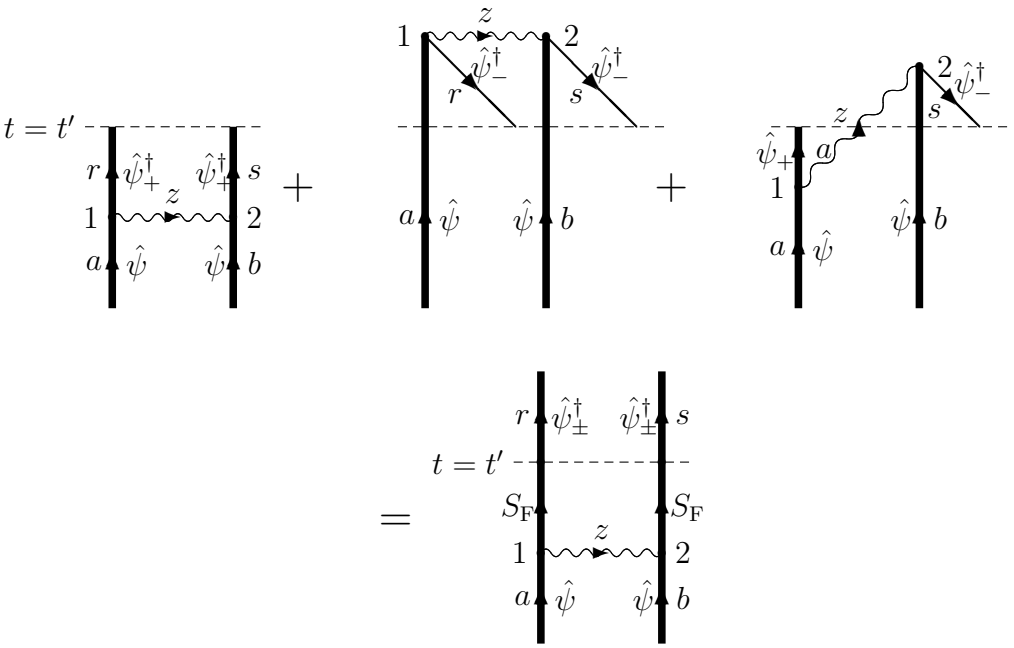

Fig. 15. The one-time evolution operator for single-photon exchange between the electrons, including forward and backward time evolution, represented by three time-ordered (Goldstone) diagrams (top) and a single Feynman diagram (bottom). The wavy line represents the photon propagator, the open, solid lines the electron-field operator and the straight line between dots the electron propagator. The subscript of the electron field operators indicates positive- and negative-energy part, respectively.

Fig:CovEvOp

integration over the electron propagators, yielding

$$U^{(2)}_{\mathrm{Cov}}(t',-\infty) = -\tfrac{1}{2}\iint \mathrm{d}^3\boldsymbol{x}'_1\mathrm{d}^3\boldsymbol{x}'_2\,\hat\psi^\dagger(x'_1)\hat\psi^\dagger(x'_2)\iint \mathrm{d}^4x_1\,\mathrm{d}^4x_2$$
$$\times\,\mathrm{i}S_{\mathrm{F}}(x'_1,x_1)\,\mathrm{i}S_{\mathrm{F}}(x'_2,x_2)\,\mathrm{i}I(x_2,x_1)\,\hat\psi(x_2)\,\hat\psi(x_1)\,\mathrm{e}^{-\gamma(|t_1|+|t_2|)} \qquad (208)$$

U2Cov3

with $x'_i = (t',\boldsymbol{x}'_i)$. (Note that x'_1 and x'_2 have the common time t'.) In analogy with the single-photon exchange (172) the 'matrix elements' become

$$\Big\langle rs\Big|U^{(2)}_{\mathrm{Cov}}(t',-\infty)\Big|ab\Big\rangle = -\iint \mathrm{d}^3\boldsymbol{x}'_1\mathrm{d}^3\boldsymbol{x}'_2\,\phi^\dagger_r(x'_1)\phi^\dagger_s(x'_2)\iint \mathrm{d}^4x_1\,\mathrm{d}^4x_2$$
$$\times\,\mathrm{i}S_{\mathrm{F}}(x'_1,x_1)\,\mathrm{i}S_{\mathrm{F}}(x'_2,x_2)\,\mathrm{i}I(x_2,x_1)\,\phi_a(x_1)\,\phi_b(x_2)\,\mathrm{e}^{-\gamma(|t_1|+|t_2|)}$$
$$= -\iint \mathrm{d}t_1\,\mathrm{d}t_2\,\Big\langle rs\Big|\boldsymbol{x}'_1\boldsymbol{x}'_2\Big\rangle\Big\langle\boldsymbol{x}'_1\boldsymbol{x}'_2\Big|\mathrm{i}S_{\mathrm{F}}(x'_1,x_1)\,\mathrm{i}S_{\mathrm{F}}(x'_2,x_2)\,\mathrm{i}I(x_2,x_1)\,\Big|\boldsymbol{x}_1\boldsymbol{x}_2\Big\rangle\Big\langle\boldsymbol{x}_1\boldsymbol{x}_2\Big|ab\Big\rangle$$
$$\times\,\mathrm{e}^{\mathrm{i}t'(\varepsilon_r+\varepsilon_s)}\,\mathrm{e}^{-\mathrm{i}t_1\varepsilon_a-\mathrm{i}t_2\varepsilon_b}\,\mathrm{e}^{-\gamma(|t_1|+|t_2|)}, \qquad (209)$$

U2Cov4

where we have explicitly shown the coordinates for the bra $\langle rs|$ and the ket $|ab\rangle$.

The result (209) is illustrated by the bottom diagram in Fig. 15. The integral

is evaluated in Appendix A.1, and the result becomes

$$\boxed{\left\langle rs\left|U^{(2)}_{\rm Cov}(t',-\infty)\right|ab\right\rangle = \left\langle rs\middle|V(q,q')\middle|ab\right\rangle \frac{{\rm e}^{-{\rm i}t'(q+q')}}{q+q'}} \qquad (210)$$

U2Cov6

$$\boxed{V(q,q') = \int {\rm d}k\, f(k)\left[\frac{1}{q-(k-{\rm i}\gamma)_r}+\frac{1}{q'-(k-{\rm i}\gamma)_s}\right],} \qquad (211)$$

SingPhotInt

where $(A)_x = (A)\,{\rm sgn}(\varepsilon_x)$ and $f(k)$ is given by (77)

Interact

$$\boxed{f(k) = -\frac{e^2}{4\pi^2\, r_{12}}\,(1-\boldsymbol{\alpha}_1\cdot\boldsymbol{\alpha}_2)\,\sin(kr_{12}).} \qquad (212)$$

fk

When the final state $|rs\rangle$ lies in the model space, the contribution to the *effective interaction* becomes, using (130),

EffInt2

$$\boxed{\langle rs|H^{(1)}_{\rm eff}|ab\rangle = \langle rs|V(q,q')|ab\rangle.} \qquad (213)$$

EffIntSP

We can now compare the result above with the S-matrix result obtained in the previous chapter. When $|rs\rangle$ has the same energy as $|ab\rangle$, this agrees with the result (181). Then the potential (211) reduces to

EnergyShift SingPhotInt

$$V(q,-q) = \int \frac{2k\,{\rm d}k\, f(k)}{q^2-k^2+{\rm i}\gamma} = V^{\rm F}_{\rm eq}(q),$$

which is the same as the S-matrix result (178). In the evolution-operator result (213), however, the initial and final states do not have to have the same energy, which makes the formalism applicable also to the quasi-degeneracy problem, using an extended model space.

EqPotF EffIntSP

SingPhotAlt

5.1.1 Single-photon exchange. Alt.

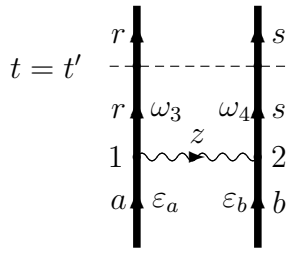

Fig. 16. The covariant evolution operator for single-photon exchange between the electrons.

Fig:SingPhotAl

We shall now derive the expression for the single-photon exchange in an alternative way, using the one-photon covariant evolution-operator method, which

will be useful in demonstrating more clearly the analogy with the Green's-function method to be discussed later.

The matrix element (209) is with the notations in Fig. 16

$$\Big\langle rs\Big|U^{(2)}_{\rm Cov}(t',-\infty)\Big|ab\Big\rangle = -\iint {\rm d}t_1\,{\rm d}t_2\,\Big\langle rs\Big|{\rm i}S_{\rm F}(x_1',x_1)$$
$$\times\,{\rm i}S_{\rm F}(x_2',x_2)\,{\rm i}I(x_2,x_1)\,\Big|ab\Big\rangle\,{\rm e}^{{\rm i}t'(\varepsilon_r+\varepsilon_s)}\,{\rm e}^{-{\rm i}t_1\varepsilon_a-{\rm i}t_2\varepsilon_b}\,{\rm e}^{-\gamma(|t_1|+|t_2|)}$$
$$= {\rm i}\iint {\rm d}t_1\,{\rm d}t_2\,\frac{\Big\langle rs\Big|I(z)\Big|ab\Big\rangle}{(\omega_3-\varepsilon_r+{\rm i}\eta_r)(\omega_4-\varepsilon_s+{\rm i}\eta_s)}$$
$$\times\,{\rm e}^{{\rm i}t'(\varepsilon_r+\varepsilon_s-\omega_3-\omega_4)}\,{\rm e}^{-{\rm i}t_1(\varepsilon_a-z-\omega_3)}\,{\rm e}^{-{\rm i}t_2(\varepsilon_b+z-\omega_4)}\,{\rm e}^{-\gamma(|t_1|+|t_2|)}, \qquad (214)$$

U2Cov4A

integrated over z and all the ω's. In analogy with the previous case, the time integrations yield the delta factors $\delta(\varepsilon_a-z-\omega_3)$ and $\delta(\varepsilon_b+z-\omega_4)$, and integrations over z to $\delta(\varepsilon_a+\varepsilon_b-\omega_3-\omega_4)$. Integrations over ω_4 then yield

$$\Big\langle rs\Big|U^{(2)}_{\rm Cov}(t',-\infty)\Big|ab\Big\rangle$$
$$= {\rm i}\int\frac{{\rm d}\omega_3}{2\pi}\,\frac{\Big\langle rs\Big|I(\varepsilon_a-\omega_3)\Big|ab\Big\rangle}{(\omega_3-\varepsilon_r+{\rm i}\gamma_r)(\varepsilon_a+\varepsilon_b-\omega_3-\varepsilon_s+{\rm i}\gamma_s)}\,{\rm e}^{-{\rm i}t'(q+q')}. \qquad (215)$$

U2Cov4A1

This is equivalent to the integral (A.3) with the substitution $\varepsilon_a-\omega_3\to z$. Rewriting the denominators in analogy with (294) and (A.5), we obtain

$$\Big\langle rs\Big|U^{(2)}_{\rm Cov}(t',-\infty)\Big|ab\Big\rangle = {\rm i}\frac{{\rm e}^{-{\rm i}t'(q+q')}}{q+q'}$$
$$\times\int\frac{{\rm d}\omega_3}{2\pi}\,\Big\langle rs\Big|I(\varepsilon_a-\omega_3)\Big|ab\Big\rangle\Big[\frac{1}{\omega_3-\varepsilon_r+{\rm i}\gamma_r}+\frac{1}{\varepsilon_a+\varepsilon_b-\omega_3-\varepsilon_s+{\rm i}\gamma_s}\Big]. \qquad (216)$$

U2Cov4A2

This can be compared with the phantom-particle equation (IV.22) in (?). The contribution to the effective Hamiltonian is then obtained by means of (130), which yields

$$H^{(1)}_{\rm eff} = {\rm i}\int\frac{{\rm d}\omega_3}{2\pi}\,\Big\langle rs\Big|I(\varepsilon_a-\omega_3)\Big|ab\Big\rangle\,\Big[\frac{1}{\omega_3-\varepsilon_r+{\rm i}\gamma_r}+\frac{1}{\varepsilon_a+\varepsilon_b-\omega_3-\varepsilon_s+{\rm i}\gamma_s}\Big]. \qquad (217)$$

SingPhotEffInt

This is identical to the result (302), obtained below with the nonhermitian form of the effective Hamiltonian in the Green's-function method.

5.2 Nonradiative two-photon exchange

ec:TwoPhoton

The QED effects can be separated into two categories, which we refer to as *nonradiative* and *radiative* effects. The radiative effects are characterized by

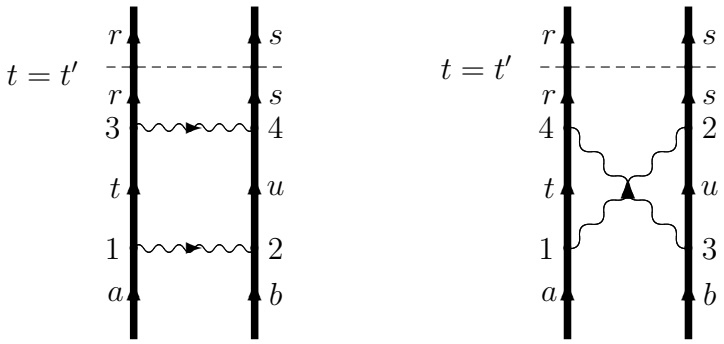

Fig. 17. The nonradiative two-photon exchange diagrams, the ladder diagram (left) and the crossed-photon diagram (right). Fig:TwoPhot

having at least one self-energy or vacuum-polarization loop, while the nonradiative effects are free from such parts. The nonradiative two-photon effect for a two-electron system is of the type shown in Fig. 17, the two-photon *ladder* and the two-photon *crossed* diagram. The ladder diagram has a substantial MBPT part in it. The crossed and the radiative diagrams have no MBPT counterpart.

The fourth-order evolution operator is according to the expansion (87) with the interaction (68)

$$\frac{1}{4!}\iiiint_{t_0}^{t} \mathrm{d}^4x_4\,\mathrm{d}^4x_3\,\mathrm{d}^4x_2\,\mathrm{d}^4x_1\;T_{\mathrm{D}}\Big[\Big(\hat{\psi}^\dagger(x)\,e\alpha^\tau A_\tau\hat{\psi}(x)\Big)_4\Big(\hat{\psi}^\dagger(x)\,e\alpha^\sigma A_\sigma\hat{\psi}(x)\Big)_3 \times\Big(\hat{\psi}^\dagger(x)\,e\alpha^\nu A_\nu\hat{\psi}(x)\Big)_2\Big(\hat{\psi}^\dagger(x)\,e\alpha^\mu A_\mu\hat{\psi}(x)\Big)_1\Big]. \tag{218}$$ U4

In order to form the two-photon exchange diagrams in Fig. 17 – the 'ladder' and the 'crossed-photon' diagrams – the contractions can be performed in 12 distinct ways, all leading to equivalent diagrams. The covariant evolution operator for the ladder diagram is then in analogy with the single-photon exchange (208)

$$U^{(4)}_{\mathrm{Cov}}(t',-\infty)_{\mathrm{Ladder}} = \tfrac{1}{2}\iint \mathrm{d}^3\boldsymbol{x}'_3\,\mathrm{d}^3\boldsymbol{x}'_4\;\hat{\psi}^\dagger(x'_3)\,\hat{\psi}^\dagger(x'_4)\iint \mathrm{d}^4x_3\,\mathrm{d}^4x_4\,\mathrm{i}S_{\mathrm{F}}(x'_3,x_3) \times \mathrm{i}S_{\mathrm{F}}(x'_4,x_4)\,\mathrm{i}I(x_4,x_3)\iint \mathrm{d}t_1\,\mathrm{d}t_2\,\mathrm{i}S_{\mathrm{F}}(x_3,x_1)\,\mathrm{i}S_{\mathrm{F}}(x_4,x_2)\,\mathrm{i}I(x_2,x_1)\,\hat{\psi}(x_1)\,\hat{\psi}(x_2) \times \mathrm{e}^{\mathrm{i}t'(\varepsilon_r+\varepsilon_s)}\,\mathrm{e}^{-\mathrm{i}t_1\varepsilon_a-\mathrm{i}t_2\varepsilon_b}\,\mathrm{e}^{-\gamma(|t_1|+|t_2|+|t_3|+|t_4|)}. \tag{219}$$ U4Cov1

The 'matrix element' then becomes after identification with the second-quantized expansion (23)

$$\Big\langle rs\Big|U^{(4)}_{\mathrm{Cov}}(t',-\infty)\Big|ab\Big\rangle = \Big\langle rs\Big|\iint \mathrm{d}^4x_3\,\mathrm{d}^4x_4\,\mathrm{i}S_{\mathrm{F}}(x'_3,x_3)\,\mathrm{i}S_{\mathrm{F}}(x'_4,x_4)\,\mathrm{i}I(x_4,x_3) \times\iint \mathrm{d}t_1\,\mathrm{d}t_2\,\mathrm{i}S_{\mathrm{F}}(x_3,x_1)\,\mathrm{i}S_{\mathrm{F}}(x_4,x_2)\,\mathrm{i}I(x_2,x_1)\Big|ab\Big\rangle \times\mathrm{e}^{\mathrm{i}t'(\varepsilon_r+\varepsilon_s)}\,\mathrm{e}^{-\mathrm{i}t_1\varepsilon_a-\mathrm{i}t_2\varepsilon_b}\,\mathrm{e}^{-\gamma(|t_1|+|t_2|+|t_3|+|t_4|)}, \tag{220}$$ U4Cov2

and similarly for the crossed diagram.

sec:SepLadd

5.2.1 *Separable ladder diagram*

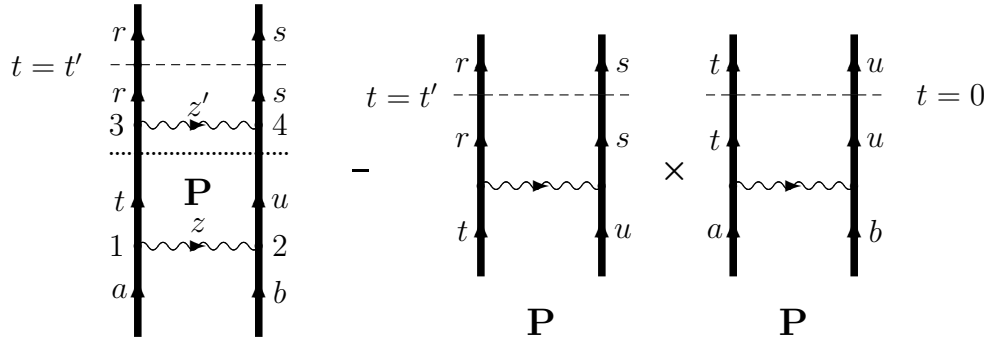

Fig. 18. Graphical representation of the reducible two-photon-photon ladder diagram and the corresponding counterterm. The dotted line represents a time with no uncontracted photon, i.e., a time after the first photon has been absorbed and before the second has been created.

TwoPhotDiag

We consider first the two-photon *ladder diagram*. Here, we distinguish between two situations, whether the two photons overlap with each other in time or not. *If the photons do not overlap in time, we refer to the diagram as being separable, and in the opposite case as being nonseparable.*

The separable two-photon ladder is illustrated by the leftmost diagram in Fig. 18. The field-theoretical evaluation is given in the Appendix A.2 (B.10), assuming all states to be *positive* energy states,

$$\left\langle rs\left|U^{(4)}_{\rm Cov}(t',-\infty)\right|ab\right\rangle_{\rm SepLadder} = \left\langle rs\middle|V(q+p',q'+p)\middle|tu\right\rangle\left\langle tu\middle|V(p,p')\middle|ab\right\rangle \times\frac{{\rm e}^{-{\rm i}t'(q+q')}}{(q+q')(p+p')}, \tag{221}$$

SepLadder

where $V(q,q')$ is the effective one-photon interaction (210), (211). The corresponding contribution to the effective interaction then becomes, using (B.10),

$$\boxed{\left\langle rs\middle|H_{\rm eff}\middle|ab\right\rangle_{\rm Sep} = \frac{\left\langle rs\middle|V(q+p',q'+p)\middle|tu\right\rangle\left\langle tu\middle|V(p,p')\middle|ab\right\rangle}{p+p'}\,.} \tag{222}$$

HeffSepLad

When the diagram is *reducible*, i.e., separable with the intermediate state in the model space, there is a *counterterm* (118), $U^{(2)}PU^{(2)}P$,

$$\left\langle rs\middle|U_{\rm Counter}\middle|ab\right\rangle = \left\langle rs\middle|U^{(2)}\middle|tu\right\rangle\left\langle tu\middle|U^{(2)}\middle|ab\right\rangle$$
$$= \left\langle rs\middle|V(q-p,q'-p')\middle|tu\right\rangle\left\langle tu\middle|V(p,p')\middle|ab\right\rangle\frac{{\rm e}^{-{\rm i}t'(q+q'-p-p')}}{(q+q'-p-p')(p+p')}. \tag{223}$$

Counter

Using the notations of (147),

$$E_{\rm in} = \varepsilon_a + \varepsilon_b,\ E_{\rm out} = \varepsilon_r + \varepsilon_s,\ \Delta E = p + p' = E_{\rm in} - \varepsilon_t - \varepsilon_u,$$

we can express the separable ladder (221) diagram as

$$\Big\langle rs \Big| U^{(4)}_{\rm Cov}(t', -\infty) \Big| ab \Big\rangle_{\rm SepLadder} =$$
$$\Big\langle rs \Big| V_2(E_{\rm in}) \Big| tu \Big\rangle \Big\langle tu \Big| V(p,p') \Big| ab \Big\rangle \, \frac{{\rm e}^{-{\rm i}t'(E_{\rm in}-E_{\rm out})}}{(E_{\rm in}-E_{\rm out})\,\Delta E} \tag{224}$$

SepLadder2

and the counterterm as

$$\Big\langle rs \Big| U_{\rm Counter} \Big| ab \Big\rangle = \Big\langle rs \Big| V_2(E_{\rm in} - \Delta E \Big| tu \Big\rangle \Big\langle tu \Big| V(p,p') \Big| ab \Big\rangle$$
$$\times \frac{{\rm e}^{-{\rm i}t'(E_{\rm in}-\Delta E-E_{\rm out})}}{(E_{\rm in}-\Delta E-E_{\rm out})\,\Delta E}, \tag{225}$$

Counter2

where $V_2(X) = V(X - \varepsilon_r - \varepsilon_u, X - \varepsilon_s - \varepsilon_t)$. The contribution to the effective interaction then becomes, using (130),

$$\frac{\Big\langle rs \Big| V_2(E_{\rm in}) \Big| tu \Big\rangle - \Big\langle rs \Big| V_2(E_{\rm in} - \Delta E) \Big| tu \Big\rangle}{\Delta E} \Big\langle tu \Big| V(p,p') \Big| ab \Big\rangle. \tag{226}$$

EffIntLadd

The leading term is here given by the *energy derivative* of the interaction,

$$\Big\langle rs \Big| \frac{\partial}{\partial E} \Big(V_2(E) \Big)_{E=E_{\rm in}} + \cdots \Big| tu \Big\rangle \Big\langle tu \Big| V(p,p') \Big| ab \Big\rangle, \tag{227}$$

LadderMSC

which demonstrates that the counterterm removes the (quasi)degeneracy of the reducible ladder diagram. This result is quite analogous to the expression for the second-order diagram, derived with time-dependent MBPT (163). A more detailed comparison with MBPT will be made in Chapter 8.

c:NonSepLadd

5.2.2 Nonseparable ladder diagram

The nonseparable ladder diagram is evaluated in Appendix B, Eq. (B.16), and the result becomes, assuming only positive-energy states are involved,

$$\Big\langle rs \Big| H_{\rm eff} \Big| ab \Big\rangle_{\rm Nonsep} = \iint {\rm d}k' {\rm d}k \, \langle rs|f(k')|tu\rangle\langle tu|f(k)|ab\rangle \times$$
$$\Big[\frac{1}{(q+p'-k')(q-k-k')(p-k)} + \frac{1}{(q'+p+k')(q'+k+k')(p'+k)} \Big]. \tag{228}$$

HeffNonsepLad

sec:CovSE

Next, we consider the radiative effects and start with the single-electron effects, treated also in the previous chapter with the S-matrix formulation, section 4.3. sec:LS

sec:SE

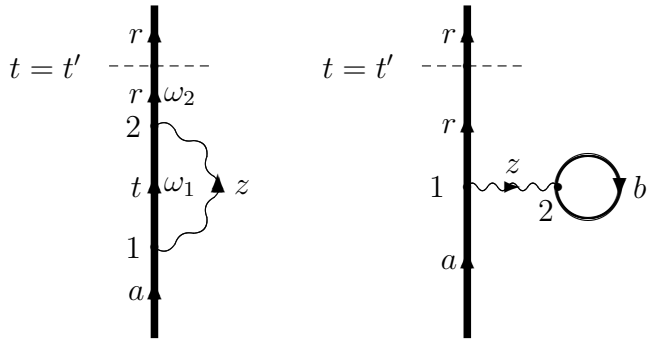

Fig. 19. The covariant-evolution-operator diagrams representing the first-order electron self-energy and vacuum polarization. Fig:LSEv

The first-order radiative effects are illustrated in Fig. 10 for the S-matrix formulation. The corresponding evolution-operator diagram are shown in Fig. 19. Here, we shall evaluate the electron self-energy diagram as an illustration. In analogy with the single-photon exchange (209) the matrix element becomes Fig:LS Fig:LSEv U2Cov4

$$\Big\langle r\Big|U^{(2)}_{\rm SE}(t',-\infty)\Big|a\Big\rangle = -\int {\rm d}^3\boldsymbol{x}'_2\,\phi^\dagger_r(\boldsymbol{x}'_2)$$
$$\times\iint {\rm d}^4x_2\,{\rm d}^4x_1\,{\rm i}S_{\rm F}(x'_2,x_2)\,{\rm i}I(x_2,x_1)\,{\rm i}S_{\rm F}(x_2,x_1)\,\phi_a(x_1)\,e^{-\gamma(|t_1|+|t_2|)}. \qquad (229)$$ SE1

Using the Fourier transform of the electron propagator (187) and of the interaction (169), this yields ElPropCoord I

$$\Big\langle r\Big|U_{\rm SE}(t',-\infty)\Big|a\Big\rangle = {\rm i}\iint\frac{{\rm d}\omega_2}{2\pi}\,\frac{{\rm d}\omega_1}{2\pi}\int\frac{{\rm d}z}{2\pi}\,\frac{\langle tr|I(z)|at\rangle}{(\omega_2-\varepsilon_r+{\rm i}\eta_r)(\omega_1-\varepsilon_t+{\rm i}\eta_t)}$$
$$\times\iint {\rm d}t_2\,{\rm d}t_2\,e^{-{\rm i}t'(\omega_2-\varepsilon_r)}\,e^{-{\rm i}t_2(\omega_1-\omega_2+z)}\,e^{-{\rm i}t_1(\varepsilon_a-\omega_1-z)}\,e^{-\gamma(|t_1|+|t_2|)}. \qquad (230)$$ SE2

Using the definition of the self-energy operator (202), the time and ω integrations yield in analogy with the single-photon exchange, treated in Appendix A.1, SelfEn SingPhotEv

$$\Big\langle r\Big|U_{\rm SE}(t',-\infty)\Big|a\Big\rangle =$$
$${\rm i}\,\frac{{\rm e}^{-{\rm i}t'(\varepsilon_a-\varepsilon_r+{\rm i}\gamma_r)}}{\varepsilon_a-\varepsilon_r+{\rm i}\gamma_r}\int\frac{{\rm d}z}{2\pi}\,\frac{\langle rt|I(z)|ta\rangle}{\varepsilon_a-\varepsilon_t-z+{\rm i}\gamma_t} = \frac{{\rm e}^{-{\rm i}t'(\varepsilon_a-\varepsilon_r+{\rm i}\gamma_r)}}{\varepsilon_a-\varepsilon_r+{\rm i}\gamma_r}\Big\langle r\Big|\Sigma(\varepsilon_a)\Big|a\Big\rangle. \qquad (231)$$ SE3

This leads to the contribution to the effective Hamiltonian, using (EffInt2 130),

$$\langle r|H_{\rm eff}^{(1)}|a\rangle = \Big\langle r\Big|\Sigma(\varepsilon_a)\Big|a\Big\rangle. \tag{232}$$

SEEffInt

The result is the same as in the S-matrix formulation (SEShift 204), when $\varepsilon_r = \varepsilon_a$. The present result, however, is valid also when the initial and final energies are different. When needed, we shall assume that the self-energy expressions are renormalized (see section sec:RenormSE 4.3.2).

5.4 Two-electron radiative effects

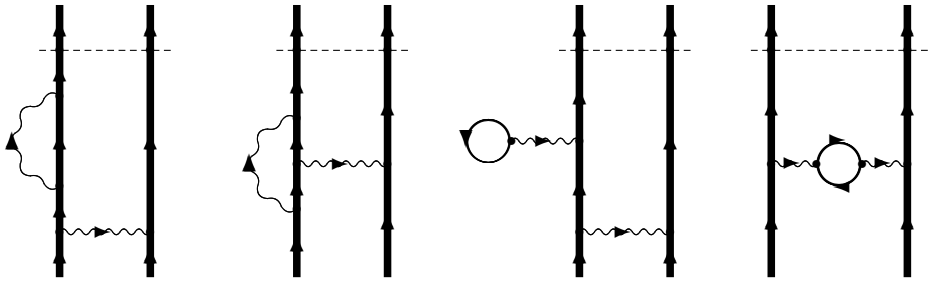

Fig. 20. The two-electron radiative effects in lowest order. The first two diagrams represent the two-electron self-energy (screened self-energy and vertex modification) and the last two represent the two-electron vacuum polarization (screened vacuum polarization and the photon self-energy).

Fig:TwoElRad

The covariant-evolution-operator diagrams for the two-electron radiative effects in lowest order are depicted in Fig. Fig:TwoElRad 20. Here, we shall treat the first of these diagrams, the screened self-energy (leftmost diagram) in some detail.

sec:ScrSEEvOp

5.4.1 Screened self-energy

The covariant evolution operator for the screened self-energy, depicted in Fig. Fig:ScrSE 21, is in analogy with the two-photon exchange (U4Cov2 220)

$$\Big\langle rs\Big|U_{\rm Cov}^{(4)}(t',-\infty)\Big|ab\Big\rangle = \iint {\rm d}t_1\,{\rm d}t_2\,\Big\langle rs\Big|\iint {\rm d}^4x_3\,{\rm d}^4x_4\,{\rm i}S_{\rm F}(x_4',x_4)\,{\rm i}S_{\rm F}(x_4,x_3)\,{\rm i}I(x_4,x_3)$$
$$\times{\rm i}S_{\rm F}(x_3,x_1)\,{\rm i}S_{\rm F}(x_2',x_2)\,{\rm i}I(x_2,x_1)\Big|ab\Big\rangle\,{\rm e}^{{\rm i}t'(\varepsilon_r+\varepsilon_s)}\,{\rm e}^{-{\rm i}t_1\varepsilon_a-{\rm i}t_2\varepsilon_b}\,{\rm e}^{-\gamma(|t_1|+|t_2|+|t_3|+|t_4|)}. \tag{233}$$

ScrSE1

Introducing the electron propagators (ElPropOp 192), this becomes after time integrations

$$\Big\langle rs\Big|U_{\rm Cov}^{(4)}(t',-\infty)\Big|ab\Big\rangle =$$
$${\rm i}\int\frac{{\rm d}\omega_3}{2\pi}\int\frac{{\rm d}\omega_4}{2\pi}\int\frac{{\rm d}\omega_5}{2\pi}\int\frac{{\rm d}z}{2\pi}\,\frac{\Big\langle r\Big|\Sigma(\omega_5)\Big|t\Big\rangle\Big\langle ts\Big|I(z)\Big|ab\Big\rangle}{(\omega_3-\varepsilon_r+{\rm i}\eta_r)(\omega_5-\varepsilon_t+{\rm i}\eta_t)(\omega_4-\varepsilon_s+{\rm i}\eta_s)}$$
$$\times\,{\rm e}^{-{\rm i}t'(\omega_3+\omega_4-\varepsilon_r-\varepsilon_s)}\,\delta(\varepsilon_a-z-\omega_5)\,\delta(\varepsilon_b+z-\omega_4)\,\delta(\omega_5-\omega_3) \tag{234}$$

ScrSEEvOp2

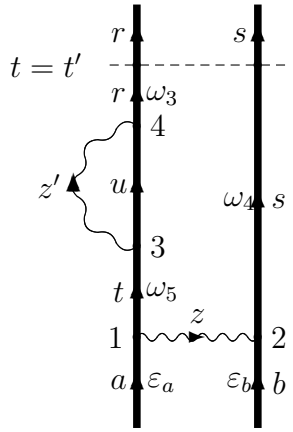

Fig. 21. The covariant-evolution-operator diagram representing the screened self-energy. (There is also a hermitian adjoint diagram, which is not necessarily identical in the nonhermitian formulation we use.)

Fig:ScrSE

and after integration over the ω's

$$\Big\langle rs\Big|U^{(4)}_{\rm Cov}(t',-\infty)\Big|ab\Big\rangle = \\ \mathrm{i}\int\frac{\mathrm{d}z}{2\pi}\,\frac{\Big\langle r\Big|\Sigma(\varepsilon_a-z)\Big|t\Big\rangle\Big\langle ts\Big|I(z)\Big|ab\Big\rangle}{(q-z+\mathrm{i}\gamma_r)(p-z+\mathrm{i}\gamma_t)(q'+z+\mathrm{i}\gamma_s)}\,\mathrm{e}^{-\mathrm{i}t'(q+q')} \qquad (235)$$

ScrSEEvOp3

with $q=\varepsilon_a-\varepsilon_r$, $p=\varepsilon_a-\varepsilon_t$, $q'=\varepsilon_b-\varepsilon_s$. Rewriting two of the denominators as before, leads to

$$\Big\langle rs\Big|U^{(4)}_{\rm Cov}(t',-\infty)\Big|ab\Big\rangle = \mathrm{i}\,\frac{\mathrm{e}^{\mathrm{i}t'(q+q')}}{(q+q')} \\ \times\int\frac{\mathrm{d}z}{2\pi}\,\frac{\Big\langle r\Big|\Sigma(\varepsilon_a-z)\Big|t\Big\rangle\Big\langle ts\Big|I(z)\Big|ab\Big\rangle}{p-z+\mathrm{i}\gamma_t}\,\Big[\frac{1}{q-z+\mathrm{i}\gamma_r}+\frac{1}{q'+z+\mathrm{i}\gamma_s}\Big]. \qquad (236)$$

The contribution to the effective Hamiltonian is then, using (130),

$$\Big\langle rs\Big|H^{(2)}_{\rm eff}\Big|ab\Big\rangle = \mathrm{i}\int\frac{\mathrm{d}z}{2\pi}\,\frac{\Big\langle r\Big|\Sigma(\varepsilon_a-z)\Big|t\Big\rangle\Big\langle ts\Big|I(z)\Big|ab\Big\rangle}{p-z+\mathrm{i}\gamma_t}\,\Big[\frac{1}{q-z+\mathrm{i}\gamma_r}+\frac{1}{q'+z+\mathrm{i}\gamma_s}\Big] \\ =-\iint\frac{\mathrm{d}z}{2\pi}\,\frac{\mathrm{d}z'}{2\pi}\,\frac{\Big\langle ru\Big|I(z')\Big|ut\Big\rangle\Big\langle ts\Big|I(z)\Big|ab\Big\rangle}{(p''-z-z'+\mathrm{i}\gamma_u)(p-z+\mathrm{i}\gamma_t)}\,\Big[\frac{1}{q-z+\mathrm{i}\gamma_r}+\frac{1}{q'+z+\mathrm{i}\gamma_s}\Big] \qquad (237)$$

ScrSEEvOp1

with $p''=\varepsilon_a-\varepsilon_u$ and with the expression (202) for the self-energy operator. The integral is evaluated in the Appendix A.3 in the Feynman gauge (77), assuming only positive-energy states are involved, which yields

$$\langle rs|H^{(2)}_{\rm eff}|ab\rangle = \iint {\rm d}k\,{\rm d}k'\,\langle ru|f(k')|ut\rangle\langle ts|f(k)|ab\rangle$$
$$\times\Big\{\frac{1}{(p''+q'-k')(p+q')}\Big[\frac{1}{p-k+{\rm i}\gamma}+\frac{1}{q'-k+{\rm i}\gamma}\Big]$$
$$+\frac{1}{(p''-k-k'+{\rm i}\gamma)(p-k+{\rm i}\gamma)}\Big[\frac{1}{p''+q'-k'+2{\rm i}\gamma}+\frac{1}{q-k+{\rm i}\gamma}\Big]\Big\}. \quad (238)$$

ScrSEEvOp4

The first term corresponds to the *separable* part, where the photons do not overlap in time, and the second term to the *nonseparable* part. The separable part can also be expressed, using the expression (203),

SelfEnInt

$$\langle rs|H^{(2)}_{\rm eff}|ab\rangle_{\rm Sep} = \langle r|\Sigma(\varepsilon_a+q')|t\rangle\int {\rm d}k\frac{\langle ts|f(k)|ab\rangle}{p+q'}\Big[\frac{1}{(p-k+{\rm i}\gamma)}+\frac{1}{(q'-k+{\rm i}\gamma)}\Big]. \quad (239)$$

ScrSESep

Reducible part

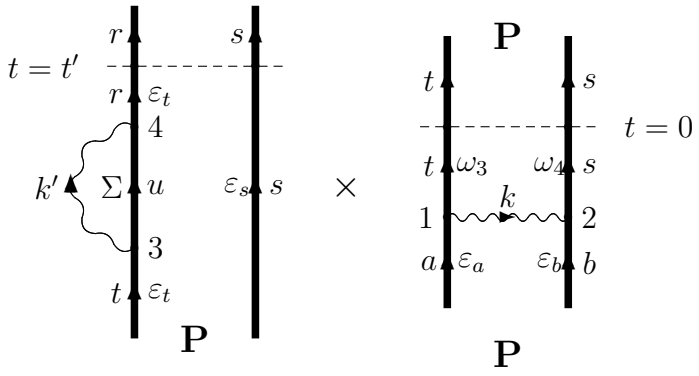

Fig. 22. The counterterm for the screened self-energy in the covariant evolution-operator method).

Fig:Counter

The separable part of the screened self-energy (239) has a *(quasi)singularity* when $\Delta = p+q' = \varepsilon_a+\varepsilon_b-\varepsilon_t-\varepsilon_s \approx 0$. This is eliminated by the counterterm in the *reduced evolution operator* (117)

UtildeExp

$$\widetilde{U}^{(4)}P = U^{(4)}P - U^{(2)}PU^{(2)}P. \quad (240)$$

Utildered

The counterterm $U^{(2)}PU^{(2)}P$, illustrated in Fig. 22, is a product of an electron self energy (232) and a single-photon exchange (211)

Fig:Counter
SEEffInt
SingPhotInt

$$\langle rs|H^{(2)}_{\rm eff}|ab\rangle_{\rm Counter} = \langle r|\Sigma(\varepsilon_t)|t\rangle$$
$$\times\int {\rm d}k\,\langle ts|f(k)|ab\rangle\Big[\frac{1}{p-k+{\rm i}\gamma}+\frac{1}{q'-k+{\rm i}\gamma}\Big]\frac{1}{p+q'}. \quad (241)$$

ScrCounterA

The difference yields the *reducible part* or the *model-space part* of the effective Hamiltonian

$$\langle rs|H^{(2)}_{\rm eff}|ab\rangle_{\rm Red} = \frac{\langle r|\Sigma(\varepsilon_t+\Delta)-\Sigma(\varepsilon_t)|t\rangle}{\Delta}$$
$$\times \int \mathrm{d}k\, \langle ts|f(k)|ab\rangle \left[\frac{1}{p-k+\mathrm{i}\gamma}+\frac{1}{q'-k+\mathrm{i}\gamma}\right] \qquad (242)$$ ScrMSCA

with $\Delta = p+q' = \varepsilon_a+\varepsilon_b-\varepsilon_t-\varepsilon_s$. In the limit of *complete degeneracy*, the first factor becomes the derivative of the self-energy with respect to the energy parameter

$$\boxed{\langle rs|H^{(2)}_{\rm eff}|ab\rangle_{\rm Red} = \left[\frac{\partial}{\partial\omega}\langle r|\Sigma(\omega)|t\rangle\right]_{\omega=\varepsilon_t}\int \mathrm{d}k\, \langle ts|f(k)|ab\rangle \left[\frac{1}{p-k+\mathrm{i}\gamma}+\frac{1}{q'-k+\mathrm{i}\gamma}\right]} \qquad (243)$$ ScrMSC1A

5.5 Fourier transform of the covariant evolution operator

Fourier

The Fourier transform of the evolution operator $U(t',-\infty)$ with respect to the time is

$$U(E) = \frac{1}{2\pi}\int \mathrm{d}t'\, \mathrm{e}^{\mathrm{i}\,Et'}\, U(t',-\infty). \qquad (244)$$ FTDef

If $U(t',-\infty)$ is of the form

$$U(t',-\infty) = F(E')\,\mathrm{e}^{-\mathrm{i}\,E't'}, \qquad (245)$$ UFT

then

$$U(E) = \delta(E-E')\,F(E'). \qquad (246)$$

Similarly, we define the Fourier transform of the *reduced* evolution operator (116) Utildet

$$\widetilde{U}(E) = \frac{1}{2\pi}\int \mathrm{d}t'\, \mathrm{e}^{\mathrm{i}\,Et'}\, \widetilde{U}(t',-\infty). \qquad (247)$$ UredFT

It follows from the form (130) EffInt2 that the energy-dependent *effective interaction* is related to the Fourier transform of the reduced evolution operator by

$$\boxed{H'_{\rm eff} = \int E\,\mathrm{d}E\,\widetilde{U}(E).} \qquad (248)$$ EffIntFT

The Fourier transform of the single-photon matrix element (210) U2Cov6 is

$$\left\langle rs\left|U^{(2)}_{\rm Cov}(E)\right|ab\right\rangle = \delta\big(E-(q+q')\big)\,\frac{\left\langle rs\middle|V(q,q')\middle|ab\right\rangle}{q+q'}, \qquad (249)$$ S2FT

and (248) EffIntFT yields the effective interaction

$$\left\langle rs\middle|H'_{\rm eff}\middle|ab\right\rangle = \left\langle rs\middle|V(q,q')\middle|ab\right\rangle \qquad (250)$$ EffInt3

in agreement with (213).

Applying the same rule to the separable two-photon matrix element (224), yields the contribution to the effective interaction

$$\left\langle rs\middle|H'_{\rm eff}\middle|ab\right\rangle_{\rm Ladder} = \frac{1}{\Delta E}\left\langle rs\middle|V_2(E_{\rm in})\middle|tu\right\rangle\left\langle tu\middle|V(p,p')\middle|ab\right\rangle, \qquad (251)$$

EffIntLadd2

and when the diagram is reducible the counterterm (225) yields

$$\left\langle rs\middle|H'_{\rm eff}\middle|ab\right\rangle_{\rm Counter} = \frac{1}{\Delta E}\left\langle rs\middle|V_2(E_{\rm in}-\Delta E)\middle|tu\right\rangle\left\langle tu\middle|V(p,p')\middle|ab\right\rangle. \qquad (252)$$

EffIntCount

This agrees with the previous result (226) in subsection 5.2.

Some applications of the covariant-evolution-operator technique are discussed in chapter 7.

6 The two-times Green's-function formalism

6.1 General

We shall now consider the two-times Green's-function method, mainly for the purpose of making comparison with the covariant-evolution-operator method, discussed in the previous chapter. For further details regarding the two-times Green's-function method, the reader is referred primarily to the recent review article by [?]) and to the thesis of [?]).

In field theory the *single-particle Green's function* is usually defined [?, Eq. 7.1) [15]

$$\mathrm{i}G(x,x_0) = \frac{\left\langle 0_{\rm H}\middle|T[\hat\psi_{\rm H}(x)\hat\psi^\dagger_{\rm H}(x_0)]\middle|0_{\rm H}\right\rangle}{\langle 0_{\rm H}|\,0_{\rm H}\rangle}, \qquad (253)$$

Green

where T is the Wick time-ordering operator (74) and $\hat\psi_{\rm H}$, $\hat\psi^\dagger_{\rm H}$ are the electron field operators in the Heisenberg representation (34). $|0_H\rangle$ is the lowest eigenstate of the Fock-space Hamiltonian, $\hat H$, in this representation – or the *'Heisenberg vacuum'* – which is time independent. This state satisfies the condition

$$\hat\psi_{\rm H}(x)\,|0_{\rm H}\rangle = 0. \qquad (254)$$

Vacuum

[15] Often the Green's function is defined using $\hat{\bar\psi}_{\rm H} = \hat\psi^\dagger_{\rm H}\gamma^0$ instead of $\hat\psi^\dagger_{\rm H}$ and sometimes without the imaginary unit; see e.g. [?, Eq. 6-1)

In the interaction picture (IP) the vacuum evolves in time according to the definition (84),

$$|0_{\rm I}(t)\rangle = U(t,t_0)\,|0_{\rm I}(t_0)\rangle. \tag{255}$$

VacIP

The 'unperturbed' vacuum in the IP is $|0\rangle = |0_{\rm I}(-\infty)\rangle$, assuming an adiabatic damping (88), and is related to the Heisenberg vacuum by

$$|0_{\rm H}\rangle = |0_{\rm I}(t=0)\rangle = U(0,-\infty)\,|0\rangle. \tag{256}$$

PertVac

The relation between operators in the HP and the IP is given in Eq. (32)

$$\hat{O}_{\rm H}(t) = {\rm e}^{{\rm i}\hat{H}'t}\,O_{\rm I}\,{\rm e}^{-{\rm i}H't} = U(0,t)\,O_{\rm I}\,U(t,0), \tag{257}$$

HPIPU

and we can then transform the Green's function (253) to the interaction picture

$${\rm i}G(x,x_0) = \frac{\Big\langle 0\Big|U(\infty,0)\,T\Big[U(0,t)\hat{\psi}(x)U(t,0)U(0,t_0)\hat{\psi}^\dagger(x_0)U(t_0,0)\Big]\,U(0,-\infty)\Big|0\Big\rangle}{\Big\langle 0\Big|U(\infty,-\infty)\Big|0\Big\rangle}, \tag{258}$$

which, using (87), can be transformed into (?, Sec. 8), (?, Eq. 3)

$$\boxed{{\rm i}G(x,x_0) = \frac{\Big\langle 0\Big|\,T\Big\{\,\exp\Big[-{\rm i}\int_{-\infty}^{\infty}{\rm d}^4\xi\,\hat{\mathcal{H}}'_{\rm I}(\xi)\Big]\,\hat{\psi}(x)\hat{\psi}^\dagger(x_0)\Big\}\,\Big|0\Big\rangle}{\Big\langle 0\Big|\,T\,\exp\Big[-{\rm i}\int_{-\infty}^{\infty}{\rm d}^4\xi\,\hat{\mathcal{H}}'_{\rm I}(\xi)\Big]\,\Big|0\Big\rangle}.} \tag{259}$$

GreenIP

It can be shown that the denominator in the expression (259) has the effect of removing all *unlinked (unconnected) diagrams*, and the result can be expressed (?, Eq. 9.5)

$$\begin{aligned}{\rm i}G(x,x_0) &= \Big\langle 0\Big|T\Big\{\,\exp\Big[-{\rm i}\int_{-\infty}^{\infty}{\rm d}^4\xi\,\mathcal{H}'(\xi)\Big]\,\hat{\psi}(x)\hat{\psi}^\dagger(x_0)\Big\}\Big|0\Big\rangle_{\rm conn}\\ &= \sum_{n=0}^{\infty}\frac{(-{\rm i})^n}{n!}\int_{-\infty}^{\infty}{\rm d}^4x_1\cdots\int_{-\infty}^{\infty}{\rm d}^4x_n\,\Big\langle 0\Big|T\Big[\mathcal{H}'(x_1)\cdots\mathcal{H}'(x_n)\,\hat{\psi}(x)\hat{\psi}^\dagger(x_0)\Big]\Big|0\Big\rangle_{\rm conn}. \end{aligned} \tag{260}$$

GreenLink

This leads to the expansion

$$\begin{aligned}&{\rm i}G_0(x,x_0) = \Big\langle 0\Big|T[\hat{\psi}(x)\hat{\psi}^\dagger(x_0)]\Big|0\Big\rangle\\ &{\rm i}G_1(x,x_0) = -{\rm i}\Big\langle 0\Big|\int_{-\infty}^{\infty}{\rm d}^4x_1\,T\Big[\mathcal{H}'(x_1)\,\hat{\psi}(x)\hat{\psi}^\dagger(x_0)\Big]\Big|0\Big\rangle_{\rm conn}\\ &{\rm i}G_2(x,x_0) = -\tfrac{1}{2}\Big\langle 0\Big|\int_{-\infty}^{\infty}{\rm d}^4x_1\int_{-\infty}^{\infty}{\rm d}^4x_2\,T\Big[\mathcal{H}'(x_1)\mathcal{H}'(x_2)\,\hat{\psi}(x)\hat{\psi}^\dagger(x_0)\Big]\Big|0\Big\rangle_{\rm conn}\\ &\text{etc.}\end{aligned} \tag{261}$$

GreenExp

The *n-particle Green's function* is defined in an analogous way

$$\mathrm{i}G(x_1', x_2' \cdots x_n'; x_{10}, x_{20} \cdots x_{n0}) = \frac{\Big\langle 0_H \Big| T\Big[\hat{\psi}_{\mathrm{H}}(x_1') \cdots \hat{\psi}_{\mathrm{H}}(x_n')\, \hat{\psi}^\dagger_{\mathrm{H}}(x_{10}) \cdots \hat{\psi}^\dagger_{\mathrm{H}}(x_{n0})\Big] \Big| 0_H \Big\rangle}{\Big\langle 0_H \Big| 0_H \Big\rangle}, \tag{262}$$

nGreen

which leads to the expansion in the interaction picture

$$\mathrm{i}G(x_1', x_2' \cdots x_n'; x_{10}, x_{20} \cdots x_{n0}) = \sum_{n=0}^{\infty} \frac{(-\mathrm{i})^n}{n!} \int_{-\infty}^{\infty} \mathrm{d}^4 x_1 \cdots \int_{-\infty}^{\infty} \mathrm{d}^4 x_n$$
$$\times \Big\langle 0 \Big| T\Big[\hat{\mathcal{H}}'(x_1) \cdots \mathcal{H}'(x_n)\, \hat{\psi}_H(x_1') \cdots \hat{\psi}_H(x_n')\, \hat{\psi}^\dagger(x_{10}) \cdots \hat{\psi}^\dagger(x_{n0})\Big] \Big| 0 \Big\rangle_{\mathrm{conn}}. \tag{263}$$

nGreenIPLink

If we set all incoming times $t_{i0} = t_0$ and all outgoing times $t_i = t'$, we have the *two-times Green's function*, extensively discussed by Shabaev *et al.* (?????). Shab02,Sh93,Sh94,SF94,ABP00

6.2 The Fourier transform of the two-times Green's function

sec:FTGF

Assuming the vacuum state is normalized, we have from the definition (253) Green

$$\mathrm{i}G(x, x_0) = \Big\langle 0_{\mathrm{H}} \Big| T\Big[\hat{\psi}_{\mathrm{H}}(x)\, \hat{\psi}^\dagger_{\mathrm{H}}(x_0)\Big] \Big| 0_{\mathrm{H}} \Big\rangle$$
$$= \Theta(t - t_0) \Big\langle 0_{\mathrm{H}} \Big| \hat{\psi}_{\mathrm{H}}(x)\, \hat{\psi}^\dagger_{\mathrm{H}}(x_0) \Big| 0_{\mathrm{H}} \Big\rangle - \Theta(t_0 - t) \Big\langle 0_{\mathrm{H}} \Big| \hat{\psi}^\dagger_{\mathrm{H}}(x_0)\, \hat{\psi}_{\mathrm{H}}(x) \Big| 0_{\mathrm{H}} \Big\rangle. \tag{264}$$

GreenH

Considering $t > t_0$, we have, from the definition (34), ElFieldHP

$$\mathrm{i}G_+(x, x_0) = \Big\langle 0_{\mathrm{H}} \Big| \hat{\psi}_{\mathrm{H}}(x)\, \hat{\psi}^\dagger_{\mathrm{H}}(x_0) \Big| 0_{\mathrm{H}} \Big\rangle = \Big\langle 0_{\mathrm{H}} \Big| \Big(\mathrm{e}^{\mathrm{i}\hat{H}t} \hat{\psi}_{\mathrm{S}}(\boldsymbol{x}) \mathrm{e}^{-\mathrm{i}\hat{H}t} \Big) \Big(\mathrm{e}^{\mathrm{i}\hat{H}t_0} \hat{\psi}^\dagger_{\mathrm{S}}(\boldsymbol{x}_0) \mathrm{e}^{-\mathrm{i}\hat{H}t_0} \Big) \Big| 0_{\mathrm{H}} \Big\rangle. \tag{265}$$

GreenH+

We insert a complete set of positive-energy eigenstates of the Hamiltonian $\hat{H}$ (27) between the field operators, HamSecQuant

$$\hat{H}\, |n\rangle = E_n\, |n\rangle, \tag{266}$$

Eigenvalue

which yields the *Lehmann representation*

$$\mathrm{i}G_+(x, x_0) = \sum_n \Big\langle 0_{\mathrm{H}} \Big| \mathrm{e}^{\mathrm{i}\hat{H}t} \hat{\psi}_{\mathrm{S}}(x) \Big| n \Big\rangle\, \mathrm{e}^{-\mathrm{i}E_n(t-t_0)} \Big\langle n \Big| \hat{\psi}^\dagger_{\mathrm{S}}(x_0)\, \mathrm{e}^{-\mathrm{i}\hat{H}t} \Big| 0_{\mathrm{H}} \Big\rangle$$
$$= \sum_n \Big\langle 0_{\mathrm{H}} \Big| \hat{\psi}_{\mathrm{S}}(x) \Big| n \Big\rangle\, \mathrm{e}^{-\mathrm{i}E_n(t-t_0)} \Big\langle n \Big| \hat{\psi}^\dagger_{\mathrm{S}}(x_0) \Big| 0_{\mathrm{H}} \Big\rangle, \tag{267}$$

Lehmann

setting the energy of the vacuum to zero. We can now perform a Fourier transform of the Green's function, including the *adiabatic damping* $\mathrm{e}^{-\gamma\tau}$ (see section 3.3), yielding ($\tau = t - t_0 > 0$) sec:GML

$$G_+(\boldsymbol{x}, \boldsymbol{x}_0, E) = \int_0^\infty \mathrm{d}\tau\, \mathrm{e}^{\mathrm{i}E\tau}\, G_+(\boldsymbol{x}, \boldsymbol{x}_0, \tau) = \sum_n \frac{\Big\langle 0_{\mathrm{H}} \Big| \hat{\psi}_S(\boldsymbol{x}) \Big| n \Big\rangle \Big\langle n \Big| \hat{\psi}^\dagger_S(\boldsymbol{x}_0) \Big| 0_{\mathrm{H}} \Big\rangle}{E - E_n + \mathrm{i}\gamma}, \tag{268}$$

GreenFT

using
$$\int_0^\infty \mathrm{d}t\, \mathrm{e}^{\mathrm{i}\alpha t}\, \mathrm{e}^{-\gamma t} = \frac{\mathrm{i}}{\alpha + \mathrm{i}\gamma}. \tag{269}$$
delta

We then see that *the poles of the Green's function represent the true eigenvalues of the system*. Assuming no degeneracy, the eigenvalues can be obtained from the formula (Shab02 ?, Eq.44)

$$\boxed{E_n = \frac{\oint_{\Gamma_n} \mathrm{d}E\, E\, G_+(\boldsymbol{x}, \boldsymbol{x}_0, E)}{\oint_{\Gamma_n} \mathrm{d}E\, G_+(\boldsymbol{x}, \boldsymbol{x}_0, E)}} \tag{270}$$
Energy

where the contour Γ_n encircles the pole in question (and no other). This formula can be compared with the corresponding formula for the covariant evolution operator (EffIntFT 248).

The eigenstates $|n\rangle$ in the eigenvalue equation (Eigenvalue 266) are *Fock states*, and the functions
$$\Psi_n(\boldsymbol{x}) = \langle n|\hat{\psi}_{\mathrm{S}}^\dagger(\boldsymbol{x})|0_{\mathrm{H}}\rangle \tag{271}$$
EigenfcnS
are the corresponding wavefunctions in configuration space (in the Schrödinger representation). [Formally, these functions can be expressed as eigenfunctions of a hypothetical Hamiltonian in configuration space (H) that corresponds to the Fock-space Hamiltonian ($\hat{H}$),
$$H\, \Psi_n(\boldsymbol{x}) = E_n\, \Psi_n(\boldsymbol{x}).] \tag{272}$$
HamHilb

We can then express the Fourier transform (GreenFT 268) of the Green's function
$$G_+(\boldsymbol{x}, \boldsymbol{x}_0, E) = \sum_n \frac{\Psi_n(\boldsymbol{x})\, \Psi_n^\dagger(\boldsymbol{x}_0)}{E - E_n + \mathrm{i}\gamma}. \tag{273}$$
GreenFT2

Note, that this is the *exact* single-particle Green's function (positive-energy or retarded part), since the states are eigenstates of the exact Hamiltonian (c.f. (ElPropFour 186)). With no degeneracy, the numerator in (Energy 270) then becomes
$$\oint_{\Gamma_n} \mathrm{d}E\, E\, G_+(\boldsymbol{x}, \boldsymbol{x}_0, E) = \Psi_n(\boldsymbol{x})\, E_n \Psi_n^\dagger(\boldsymbol{x}_0) \tag{274}$$
IntE

with no summation over n, and since the denominator is then $\Psi_n(\boldsymbol{x})\, \Psi_n^\dagger(\boldsymbol{x}_0)$, the result (Energy 270) follows directly.

The retarded Green's function (GreenFT2 273) can also be written
$$G_+(\boldsymbol{x}, \boldsymbol{x}_0, E) = \sum_n \frac{\langle \boldsymbol{x}|\Psi_n\rangle\, \langle \Psi_n|\boldsymbol{x}_0\rangle}{E - E_n + \mathrm{i}\gamma}, \tag{275}$$
GreenFT3

which is the coordinate representation of a (retarded) *'Green's-function operator'* (c.f. Eq. (ElPropDiracFour 188))
$$\hat{G}_+(E) = \sum_n \frac{|\Psi_n\rangle\, \langle \Psi_n|}{E - E_n + \mathrm{i}\gamma}. \tag{276}$$
GreenOp

The single-particle Green's function depends on time through a single time variable $\tau = t - t_0$, as follows from the Lehmann representation (267). The procedure above can easily be generalized to many particles, if we *set all final times equal to* t *and all initial times equal to* t_0.

6.3 Extended model space. (Quasi)degeneracy

Degen

Essentially following Shabaev (?, Sec. 2.5.8), (??) we shall now extend the treatment of the two-times-Green's-function formalism to the case of degeneracy or quasi-degeneracy in the model space by means of an *extended model space*, in close analogy with the treatment of time-independent and time-dependent MBPT in the previous sections (sect. 2.2 and 3.3.2) (see also (?)). As in section 2.2, we introduce a *model space* (D) of dimensionality d, which contains the model states of all degenerate or quasi-degenerate states. The model space is spanned by eigenfunctions of the unperturbed Hamiltonian

$$H_0\Phi_i = E_0^i\Phi_i \qquad (i = 1, 2\cdots d). \tag{277}$$

BasisFcns1

The matrix of the retarded Green's-function operator (276) in this basis is then

$$\langle\Phi_i|\hat{G}_+(E)|\Phi_j\rangle = \langle i|\hat{G}_+(E)|j\rangle = \sum_n \frac{\langle i|\Psi_n\rangle\,\langle\Psi_n|j\rangle}{E - E_n + \mathrm{i}\gamma}. \tag{278}$$

Gmatrix

$\langle i|\Psi_n\rangle$ is the projection of the state $|\Psi_n\rangle$ onto the model-space state $|i\rangle$, and the entire projection,

$$\hat{P}\,|\Psi_n\rangle = \sum_{i=1}^{d} |i\rangle\langle i|\Psi_n\rangle = |\Psi_n^0\rangle, \tag{279}$$

ModelFcn

is the *zeroth-order or model state* corresponding to the *target state* $|\Psi_n\rangle$ in intermediate normalization (12).

We now construct the $\mathcal{P}$ matrix with the elements

$$\mathcal{P}_{ij} = \langle i|\hat{\mathcal{P}}|j\rangle = \frac{1}{2\pi\mathrm{i}}\oint_{\Gamma_D} \mathrm{d}E\,\langle i|\hat{G}_+(E)|j\rangle = \sum_D \langle i|\Psi_n\rangle\langle\Psi_n|j\rangle = \sum_D \langle i|\Psi_n^0\rangle\langle\Psi_n^0|j\rangle \tag{280}$$

Pmatrix

and the analogous $\mathcal{K}$ matrix

$$\mathcal{K}_{ij} = \langle i|\hat{\mathcal{K}}|j\rangle = \frac{1}{2\pi\mathrm{i}}\oint_{\Gamma_D} \mathrm{d}E\,E\,\langle i|\hat{G}_+(E)|j\rangle = \sum_D \langle i|\Psi_n\rangle E_n\langle\Psi_n|j\rangle = \sum_D \langle i|\Psi_n^0\rangle E_n\langle\Psi_n^0|j\rangle. \tag{281}$$

Kmatrix

Here, the integration is performed around all poles corresponding to the target states, and the summations are then restricted to these states. $\hat{\mathcal{P}}$, $\hat{\mathcal{K}}$ are the

corresponding *operators*

$$\hat{\mathcal{P}} = \sum_D |\Psi_n^0\rangle\langle\Psi_n^0| \,; \qquad \hat{\mathcal{K}} = \sum_D |\Psi_n^0\rangle E_n \langle\Psi_n^0|. \tag{282}$$

PKop

The model states $|\Psi_n^0\rangle$ are not necessarily orthonormal. For that reason we introduce a '*dual set*' of states in the model space, $|\widetilde{\Psi}_n^0\rangle$, defined by

$$\langle\Psi_m^0|\widetilde{\Psi}_n^0\rangle = \langle\widetilde{\Psi}_n^0|\Psi_m^0\rangle = \delta_{mn}. \tag{283}$$

DualStates

It then follows that

$$\hat{\mathcal{P}}\,|\widetilde{\Psi}_n^0\rangle = |\Psi_n^0\rangle \quad \text{and} \quad \hat{\mathcal{P}}^{-1}|\Psi_n^0\rangle = |\widetilde{\Psi}_n^0\rangle. \tag{284}$$

PDual

With these notations

$$\hat{\mathcal{P}}^{-1} = \sum_D |\widetilde{\Psi}_n^0\rangle\langle\widetilde{\Psi}_n^0|, \tag{285}$$

Pinv

and the standard projection operator for the model space (15) becomes

$$\hat{P} = \sum_D |\Psi_n^0\rangle\langle\widetilde{\Psi}_n^0| = \sum_D |\widetilde{\Psi}_n^0\rangle\langle\Psi_n^0|. \tag{286}$$

P

It also follows that

$$\hat{\mathcal{K}}\,\hat{\mathcal{P}}^{-1}|\Psi_n^0\rangle = E_n\,|\Psi_n^0\rangle, \tag{287}$$

EffHamNonHerm

which implies that

$$\boxed{\hat{\mathcal{K}}\,\hat{\mathcal{P}}^{-1} = \sum_D |\Psi_n^0\rangle E_n \langle\widetilde{\Psi}_n^0|} \tag{288}$$

EffHamG

is an *effective Hamiltonian*, which operates within the model space and generates the exact energies of the corresponding target states. This is completely equivalent to the effective Hamiltonian introduced in the MBPT section (13). In both cases the operator is *nonhermitian*, and the eigenstates are the model states, which are in general nonorthogonal. As shown by (???), (??), it is possible to express the effective Hamiltonian (288) in a *hermitian form*

$$\boxed{\left(\hat{\mathcal{P}}^{-1/2}\hat{\mathcal{K}}\hat{\mathcal{P}}^{-1/2}\right)\left|\hat{\mathcal{P}}^{-1/2}\Psi_n^0\right\rangle = E_n\left|\hat{\mathcal{P}}^{-1/2}\Psi_n^0\right\rangle.} \tag{289}$$

EffHamHerm

This is equivalent to the hermitian form of the MBPT effective Hamiltonian introduced by des Cloizeaux (??).

The two-times Green's function for single-photon exchange, represented in Fig. 23, is obtained from the expansion (263), considering only relevant contractions for this case,

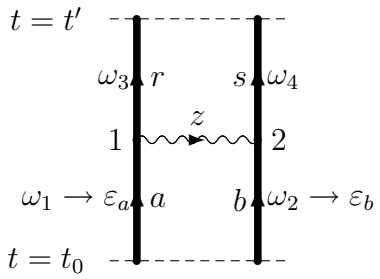

Fig. 23. The two-times Green's function for single-photon exchange between the electrons. Fig:SingPhotGF

$$
\begin{aligned}
&\mathrm{i}G(x_1', x_2'; x_{10}, x_{20}) = \\
&= -\tfrac{1}{2} \iint \mathrm{d}^4x_1 \mathrm{d}^4x_2 \left\langle 0 \middle| T\Big[\hat{\mathcal{H}}'(x_1)\hat{\mathcal{H}}'(x_2)\, \hat{\psi}(x_1')\hat{\psi}(x_2')\, \hat{\psi}^\dagger(x_{10})\hat{\psi}^\dagger(x_{20})\Big] \middle| 0 \right\rangle \\
&= -\tfrac{1}{2} \iint \mathrm{d}^4x_1\, \mathrm{d}^4x_2\, \mathrm{i}S_\mathrm{F}(x_1', x_1)\, \mathrm{i}S_\mathrm{F}(x_2', x_2)\, \mathrm{i}I(x_2, x_1)\, \mathrm{i}S_\mathrm{F}(x_1, x_{10})\, \mathrm{i}S_\mathrm{F}(x_2, x_{20}), \quad (290)
\end{aligned}
$$

GreenSingPhot

using (68) $\hat{\mathcal{H}}_\mathrm{I}'(x) = -e\hat{\psi}^\dagger(x)\, \alpha^\mu A_\mu \hat{\psi}(x)$ and (169) $I(x_2, x_1) = e\alpha_1^\mu D_{\mathrm{F}\nu\mu}(x_2 - x_1)\, e\alpha_2^\nu$. We shall now evaluate this expression in some detail.

Using the form (187) of the electron propagator, we have

$$
\begin{aligned}
&G(x_1', x_2'; x_{10}, x_{20}) = -\frac{1}{2} \iint \mathrm{d}^4x_1\, \mathrm{d}^4x_2\, \frac{\langle \boldsymbol{x}_1'|r\rangle\langle r|\boldsymbol{x}_1\rangle}{\omega_3 - \varepsilon_r + \mathrm{i}\eta_r}\, \frac{\langle \boldsymbol{x}_2'|s\rangle\langle s|\boldsymbol{x}_2\rangle}{\omega_4 - \varepsilon_s + \mathrm{i}\eta_s}\, I(\boldsymbol{x}_2, \boldsymbol{x}_1, z) \\
&\times \frac{\langle \boldsymbol{x}_1|a\rangle\langle a|\boldsymbol{x}_{10}\rangle}{\omega_1 - \varepsilon_a + \mathrm{i}\eta_a}\, \frac{\langle \boldsymbol{x}_2|b\rangle\langle b|\boldsymbol{x}_{20}\rangle}{\omega_2 - \varepsilon_b + \mathrm{i}\eta_b}\, \mathrm{e}^{-\mathrm{i}\omega_3(t'-t_1)}\, \mathrm{e}^{-\mathrm{i}\omega_4(t'-t_2)}\, \mathrm{e}^{-\mathrm{i}z(t_2-t_1)}\, \mathrm{e}^{-\mathrm{i}\omega_1(t_1-t_0)}\, \mathrm{e}^{-\mathrm{i}\omega_2(t_2-t_0)}, \quad (291)
\end{aligned}
$$

SingPh

integrated also over z and the ω's. The time integrations of t_1 and t_2, performed over all times, yield according to the formula (174) the factors $\delta(\omega_1 - z - \omega_3)$ and $\delta(\omega_2 + z - \omega_4)$, respectively, and the integration over z leads to $\delta(\omega_1 + \omega_2 - \omega_3 - \omega_4)$. As in the covariant-evolution-operator method, the adiabatic damping can here be performed individually for each vertex, and we can therefore directly replace the time integrations (174) by Dirac delta functions.

The Fourier transform of $G(x_1', x_2'; x_{10}, x_{20})$ with respect to the times t' and t_0 is

$$
\begin{aligned}
&\frac{1}{(2\pi)^2} \iint \mathrm{d}t'\, \mathrm{d}t_0\, \mathrm{e}^{\mathrm{i}E't'}\, \mathrm{e}^{-\mathrm{i}Et_0}\, G(x_1', x_2'; x_{10}, x_{20}) \\
&\Rightarrow \delta(E' - \omega_3 - \omega_4)\, \delta(E - \omega_1 - \omega_2)\, G(E, E').
\end{aligned}
$$

Integrations over ω_2 and ω_4 lead to the delta function $\delta(E' - E)$, which can be eliminated together with the delta function $\delta(\omega_1 + \omega_2 - \omega_3 - \omega_4)$ above, yielding the matrix element (c.f. 209)

$$\Big\langle rs\Big|G(E)\Big|ab\Big\rangle = -\iint \frac{\mathrm{d}\omega_1}{2\pi}\,\frac{\mathrm{d}\omega_3}{2\pi}$$
$$\times \frac{\Big\langle rs\Big|I(\omega_1-\omega_3)\Big|ab\Big\rangle}{(\omega_3-\varepsilon_r+\mathrm{i}\gamma_r)(E-\omega_3-\varepsilon_s+\mathrm{i}\gamma_s)\,(\omega_1-\varepsilon_a+\mathrm{i}\gamma_a)\,(E-\omega_1-\varepsilon_b+\mathrm{i}\gamma_b)}. \quad (292)$$ GF

The effective Hamiltonian is given by (289) EffHamHerm

$$H_{\mathrm{eff}} = \mathcal{P}^{-1/2}\,\mathcal{K}\,\mathcal{P}^{-1/2} \quad (293a)$$ HeffG

$$\mathcal{K} = \frac{1}{2\pi\mathrm{i}}\oint_\Gamma E\,\mathrm{d}E\,G(E) \quad (293b)$$ K

$$\mathcal{P} = \frac{1}{2\pi\mathrm{i}}\oint_\Gamma \mathrm{d}E\,G(E), \quad (293c)$$ PG

where the integration Γ should be performed in the positive direction and enclose the unperturbed energies of the initial ($E^0_{\mathrm{in}} = \varepsilon_a + \varepsilon_b$) and final states ($E^0_{\mathrm{out}} = \varepsilon_r + \varepsilon_s$) but no other unperturbed energies.

The denominators in (292) GF can be rewritten as

$$\left[\frac{1}{(\omega_3-\varepsilon_r+\mathrm{i}\gamma_r)}+\frac{1}{(E-\omega_3-\varepsilon_s+\mathrm{i}\gamma_s)}\right]\frac{1}{E-E^0_{\mathrm{out}}+\mathrm{i}\gamma_r+\mathrm{i}\gamma_s}$$
$$\times\left[\frac{1}{(\omega_1-\varepsilon_a+\mathrm{i}\gamma_a)}+\frac{1}{(E-\omega_1-\varepsilon_b+\mathrm{i}\gamma_b)}\right]\frac{1}{E-E^0_{\mathrm{in}}+\mathrm{i}\gamma_a+\mathrm{i}\gamma_b}, \quad (294)$$ Phantom

which corresponds to the *phantom-particle diagrams*, discussed by LeBigot (?, LeB01 Eq. IV.24). In the $\mathcal{K}$ integral (293b) K the poles E^0_{in} and E^0_{out} contribute. The former yields

$$\left[\frac{1}{(\omega_3-\varepsilon_r+\mathrm{i}\gamma_r)}+\frac{1}{(E^0_{\mathrm{in}}-\omega_3-\varepsilon_s+\mathrm{i}\gamma_s)}\right]\frac{E^0_{\mathrm{in}}}{E^0_{\mathrm{in}}-E^0_{\mathrm{out}}}$$
$$\times\left[\frac{1}{(\omega_1-\varepsilon_a+\mathrm{i}\gamma_a)}+\frac{1}{(\varepsilon_a-\omega_1+\mathrm{i}\gamma_b)}\right],$$

where the last bracket leads to the delta function $-2\pi\mathrm{i}\,\delta(\omega_1-\varepsilon_a)$ (indicated by $\omega_1 \to \varepsilon_a$ in Fig. 23) Fig:SingPhotGF. Similarly, the other pole yields

$$-2\pi\mathrm{i}\,\delta(\omega_3-\varepsilon_r)\,\frac{E^0_{\mathrm{out}}}{E^0_{\mathrm{out}}-E^0_{\mathrm{in}}}\left[\frac{1}{(\omega_1-\varepsilon_a+\mathrm{i}\gamma_a)}+\frac{1}{(E^0_{\mathrm{out}}-\omega_1-\varepsilon_b+\mathrm{i}\gamma_b)}\right].$$

Integrating the first contribution over ω_1 and the second over ω_3, gives the matrix elements

$$\langle rs|\hat{\mathcal{K}}|ab\rangle =$$
$$\mathrm{i}\int\frac{\mathrm{d}\omega_3}{2\pi}\,\langle rs\,|I(\varepsilon_a-\omega_3)|\,ab\rangle\,\frac{E^0_{\mathrm{in}}}{E^0_{\mathrm{in}}-E^0_{\mathrm{out}}}\left[\frac{1}{(\omega_3-\varepsilon_r+\mathrm{i}\gamma_r)}+\frac{1}{(E^0_{\mathrm{in}}-\omega_3-\varepsilon_s+\mathrm{i}\gamma_s)}\right]$$
$$+\mathrm{i}\int\frac{\mathrm{d}\omega_1}{2\pi}\,\langle rs\,|I(\omega_1-\varepsilon_r)|\,ab\rangle\,\frac{E^0_{\mathrm{out}}}{E^0_{\mathrm{out}}-E^0_{\mathrm{in}}}\left[\frac{1}{(\omega_1-\varepsilon_a+\mathrm{i}\gamma_a)}+\frac{1}{(E^0_{\mathrm{out}}-\omega_1-\varepsilon_b+\mathrm{i}\gamma_b)}\right], \quad (295)$$ Kelem

which is identical to the Eq. (25) in [?]. ABP00

In a similar way we obtain the $\mathcal{P}$ integral (293c) PG

$$\begin{aligned}
&\langle rs|\hat{\mathcal{P}}|ab\rangle = \\
&\mathrm{i}\int\frac{\mathrm{d}\omega_3}{2\pi}\,\langle rs\,|I(\varepsilon_a-\omega_3)|\,ab\rangle\,\frac{1}{E^0_{\rm in}-E^0_{\rm out}}\left[\frac{1}{(\omega_3-\varepsilon_r+\mathrm{i}\gamma_r)}+\frac{1}{(E^0_{\rm in}-\omega_3-\varepsilon_s+\mathrm{i}\gamma_s)}\right]\\
&+\mathrm{i}\int\frac{\mathrm{d}\omega_1}{2\pi}\,\langle rs\,|I(\omega_1-\varepsilon_r)|\,ab\rangle\,\frac{1}{E^0_{\rm out}-E^0_{\rm in}}\left[\frac{1}{(\omega_1-\varepsilon_a+\mathrm{i}\gamma_a)}+\frac{1}{(E^0_{\rm out}-\omega_1-\varepsilon_b+\mathrm{i}\gamma_b)}\right], \quad (296)
\end{aligned}$$ Pelem

which is the same as Eq. (26) in [?]. Expanding (293a) yields in first order ABP00 HeffG

$$H^{(1)}_{\rm eff}=\mathcal{K}^{(1)}-\frac{1}{2}\mathcal{P}^{(1)}\mathcal{K}^{(0)}-\frac{1}{2}\mathcal{K}^{(0)}\mathcal{P}^{(1)}, \quad (297)$$ HeffG1

where $\mathcal{K}^{(0)}_{ij}=\delta_{ij}\,E^0_i$. This yields the contribution to the matrix element

$$\begin{aligned}
&\langle rs|H^{(1)}_{\rm eff}|ab\rangle=\langle rs|\mathcal{K}^{(1)}|ab\rangle-\frac{1}{2}\left(E^0_{\rm in}+E^0_{\rm out}\right)\langle rs|\mathcal{P}^{(1)}|ab\rangle\\
&=\frac{\mathrm{i}}{2}\int\frac{\mathrm{d}\omega_3}{2\pi}\,\langle rs\,|I(\varepsilon_a-\omega_3)|\,ab\rangle\left[\frac{1}{(\omega_3-\varepsilon_r+\mathrm{i}\gamma_r)}+\frac{1}{(E^0_{\rm in}-\omega_3-\varepsilon_s+\mathrm{i}\gamma_s)}\right]\\
&+\frac{\mathrm{i}}{2}\int\frac{\mathrm{d}\omega_1}{2\pi}\,\langle rs\,|I(\omega_1-\varepsilon_r)|\,ab\rangle\left[\frac{1}{(\omega_1-\varepsilon_a+\mathrm{i}\gamma_a)}+\frac{1}{(E^0_{\rm out}-\omega_1-\varepsilon_b+\mathrm{i}\gamma_b)}\right]. \quad (298)
\end{aligned}$$ HeffG2

The photon interaction $I(z)$ has in the Feynman gauge the form (77) Interact

$$I(z)=\int\mathrm{d}k\,\frac{2k\,f(k)}{z^2-k^2+\mathrm{i}\eta};\qquad f(k)=-\frac{\mathrm{e}^2\alpha_1^\mu\,\alpha_{2\mu}}{4\pi^2\,r_{12}}\,\sin(k\,r_{21}).$$

Nonherm

Assuming r and s to be *positive-energy* states, we integrate over ω_3 in the negative half plane (poles at $\varepsilon_r-\mathrm{i}\gamma$ and $\varepsilon_a+k-\mathrm{i}\eta$), which gives

$$\begin{aligned}
&\tfrac{1}{2}\int\mathrm{d}k\,\langle rs\,|f(k)|\,ab\rangle\left[\frac{2k}{q^2-k^2+\mathrm{i}\gamma}+\frac{1}{q+k+\mathrm{i}\gamma}+\frac{1}{q'-k+\mathrm{i}\gamma}\right]\\
&=\tfrac{1}{2}\int\mathrm{d}k\,\langle rs\,|f(k)|\,ab\rangle\left[\frac{1}{q-k+\mathrm{i}\gamma}+\frac{1}{q'-k+\mathrm{i}\gamma}\right], \quad (299a)
\end{aligned}$$

where $q=\varepsilon_a-\varepsilon_r$ and $q'=\varepsilon_b-\varepsilon_s$. Similarly for ω_1

$$-\tfrac{1}{2}\int\mathrm{d}k\,\langle rs\,|f(k)|\,ab\rangle\left[\frac{1}{q+k-\mathrm{i}\gamma}+\frac{1}{q'+k-\mathrm{i}\gamma}\right]. \quad (299b)$$

This gives the final result

$$\langle rs|H^{(1)}_{\rm eff}|ab\rangle=\tfrac{1}{2}\int\mathrm{d}k\,\langle rs\,|f(k)|\,ab\rangle\left[\frac{2k}{q^2-k^2+\mathrm{i}\gamma}+\frac{2k}{q'^{\,2}-k^2+\mathrm{i}\gamma}\right], \quad (300)$$

which agrees with the result (29) of [ABPQQ ?]. This is identical to the *Mittleman potential* [M172 (?)].

If we instead use the *nonhermitian form* of the effective Hamiltonian (288), we have in place of (297)

$$H^{(1)}_{\rm eff} = \mathcal{K}^{(1)} - \mathcal{K}^{(0)}\mathcal{P}^{(1)} \Rightarrow \langle rs|H^{(1)}_{\rm eff}|ab\rangle = \langle rs|\mathcal{K}^{(1)}|ab\rangle - E_{\rm out}\,\langle rs|\mathcal{P}^{(1)}|ab\rangle, \tag{301}$$

HeffGnH

which becomes

$$\langle rs|H^{(1)}_{\rm eff}|ab\rangle = {\rm i}\int \frac{{\rm d}\omega_3}{2\pi}\ \langle rs\,|I(\varepsilon_a-\omega_3)|\,ab\rangle\ \left[\frac{1}{(\omega_3-\varepsilon_r+{\rm i}\gamma_r)}+\frac{1}{(E^0_{\rm in}-\omega_3-\varepsilon_s+{\rm i}\gamma_s)}\right]. \tag{302}$$

HeffGnH2

This is identical to the result of the evolution-operator method with the substitutions $\omega_3 \to \varepsilon_a - z$ and $E^0_{\rm in} = \varepsilon_a + \varepsilon_b$ and leads with the Feynman gauge to the result of the covariant evolution-operator method (213), (A.8), where also a nonhermitian effective Hamiltonian is used,

$$\langle rs|H^{(1)}_{\rm eff}|ab\rangle = \int {\rm d}k\ \langle rs\,|f(k)|\,ab\rangle\ \left[\frac{1}{q-k+{\rm i}\gamma}+\frac{1}{q'-k+{\rm i}\gamma}\right]. \tag{303}$$

HeffGnH3

6.4 Screened self-energy

sec:ScrSEGF

6.4.1 Irreducible part

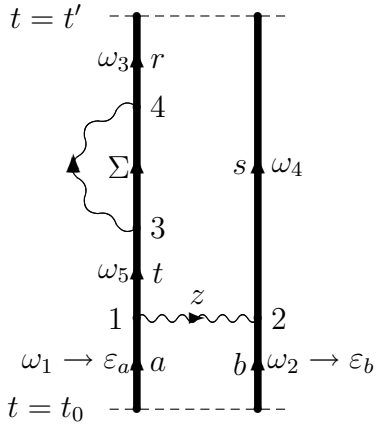

Fig. 24. The two-times Green's-function diagram representing the screened self-energy.

Fig:ScrSEGF

As a second example we consider the two-times Green's function for the screened self-energy, depicted in Fig. 24,

$$
\begin{aligned}
G(x_1', x_2'; x_{10}, x_{20}) &= \frac{\mathrm{i}}{2} \iint \mathrm{d}^4x_1\, \mathrm{d}^4x_2 \iint \mathrm{d}^4x_3\, \mathrm{d}^4x_4 \\
&\times \mathrm{i}S_{\mathrm{F}}(\boldsymbol{x}_4', \boldsymbol{x}_4, \omega_3)\mathrm{i}S_{\mathrm{F}}(\boldsymbol{x}_2', \boldsymbol{x}_2, \omega_4)\mathrm{i}\Sigma(\boldsymbol{x}_4, \boldsymbol{x}_3, \omega_5)\mathrm{i}S_{\mathrm{F}}(\boldsymbol{x}_3, \boldsymbol{x}_1, \omega_5)\mathrm{i}I(\boldsymbol{x}_2, \boldsymbol{x}_1, z) \\
&\times \mathrm{i}S_{\mathrm{F}}(\boldsymbol{x}_1, \boldsymbol{x}_{10}, \omega_1)\mathrm{i}S_{\mathrm{F}}(\boldsymbol{x}_2, \boldsymbol{x}_{20}, \omega_2) \\
&\times \mathrm{e}^{-\mathrm{i}t'(\omega_3+\omega_4)}\ \mathrm{e}^{-\mathrm{i}t_4(\omega_5-\omega_3)}\, \mathrm{e}^{-\mathrm{i}t_1(\omega_1-z-\omega_5)}\, \mathrm{e}^{-\mathrm{i}t_2(\omega_2+z-\omega_4)}\, \mathrm{e}^{\mathrm{i}t_0(\omega_1+\omega_2)} \qquad (304)
\end{aligned}
$$

ScrSEGF

(leaving out the ω and z integrations). Here, Σ represents the self-energy operator (SelfEn 202). After time integrations this becomes

$$
\begin{aligned}
G(x_1', x_2'; x_{10}, x_{20}) &= \tfrac{1}{2} \iint \mathrm{d}^3\boldsymbol{x}_1\, \mathrm{d}^3\boldsymbol{x}_2 \iint \mathrm{d}^3\boldsymbol{x}_3\, \mathrm{d}^3\boldsymbol{x}_4\, \frac{\langle \boldsymbol{x}_4'|r\rangle\langle r|\boldsymbol{x}_4\rangle}{\omega_3 - \varepsilon_r + \mathrm{i}\gamma_r}\, \frac{\langle \boldsymbol{x}_2'|s\rangle\langle s|\boldsymbol{x}_2\rangle}{\omega_4 - \varepsilon_s + \mathrm{i}\gamma_s} \\
&\times \Sigma(\boldsymbol{x}_4, \boldsymbol{x}_3, \omega_5)\, \frac{\langle \boldsymbol{x}_3|t\rangle\langle t|\boldsymbol{x}_1\rangle}{\omega_5 - \varepsilon_t + \mathrm{i}\gamma_t}\, I(z)\, \frac{\langle \boldsymbol{x}_1|a\rangle\langle a|\boldsymbol{x}_{10}\rangle}{\omega_1 - \varepsilon_a + \mathrm{i}\gamma_a}\, \frac{\langle \boldsymbol{x}_2|b\rangle\langle b|\boldsymbol{x}_{20}\rangle}{\omega_2 - \varepsilon_b + \mathrm{i}\gamma_b} \\
&\times \mathrm{e}^{-\mathrm{i}t'(\omega_3+\omega_4)}\ \mathrm{e}^{\mathrm{i}t_0(\omega_1+\omega_2)} \delta(\omega_1 - z - \omega_5)\, \delta(\omega_2 + z - \omega_4)\, \delta(\omega_5 - \omega_3). \qquad (305)
\end{aligned}
$$

Integration over z and ω_5 gives as before $\delta(\omega_1 + \omega_2 - \omega_3 - \omega_4)$. The Fourier transform leads in the same way as the single-photon exchange (GF 292) to

$$
\begin{aligned}
\big\langle rs\big|G(E)\big|ab\big\rangle &= \iint \frac{\mathrm{d}\omega_1}{2\pi}\, \frac{\mathrm{d}\omega_3}{2\pi} \\
&\times \frac{\big\langle r\big|\Sigma(\omega_3)\big|t\big\rangle\, \big\langle ts\big|I(\omega_1 - \omega_3)\big|ab\big\rangle}{(\omega_3 - \varepsilon_r + \mathrm{i}\gamma_r)(E - \omega_3 - \varepsilon_s + \mathrm{i}\gamma_s)\, (\omega_3 - \varepsilon_t + \mathrm{i}\gamma_t)\, (\omega_1 - \varepsilon_a + \mathrm{i}\gamma_a)\, (E - \omega_1 - \varepsilon_b + \mathrm{i}\gamma_b)}, \qquad (306)
\end{aligned}
$$

ScrSEFT

which is equivalent to the results of (LIS01 ?) and (LeB01 ?, Eq. IV.9). The treatment is then quite analogous to the single-photon exchange, and we obtain instead of the expression (HeffG2 298)

$$
\begin{aligned}
&\langle rs|H_{\mathrm{eff}}^{(1)}|ab\rangle = \\
&-\frac{\mathrm{i}}{2} \int \frac{\mathrm{d}\omega_3}{2\pi}\, \frac{\big\langle r\big|\Sigma(\omega_3)\big|t\big\rangle\, \big\langle ts\,\big|I(\varepsilon_a - \omega_3)\big|\, ab\big\rangle}{\omega_3 - \varepsilon_t + \mathrm{i}\gamma_t} \left[\frac{1}{(\omega_3 - \varepsilon_r + \mathrm{i}\gamma_r)} + \frac{1}{(E_{\mathrm{in}}^0 - \omega_3 - \varepsilon_s + \mathrm{i}\gamma_s)}\right] \\
&-\frac{\mathrm{i}}{2} \int \frac{\mathrm{d}\omega_1}{2\pi}\, \frac{\big\langle r\big|\Sigma(\omega_3)\big|t\big\rangle\, \big\langle ts\,\big|I(\omega_1 - \varepsilon_r)\big|\, ab\big\rangle}{\omega_3 - \varepsilon_t + \mathrm{i}\gamma_t} \left[\frac{1}{(\omega_1 - \varepsilon_a + \mathrm{i}\gamma_a)} + \frac{1}{(E_{\mathrm{out}}^0 - \omega_1 - \varepsilon_b + \mathrm{i}\gamma_b)}\right]. \qquad (307)
\end{aligned}
$$

ScrSEFT

Using instead the *nonhermitian form* of the effective Hamiltonian, leads in analogy with single-photon result (HeffGnH2 302) to the simpler expression

$$
\begin{aligned}
&\langle rs|H_{\mathrm{eff}}^{(1)}|ab\rangle = \\
&= -\mathrm{i} \int \frac{\mathrm{d}\omega_3}{2\pi}\, \frac{\big\langle r\big|\Sigma(\omega_3)\big|t\big\rangle\, \big\langle ts\,\big|I(\varepsilon_a - \omega_3)\big|\, ab\big\rangle}{\omega_3 - \varepsilon_t + \mathrm{i}\gamma_t} \left[\frac{1}{(\omega_3 - \varepsilon_r + \mathrm{i}\gamma_r)} + \frac{1}{(E_{\mathrm{in}}^0 - \omega_3 - \varepsilon_s + \mathrm{i}\gamma_s)}\right]. \qquad (308)
\end{aligned}
$$

ScrSEnc

This is identical to the evolution-operator result (ScrSEEv0p1 237), if we make the substitution $\omega_3 \to \varepsilon_a - z$. This expression contains a *(quasi)singularity*, when the intermediate state is *(quasi)degenerate* with the initial one, $E_{\mathrm{in}}^0 = \varepsilon_a + \varepsilon_b \approx \varepsilon_s + \varepsilon_t$. In the evolution-operator method this singularity is eliminated by the counterterm (UtildeExp 117), and in the Green's-function method it will be eliminated by a similar counterterm, as will be shown below.

6.4.2 *Reducible part*

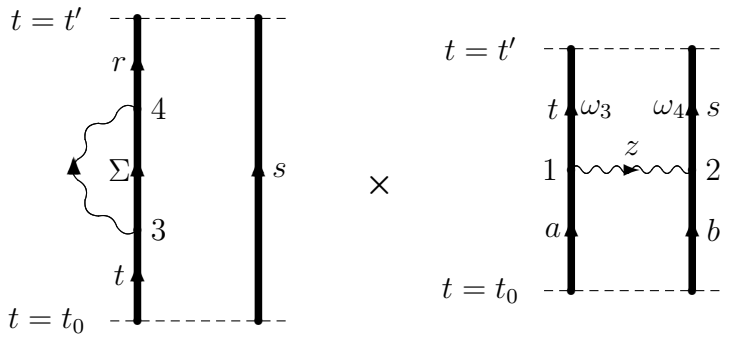

Fig. 25. The counterterm for the screened self-energy in the Green's-function method (c.f. Fig. 22). Fig:Counter Fig:CounterGF

In order to evaluate the reducible part of the screened self-energy diagram, i.e., when the intermediate state lies in the model space, one has to consider also products of first-order contributions to the $\mathcal{K}$ and $\mathcal{P}$ integrals (??), shown in Fig. 25. The contribution to the *nonhermitian* effective Hamiltonian (288) is $-\mathcal{K}^{(1)}\,\mathcal{P}^{(1)}$. LIS01,LeB01 Fig:CounterGF EffHamG

From (296) we have Pelem

$$\begin{aligned}
&\langle rs|\mathcal{P}^{(1)}|ab\rangle = \mathrm{i}\int\frac{\mathrm{d}\omega_3}{2\pi}\;\langle rs\,|I(\varepsilon_a-\omega_3)|\,ab\rangle\;\frac{1}{E^0_{\rm in}-E^0_{\rm out}}\\
&\times\left[\frac{1}{(\omega_3-\varepsilon_r+\mathrm{i}\gamma_r)}+\frac{1}{(E^0_{\rm in}-\omega_3-\varepsilon_s+\mathrm{i}\gamma_s)}\right]\\
&=\mathrm{i}\int\frac{\mathrm{d}\omega_3}{2\pi}\;\langle rs\,|I(\varepsilon_a-\omega_3)|\,ab\rangle\;\frac{1}{(\omega_3-\varepsilon_r+\mathrm{i}\gamma_r)\,(E^0_{\rm in}-\omega_3-\varepsilon_s+\mathrm{i}\gamma_s)}
\end{aligned}\tag{309}$$

CounterP

and together with the self-energy $\mathcal{K}$ part this yields

$$\langle rs|H^{(1)}_{\rm eff}|ab\rangle_{\rm Counter}=\mathrm{i}\langle r|\Sigma(\varepsilon_t)|t\rangle\int\frac{\mathrm{d}\omega_3}{2\pi}\frac{\langle ts|I(\varepsilon_a-\omega_3)|ab\rangle}{(\omega_3-\varepsilon_t+\mathrm{i}\gamma_t)(\varepsilon_a+\varepsilon_b-\omega_3-\varepsilon_s+\mathrm{i}\gamma_s)}.\tag{310}$$

CounterGF

This removes the singularity of the effective-interaction result (308). ScrSEnonHerm

6.5 *General comparison between the Green's-function and the evolution-operator methods*

sec:Comp

We shall now compare the two methods for bound-state QED discussed above, the two-times Green's-function and the covariant-evolution-operator methods, and we take the single-photon exchange between the electrons as an example. As pointed out before, both these methods are, in principle, *two-times methods*, although in the covariant-evolution-operator method the initial time is

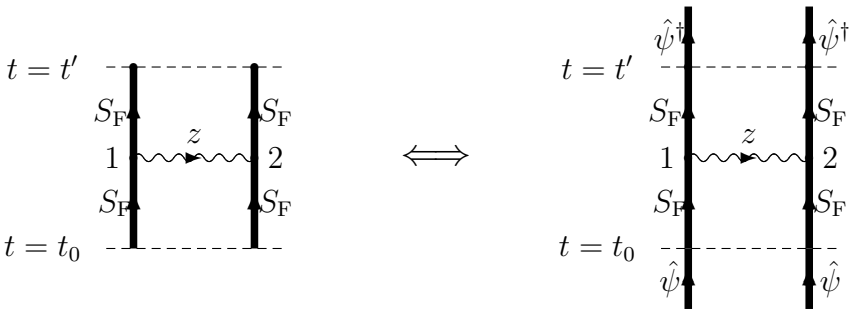

Fig. 26. The two-times Green's function for single-photon exchange between the electrons is represented by the diagram on the left, and the corresponding two-times covariant evolution operator by the diagram on the right.

Fig:SingPhotCo

normally set to $t_0 = -\infty$, which simplifies the handling considerably (Sect. 5.1). In order to make the comparison with the two-times Green's-function method more transparent, however, we shall use the original two-times form also of the evolution-operator method.

sec:SingPhotCov

The two-times Green's-function expression for the single-photon exchange (290)

GreenSingPhot

$$\begin{aligned}
&\mathrm{i}G(x_1', x_2'; x_{10}, x_{20}) \\
&= -\tfrac{1}{2} \iint \mathrm{d}^4x_1 \mathrm{d}^4x_2 \left\langle 0 \middle| T\left[\hat{\mathcal{H}}'(x_1)\hat{\mathcal{H}}'(x_2)\, \hat{\psi}(x_1')\hat{\psi}(x_2')\, \hat{\psi}^\dagger(x_{10})\hat{\psi}^\dagger(x_{20})\right] \middle| 0 \right\rangle \\
&= -\tfrac{1}{2} \iint \mathrm{d}^4x_1\, \mathrm{d}^4x_2\, \mathrm{i}S_\mathrm{F}(x_1', x_1)\, \mathrm{i}S_\mathrm{F}(x_2', x_2)\, \mathrm{i}I(x_2, x_1)\, \mathrm{i}S_\mathrm{F}(x_1, x_{10})\, \mathrm{i}S_\mathrm{F}(x_2, x_{20}) \quad (311)
\end{aligned}$$

GreenSingPhot

is represented by the first diagram in Fig. 26. This we shall compare with the corresponding *two-times covariant-evolution operator*, which by a straightforward generalization of the single-time result (208) is given by

Fig:SingPhotComp

U2Cov3

$$\begin{aligned}
&U^{(2)}_\mathrm{Cov}(t', t_0) = -\tfrac{1}{2} \iint \mathrm{d}^3\boldsymbol{x}_1' \mathrm{d}^3\boldsymbol{x}_2'\, \hat{\psi}^\dagger(x_1')\hat{\psi}^\dagger(x_2') \iint \mathrm{d}^4x_1\, \mathrm{d}^4x_2\, \mathrm{i}S_\mathrm{F}(x_1', x_1) \\
&\times \mathrm{i}S_\mathrm{F}(x_2', x_2)\, \mathrm{i}I(x_2, x_1) \iint \mathrm{d}^3\boldsymbol{x}_{10} \mathrm{d}^3\boldsymbol{x}_{20}\, \mathrm{i}S_\mathrm{F}(x_1, x_{10})\, \mathrm{i}S_\mathrm{F}(x_2, x_{20}) \hat{\psi}(x_{10})\hat{\psi}(x_{20}) \quad (312)
\end{aligned}$$

U2TT

and represented by the second diagram in the figure. This comparison yields in the present case the following *relation between the two-times Green's function and the two-times covariant evolution operator*

$$U^{(2)}_\mathrm{Cov}(t', t_0) = \iint \mathrm{d}^3\boldsymbol{x}_1' \mathrm{d}^3\boldsymbol{x}_2' \iint \mathrm{d}^3\boldsymbol{x}_{10} \mathrm{d}^3\boldsymbol{x}_{20}\, \hat{\psi}^\dagger(x_1')\hat{\psi}^\dagger(x_2')\, \mathrm{i}G(x_1', x_2'; x_{10}, x_{20})\, \hat{\psi}(x_{10})\hat{\psi}(x_{20}) \quad (313)$$

Comp

– a relation that holds for any two-particle Green's function/evolution operator and can easily be generalized to the n-particle case.

It should be noted that the evolution operator is an *operator*, acting in the Fock space, while the Green's function is a *function* of the time and space coordinates.

It is now interesting to compare the two methods in some more detail. Starting with the single-photon exchange in the GF method, we see that in the nonhermitian case (302) it is the pole $E = E^0_{\rm in}$ in the 'phantom-particle' expression (294) that contributes. The denominators, originating from the propagators of the incoming lines, lead here to the delta factor $\delta(\omega_1 - \varepsilon_a)$. In the evolution-operator method, the initial time is set to $t_0 \to -\infty$ and ω_1 to ε_a from the onset. We also see that the denominator $E^0_{\rm in} - E^0_{\rm out}$ of $\hat{\mathcal{K}}^{(1)}$ is eliminated in the expression for the effective Hamiltonian, $H^{(1)}_{\rm eff} = \mathcal{K}^{(1)} - \mathcal{K}^{(0)}\mathcal{P}^{(1)}$. In the evolution-operator method the corresponding denominator is eliminated (217) by means of the time derivative. The situation is similar for the screened self-energy.

The observations above are quite general. The two-times Green's-function and covariant-evolution-operator methods are quite analogous. After time integrations both expressions depend generally on the initial and final time (although the initial time is in the latter method normally set to $t_0 = -\infty$). In the GF method a Fourier transform is performed and the effective Hamiltonian is constructed by integrations over the energy. In the evolution-operator method the same expression is obtained by means of time derivation. In the GF method with nonhermitian effective Hamiltonian the combined denominator from the propagators of the outgoing lines is eliminated by the energy integration and in the evolution-operator method by the time derivation. In the GF method the energy integration has the effect that the energy parameters of the propagators are replaced by the orbital energies. In the (one-time) evolution-operator method this is set from the onset.(C.f. Table IV.1 in the thesis of ?).

Some applications of the two-times-Green's-function technique are briefly described in chapter 7. For further information the reader is referred to the review article by ?).

7 Applications

sec:Appl

The bound-state techniques described here can be applied to various problems in QED. Here, we shall summarize some applications on *stationary* problems. For *dynamical* problems, like photoionization and radiative electron capture (REC) we refer to the current literature (???).

7.1.1 Lamb shift

Pioneering works on the problem of bound-state QED calculations were carried out by [BLS59] (?) and [DJ71] (?) within the framework of the S-matrix formulation. Later the numerical technique was developed to a high degree of sophistication mainly for the first-order self-energy of hydrogenlike ions by [Mo75,Mo82,Mo85,Mo92] (????). This technique was originally best suited for heavy ions, but a technique was later developed and applied also to low-Z ions [JMS99] (?), and this represents the most accurate result at present for neutral hydrogen and singly ionized helium. Accurate calculations of the first-order vacuum polarization on these ions, including the Wichmann-Kroll term, have been performed by [PLS93] (?), [Wichmann98] (?).

In order to reach a numerical accuracy for light elements that can match the analytical approach ($\alpha - Z\alpha$ expansion) for light elements, it is necessary to consider also the two-photon contributions. This is computationally quite challenging and has only recently been possible to attack in a more comprehensive way. A number of more or less complete calculations have appeared during the last years [MalS98,LNPS00,Ye00,YS01,JPac02] (??????).

sec:Hfs

7.1.2 Hyperfine structure and Zeeman effect

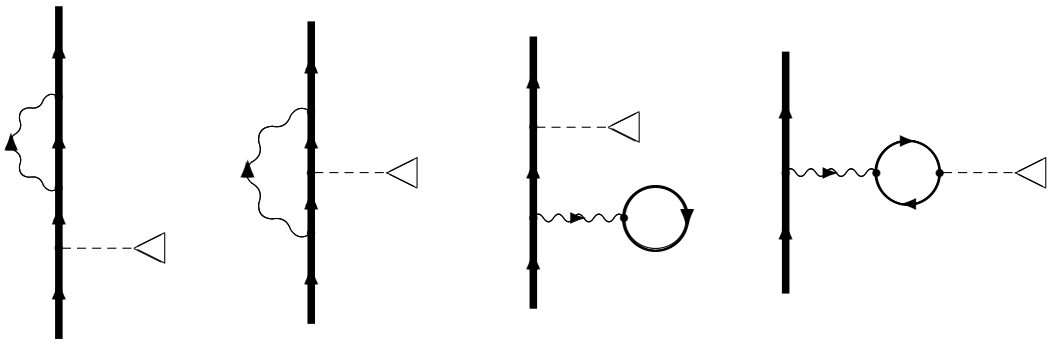

Fig. 27. The diagrams representing the lowest-order QED corrections to an additional perturbation like the hyperfine structure or Zeeman effect for hydrogenlike ions.

Fig:Hfs

The S-matrix formalism has been used also for accurate calculations for hydrogenlike ions of the effect of an 'external' perturbation, like the hyperfine structure or the Zeeman effect (atomic g-factor) [PSG96,PSS97,SPS98,BCS97,BLP00,ASP01,YIS02] (????????). The diagrams in lowest order are depicted in Fig. [Fig:Hfs] 27.

The hyperfine structure of some heavy hydrogenlike ions has been studied with the SuperEBIT at Livermore and at GSI in Darmstadt. The QED effects

are here of the order of 0.5% and clearly observable within the experimental accuracy. This effect, however, is normally overshadowed by the nuclear effect. Therefore, comparison between theory and experiment is here mainly used to extract information about the nucleus, particularly the nuclear magnetization [BUW01,MGu01] (??).

The atomic g-factor has been measured with extreme precision for some light hydrogenlike ions at the university of Mainz, and the agreement with the theoretical predictions is very good. Here, the comparison between theory and experiment can actually be used to improve the atomic value of the electron mass [HBH00,BHH02,YIS02] (???).

7.2 Applications on heliumlike ions

The nonradiative part of the two-photon interaction for the ground states of heliumlike ions (Fig. 17) has been evaluated using the S-matrix formulation by [BMJ93] (?) and [LPS95] (?). The radiative effects (Fig. 20) for the same systems have been evaluated by [PSS96] (?), using the S-matrix formalism, and by [YAS97] (?) using the two-times Green's-function method. The results obtained are in good agreement with the experimental results obtained with the SuperEBIT at Livermore [MES95] (?), although the QED effects are barely detectable.

The nonradiative diagrams for the excited $1s2s$ states of heliumlike ions have also been evaluated by means of the S-matrix formulation [MS00,ALP01,ASL02] (???) as well as of the $1s2p$ states, excluding the quasi-degenerate $J = 1$ states [MS00] (?). Recently, the covariant evolution-operator technique has been applied to the $1s2p$ states of some lighter elements, including the quasi-degenerate $J = 1$ states, and the results obtained agree well with the experimental fine-structure results [LAS01,BAs02] (??). The screened-self-energy diagrams for these states of some heavier elements have also been evaluated using the two-times Green's-function technique by Indelicato et al. [LIS01,LeB01] (??) and the vacuum-polarization screening corrections by Yerokhin et al. [ABP00] (?).

The experimental results for the fine structure of some heliumlike ions together with the theoretical results are given in Table 1. As discussed in the Introduction, the results of [PJS94] (?) are obtained by means of relativistic MBPT with the QED corrections added in lowest order in $\alpha - Z\alpha$, and the results of [Dr88] (?) with nonrelativistic Hylleraas-type wavefunction and relativistic as well as QED corrections to lowest order. The results of [BAs02,ZAS01] (?), (?) are obtained by means of the covariant evolution-operator method to second order with higher-order MBPT corrections added. Only the nonradiative QED parts are fully calculated and the remaining effects taken from the power expansion. Full QED calculations are now under way.

Table 1
The $1s2p$ fine-structure separations of some heliumlike ions.
Values for $Z = 2, 3$ given in MHz and for $Z \geq 9$ in μH (1μH= 27.2 μeV).

Z	$^3P_1 - ^3P_0$	$^3P_2 - ^3P_0$	$^3P_2 - ^3P_1$	
2	29616.9509(9)		2291.1759(10)	Expt'l [1]
	29616.9496(10)		2291.1736(11)	Theory [2]
3	155704.27(66)		-62678.41(66)	Expt'l [3]
	155703.4(1,5)		-62679.4(5)	Drake [4]
9	701(10)		4364,517(6)	Expt'l [5]
	680	5050	4362(5)	Drake [4]
	690	5050	4364	Plante [6]
	690	5050	4364	Åsén [7]
10	1371(7)	8458(2)		Expt'l [8]
	1361(6)	8455(6)	265880	Drake [4]
	1370	8469	265860	Plante [6]
	1370	8460	265880	Åsén [7]
18		124960(30)		Expt'l [9]
		124810(60)		Drake [4]
		124942		Plante [6]
		124940		Åsén [7]

1 GLH01 ??) 2 ??) 3 ??) 4 ??) 5 MMT99 ?)
6 PJS94 LAS01 ?) 7 ??) 8 ?) 9 ?)

It can be seen from the comparison in the table that the difference between the QED effects to leading order and the all-order result is hardly noticeable with the present numerical accuracy. For argon there is a significant difference between the result of Drake and the other theoretical results, which is expected to be due to the approximation of the relativistic effect in the method of Drake. It would be a challenge to try to reproduce with the evolution-operator method the accurate result for the separation $^3P_2 - ^3P_1$ in heliumlike fluorine, which would most likely test higher-order (in $Z\alpha$) QED corrections. It is presently unclear if this accuracy can be reached with the present technique. The experimental accuracy obtained for single ionized lithium and, in particular, for neutral helium, is definitely out of reach at present. An improved technique,

which might be applicable in these cases, will be discussed in the next chapter.

7.3 Applications on lithiumlike ions

Lithiumlike ions can to a large extent be treated as a single-electron system with nonCoulombic potential. Early calculations with this approach were performed in order to calculate the Lamb shift of the $1s2p$ transitions of Li-like uranium [B192,B193,LPS93] (???), and the results were in excellent agreement with the accurate experimental results of [SBB91] (?). More elaborate calculations, including the two- and three-electron interactions, have now been performed particularly by [YAB99,YAS01] (??), [BYAS01] (?).

8 Possibilities of merging of QED with MBPT

MBPT/QED

We have in the previous sections considered three different methods for bound-state QED calculations, the S-matrix, the covariant-evolution-operator and the two-times Green's-function methods. The latter two methods have the advantage compared to the S-matrix formulation that they can be used with an extended model space and thereby be applicable also to a quasi-degenerate situation. All three methods, however, have the shortcoming that in practice electron correlation can only be evaluated to relatively low order. This limits the accuracy, for instance, for simple systems with low nuclear charge, for which the electron correlation is comparatively strong.

We know that in MBPT the electron correlation can be treated to essentially all orders, as discussed in section [sec:AllOrder] 2.5. In the present section we shall consider the possibility of introducing some of these ideas into bound-state QED.

In principle, all electromagnetic interactions between electrons could be treated entirely within the QED framework by considering one-, two-, three- ... photon interactions. In practice, however, it is presently hardly possible to go beyond two-photon interactions in any reasonably complete manner. For that reason, it would be highly desirable to be able to supplement the QED calculations to second order, say, with higher-order effects using MBPT methods. A simple and straightforward way that has been applied to heliumlike ions is to add effects of third and higher orders from MBPT to the second-order QED results [PSS96,LAS01,BAs02] (???). In order to achieve higher accuracy, however, particularly for very light elements, it is necessary to *combine* the two effects in a more complete way, which would imply that the QED effects are evaluated by means of *correlated* wavefunctions, rather than with simple hydrogenic ones.

In the method developed by Drake, very accurate non-relativistic two-electron, correlated wavefunctions are constructed, using the method of Hylleraas, where the interelectronic distance r_{12} is explicitly used. The disadvantage with this technique when applied to QED calculations is that the QED effects – as well as relativistic effects – have to be evaluated analytically, using (the lowest-order) analytical expressions. Such an approach is superior to other available methods for very light elements, where electron correlation is relatively strong and the QED effects quite small. For heavier elements, on the other hand, the approach cannot compete with available numerical QED approaches. By combining the numerical QED technique with the MBPT technique, as will be outlined in the present section, it is expected that the QED effects can be accurately evaluated by means of *correlated* wavefunctions, thus combining the advantages of the two approaches.

The covariant-evolution-operator method is particularly suited as a basis for the combined approach, because of its formal analogy with MBPT, as demonstrated, for instance, in the two-photon case. This analogy remains also in higher orders. One possibility could therefore be to restrict the full QED calculations to the lowest orders and to evaluate the remaining (smaller) terms by a combination of QED and (relativistic) MBPT. This can be done by modifying the coupled-cluster equations, particularly the pair equation, to include also QED effects.

Below we shall first demonstrate the close analogy between the QED treated by the covariant evolution-operator method and the traditional MBPT. Then we shall see how this analogy can be used to derive two-electron or pair equations to generate certain QED effects to all orders. Eventually, this will lead to the complete *Bethe-Salpeter equation* [BS51,BS57] (??). Finally, we shall discuss some practical schemes for generating combined QED-MBPT effects of high order.

8.1 Comparison of QED with MBPT

In standard MBPT the second-order contribution to the energy or the effective interaction due to the electron-electron interaction, V, is

$$\sum_{|tu\rangle\in Q} \frac{\left\langle rs\middle|V\middle|tu\right\rangle \left\langle tu\middle|V\middle|ab\right\rangle}{\Delta E}\,, \tag{314}$$

MBPT2SepLadd

where the denominator is equal to the negative of the excitation energy of the intermediate state, $\Delta E = \varepsilon_a + \varepsilon_b - \varepsilon_t - \varepsilon_u$, and the summation runs over states in the complementary space (Q). This can be compared with the contribution

due to the *separable* two-photon diagram (222)

$$\sum_{|tu\rangle\in Q} \frac{\Big\langle rs\Big|V(q+p',q'+p)\Big|tu\Big\rangle\Big\langle tu\Big|V(p,p')\Big|ab\Big\rangle}{\Delta E} + \text{MSC}. \tag{315}$$

SepLadd

where

$$V(q,q') = \int \mathrm{d}k\, f(k)\left[\frac{1}{q-k+\mathrm{i}\gamma}+\frac{1}{q'-k+\mathrm{i}\gamma}\right],$$

assuming only positive-energy states are involved. The first term in (315) is here very similar to the MBPT expression and represents the *irreducible* part for which the intermediate state lies in the Q space. The term 'MSC' represents the *Model-Space Contributions*, introduced in section 3.3.1, i.e., contributions due to the *reducible* part, for which the intermediate state lies in the model space.

The lowest-order contributions to the effective interaction due to multi-photon exchange then become

$$\begin{aligned}\Big\langle rs\Big|H^{(1)}_{\text{eff}}\Big|ab\Big\rangle &= \langle rs|V(q,q')|ab\rangle \\ \Big\langle rs\Big|H^{(2)}_{\text{eff}}\Big|ab\Big\rangle &= \sum_{|tu\rangle\in Q} \frac{\Big\langle rs\Big|V(q+p',q'+p)\Big|tu\Big\rangle\Big\langle tu\Big|V(p,p')\Big|ab\Big\rangle}{\Delta E} \\ &\quad + \text{MSC} + \Big\langle rs\Big|V_2\Big|ab\Big\rangle_{\text{Nonsep}}.\end{aligned} \tag{316}$$

OneTwoPhot

The difference from the corresponding MBPT results is here that the interactions are *time-dependent* (retarded), which also leads to the appearance of the model-space contribution (MSC) and the *nonseparable* part, represented by the last two terms of the second equation. We shall now utilize this close analogy between the QED and the MBPT results in order to indicate how the schemes can be combined in a systematic fashion.

8.2 The Bethe-Salpeter equation

sec:BS

The pair equation with instantaneous Coulomb interactions, discussed in the many-body section 2.5, can straightforwardly be generalized to include the full QED photons. In analogy with the expression for the separable two-photon ladder above, we can set up a pair equation by replacing the interaction in the MBPT equation (56) by the corresponding two-photon expressions

$$\begin{aligned}\left(q+q'\right) s^{rs}_{ab} &= \langle rs|V(q,q')|ab\rangle \\ &+\langle rs|V(q+p',q'+p)|tu\rangle\, s^{tu}_{ab} + \text{MSC}\,,\end{aligned} \tag{317}$$

PairEqSP

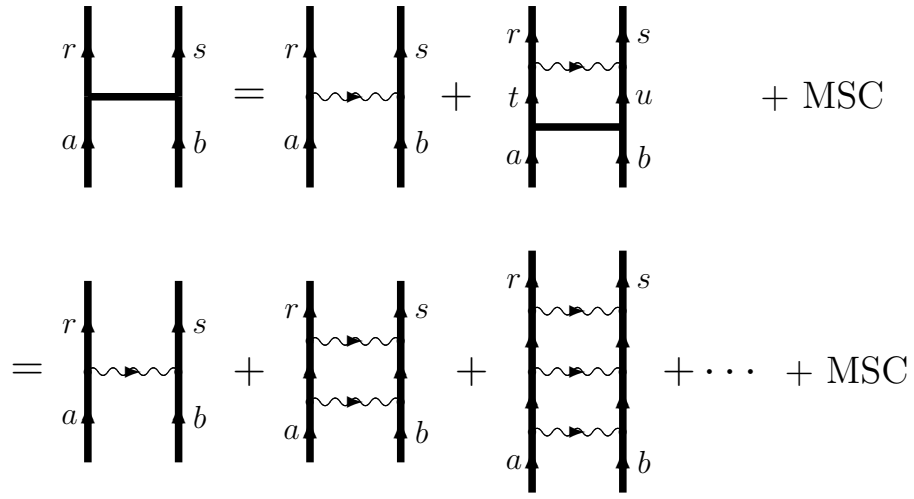

Fig. 28. The pair equation for a two-electron system, using the full QED one-photon interaction between the electrons, in analogy with the MBPT pair function in Fig. 2. This generates an infinite sequence of ladder single-photon diagrams in addition to model-space contributions (MSC).

where $q = \varepsilon_a - \varepsilon_r$, $q' = \varepsilon_b - \varepsilon_s$, $p = \varepsilon_a - \varepsilon_t$, $p' = \varepsilon_b - \varepsilon_u$. The folded term is constructed in analogy with the corresponding MBPT expression in (55) and model-space contribution, as described in section 5. The equation (317) will generate an infinite sequence of single-photon ladders (including folded diagrams and MSC), as indicated in Fig. 28.

The iteration scheme of the single-photon exchange (V_1) above can in principle be applied also to the nonseparable *two-photon* exchange ($V_2^{\rm Nonsep}$) etc. Including the nonseparable interactions to *all orders*

$$V^{\rm Nonsep} = V_1 + V_2^{\rm Nonsep} + V_3^{\rm Nonsep} + \dots \tag{318}$$

leads to the complete *Bethe-Salpeter equation* (?, p. 562)

$$\langle rs|V_{\rm BS}|ab\rangle = \langle rs|ab\rangle + \frac{\langle rs|V^{\rm Nonsep}|tu\rangle\langle tu|V_{\rm BS}|ab\rangle}{\Delta E} + \text{MSC}. \tag{319}$$

This is illustrated in Fig. 29. The contribution to the energy – or the effective interaction – is then obtained by closing the function by a final interaction, in analogy with the MBPT case in Fig. 3. The two-particle interactions contain here also radiative parts, with self-energy and vacuum polarization loops, which, of course, have to be properly renormalized. In principle, also the one-particle radiative effects, can be iterated in a similar way by means of a single-particle equation. This can then be coupled to the two-particle equation in the same way as in the MBPT case (53).

The result (319) can also be represented in the form of a Green's-function

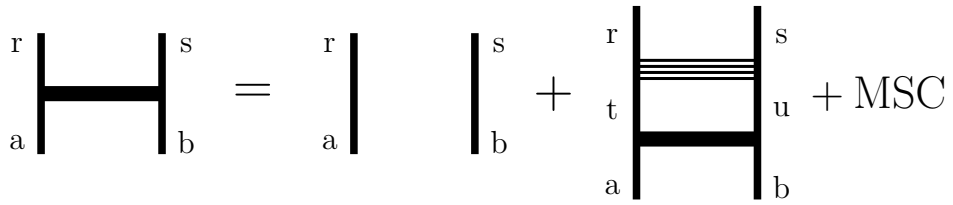

Fig. 29. Graphical representation of the complete Bethe-Salpeter equation in the form of a Dyson equation. The solid area represents the complete two-particle interaction, including no interaction, and the dashed area the nonseparable part (318). The intermediate state lies in the Q space. The MSC represents the model-space contribution of the reducible part.

NonSep

Fig:BS

equation

$$G(x_1', x_2', x_{10}, x_{20}) = \mathrm{i}S_{\mathrm{F}}(x_1', x_{10})\,\mathrm{i}S_{\mathrm{F}}(x_2', x_{20}) + \int \mathrm{d}^4x_1'' \int \mathrm{d}^4x_2''\, \overline{K}(x_1', x_2', x_1'', x_2'')\, G(x_1'', x_2'', x_{10}, x_{20}) + \mathrm{MSC}, \tag{320}$$

V.38

where $\overline{K}$ represents a *kernel of all nonseparable interactions*. This can be illustrated by the same figure, if we interpret the lines as electron propagators.

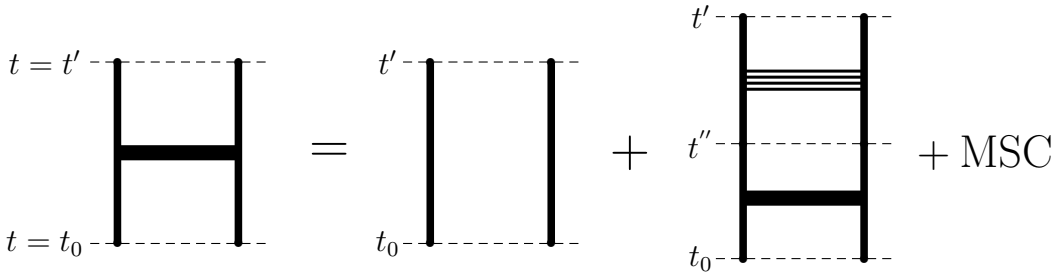

Fig. 30. Graphical representation of the complete Bethe-Salpeter equation in the form of the Green's-function equations (320) and (321).

V.38 V.38E

Fig:BS2

The Green's function depends only on the *relative* times, and by setting the initial times equal, $t_{10} = t_{20} = t_0$, as well as the final times, $t_1' = t_2' = t'$ and $t_1'' = t_2'' = t''$, we can make a Fourier transform with respect to the time *differences* $\tau' = t' - t_0$ and $\tau'' = t'' - t_0$, which leads to

$$G(\boldsymbol{x}_1', \boldsymbol{x}_2', \boldsymbol{x}_{10}, \boldsymbol{x}_{20}, E) = \int \frac{\mathrm{d}\omega}{2\pi}\, \mathrm{i}S_{\mathrm{F}}(\boldsymbol{x}_1', \boldsymbol{x}_{10}, \omega)\, \mathrm{i}S_{\mathrm{F}}(\boldsymbol{x}_2', \boldsymbol{x}_{20}, E - \omega) + \int \mathrm{d}^3\boldsymbol{x}_1'' \int \mathrm{d}^3\boldsymbol{x}_2''\, \overline{K}(\boldsymbol{x}_1', \boldsymbol{x}_2', \boldsymbol{x}_1'', \boldsymbol{x}_2'', E)\, G(\boldsymbol{x}_1'', \boldsymbol{x}_2'', \boldsymbol{x}_{10}, \boldsymbol{x}_{20}, E) + \mathrm{MSC}, \tag{321}$$

V.38E

where E is the energy parameter.

The procedure indicated here represents a generalization of the all-order procedures, discussed in section 2.5. It is clear that the nonseparable multi-photon

sec:AllOrder

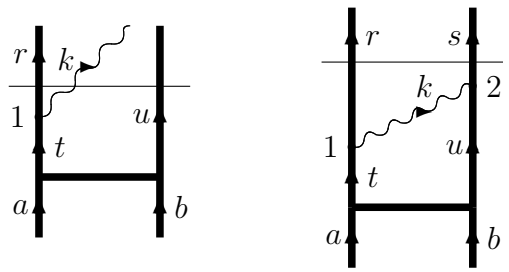

Fig. 31. The pair function with an uncontracted photon (left) and with a completed photon exchange (right). Fig:PhotPf1

interactions can be handled very much like the interactions in standard MBPT – but will obviously be considerably more time consuming. It is important that only the nonseparable parts of the interactions are iterated, in order to avoid double-counting. *The nonseparable interactions are free from singularities.* The intermediate states between the interactions are restricted to the Q space, as in ordinary MBPT, while inside the interactions *all* intermediate states (Q as well as P space) should be included. In addition, there will be finite model-space contributions (MSC) of the reducible part, which can be obtained as indicated earlier.

8.3 Pair functions with 'uncontracted' photons

sec:PhotPf

We shall now consider an alternative approach for generating higher-order diagrams, based upon a combination of the MBPT and QED approaches. We have seen in section 3 that the field-theoretical perturbation (68) due to the interaction between the electrons and the photon field can create or destroy a virtual photon. A contraction between two such operators is needed to form an interaction between the electrons. We consider now a standard MBPT *pair function* (57) *which is perturbed by a single perturbation* (68). This leads to a pair function with what we shall refer to as an *uncontracted photon*, depicted in Fig. 31 (left). Assuming the MBPT pair functions is $|\rho_{ab}\rangle = s^{tu}_{ab}|ab\rangle$, the modified function with an uncontracted photon can be expressed $|\rho^{+}_{ab,k}\rangle = s^{ru+}_{ab}(k)|ab\rangle$, where

$$s^{ru+}_{ab}(k) = \frac{\langle r|\hat{\mathcal{H}}'|t\rangle\, s^{tu}_{ab}}{\varepsilon_a - \varepsilon_r + \varepsilon_b - \varepsilon_u - k + \mathrm{i}\gamma}, \tag{322}$$

PhotPf

assuming that only positive-energy states are involved. $\hat{\mathcal{H}}'$ is here the interaction (68), operating on a single electron. The denominator above is obtained using the general scheme derived in Appendix C. The pair function then satisfies the equation

$$\Big(\varepsilon_a + \varepsilon_b - h_0(1) - h_0(2) - k\Big)\, \rho^{+}_{ab}(1,2,k) = Q\hat{\mathcal{H}}'(1)\rho_{ab}(1,2), \tag{323}$$

PhotPf2

where h_0 is the single-electron Schrödinger (7) or Dirac (62) Hamiltonian. The Q projection operator assures that the r.h.s. is orthogonal to the initial state $|ab\rangle$.

In order to complete the photon exchange, as indicated in the second diagram in Fig. 31, we operate with a second interaction, $\hat{\mathcal{H}}'(2)$, which after contraction leads to the electron-electron interaction (77). The function $f(k)$

$$f(k) = -\frac{e^2}{4\pi^2\, r_{12}}\,(1 - \boldsymbol{\alpha}_1 \cdot \boldsymbol{\alpha}_2)\,\sin(kr_{12})$$

is expanded in spherical waves according to (80)

$$\frac{\sin kr_{12}}{kr_{12}} = \sum_{k=0}^{\infty}(2l+1) j_l(kr_1) j_l(kr_2)\, \boldsymbol{C}^k(1) \cdot \boldsymbol{C}^k(2), \tag{324}$$

SphW3

and then it is essentially the Bessel function $j_l(kr)$ that appears in the radial part of the equation above in the place of $\hat{\mathcal{H}}'$. This procedure requires evidently one pair function for each value of the photon momentum k. With the denominator in (322), the contribution to the interaction from the full photon exchange becomes

$$\int \frac{\mathrm{d}k\, f(k)}{q + p' - k + \mathrm{i}\gamma},$$

corresponding to the first part of the interaction in the expressions (211), (222). The second part of the interaction corresponds to a photon that is emitted from the second electron.

The pair function with an uncontracted photon can also be iterated further with instantaneous interactions (V), before closing the photon and before making the k-integration. This leads to effects depicted in Fig. 32 and corresponds to the pair equation

$$\Big(\varepsilon_a + \varepsilon_b - h_0(1) - h_0(2) - k\Big)\,\rho^+_{ab}(1,2,k) = Q\Big(\hat{\mathcal{H}}'(1)\rho_{ab}(1,2) + V\rho^+_{ab}(1,2,k)\Big). \tag{325}$$

PhotPf3

Then the pair function can be 'closed' by a second interaction, $\hat{\mathcal{H}}(2)$, as before, and performing the k integration leads to the corresponding contribution to the energy or the effective interaction, depicted in Fig. 33. By solving the corresponding pair equation, we obtain a new pair function with contracted photons only, which can then be iterated in the same way as the standard MBPT pair function, as indicated in Fig. 34. It can also be used a new input for the whole scheme above, yielding repeated effects of the type illustrated in the last diagram in the figure. In that diagram we have also indicated that the vacuum-polarization (Uehling part) can be included, by modifying the orbitals, and the photon self-energy by modifying the photon propagator, as discussed in section 4.3.3.

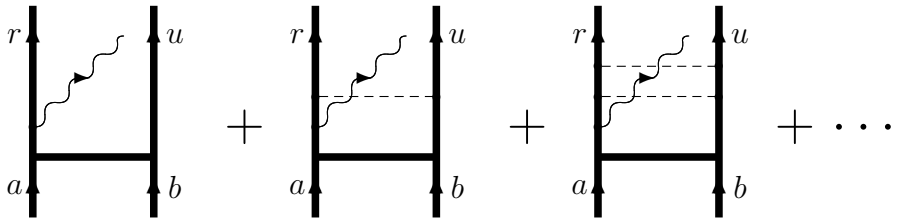

Fig. 32. The pair function with an uncontracted photon can also be iterated with instantaneous interactions before closing the photon.

Fig:PhotPf2

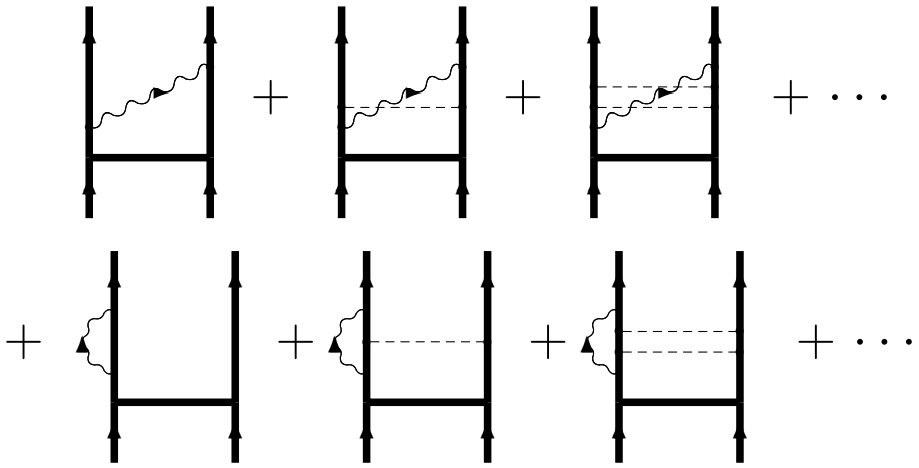

Fig. 33. Closing the uncontracted photon in the pair function illustrated in Fig. 32 can yield a new pair function including the effects indicated.

Fig:PhotPf2

Fig:PhotPf3

The effects obtained with the procedure indicated here include the entire effect due to the exchange of a single QED photon as well as the completely separable parts of two-, three-,... photon exchange. In addition, it contains most if the effect of *nonseparable* two-, three-,... photon exchange. For instance, the diagrams in Figs 33 and 34 contain the effects of two crossed photons, the vertex correction, and the screened electron self-energy, where one of the photons is retarded and the other is instantaneous. Also much of the vacuum-polarization effects, including the Uehling part of the photon self-energy, can be included, as indicated in Fig. 34. (Of course, the self-energy and vertex parts have to be properly renormalized.) Most importantly, however, these effects are evaluated by means of *correlated* wavefunctions instead of pure hydrogenic ones. When the effects are iterated, a good approximation to the full Bethe-Salpeter equation would be achieved. Work in realizing this scheme is now under way at our laboratory.

Fig:PhotPf3Photpf4

Fig:PhotPf4

In order to include the full two-photon effects with correlated wavefunctions, it will be necessary to generate pair functions with *two* 'uncontracted' photons. Then also effects of the type shown in Fig. 35 could be included. This would then represent the next step towards the solution of the full Bethe-Salpeter equation. Although straightforward in principle, this step does not seem to be

Fig:PhotPf5

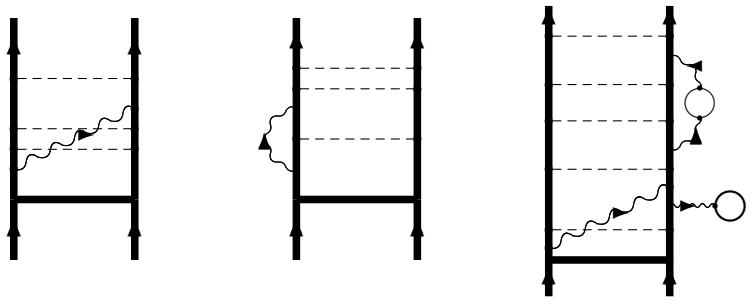

Fig:PhotPf3

Fig. 34. The pair function in Fig. 33 can be iterated further with instantaneous interactions, as well as with an uncontracted photon, leading to effects of the type indicated. In the last diagram we have also included the vacuum-polarization part, which can be obtained by modifying the orbitals and the Uehling part of the photon self-energy by modifying the photon propagator.

Fig:PhotPf4

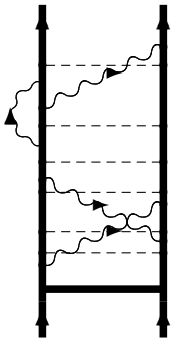

Fig. 35. By means of pair functions with *two* uncontracted photons effects of the type indicated can be evaluated.

Fig:PhotPf5

computationally feasible, however, for the time being.

9 Conclusions and outlook

In this work we have concentrated on two-electron ions for several reasons. Firstly, hydrogenlike ions have been extensively treated in the review article on the S-matrix formulation by [?]. Secondly, there has been a rapid development concerning heliumlike ions lately – experimentally as well as theoretically – a development we expect to continue for quite some time to come. Heliumlike ions represent the simplest systems where the interplay between QED effects and electron correlation can be studied, and here several interesting and challenging problems will emerge. For light elements the electron correlation is so strong that it can not be handled to a sufficient degree of accuracy with the currently available methods for bound-state QED. Furthermore, these systems contain levels which are very close in energy, which represents another

MPS98

theoretical challenge.

Experimentally, some fine-structure separations in light-medium-heavy heliumlike ions can now be measured with an accuracy up to 1 ppm , as in heliumlike fluorine [MMT99] (see Table in Section [sec:Appl]). Calculations are now under way at our laboratory in order to try to reproduce this value. It is unclear, though, whether this can be achieved with the current technique. Under way are also some efforts to realize the modified scheme, presented in the previous main section, where pair functions with an uncontracted photon are generated. It is expected that this technique will improve the accuracy considerably in cases where the electron correlation plays a major role.

The fine-structure separation in neutral helium is of particular interest. Here, the experimental accuracy is as high as 30 ppb, and it is anticipated that the accuracy could be improved by another order of magnitude [GLH01]. Since the fine-structure is due entirely to relativity and QED (proportional to α^2 in leading order), a comparison between theory and experiment may yield a value of the fine-structure constant with an accuracy comparable to (in principle half) the experimental uncertainty. The first evaluation of this constant from the experimental data and available theoretical estimates yielded a value with an uncertainty of 23 ppb, which however deviated four standard deviations from the accepted, and more accurate, value obtained mainly from the free-electron g-factor [MT00]. According to newer estimates, the theoretical uncertainty had been underestimated, and the new value agrees with the accepted value but with a larger uncertainty of about 200 ppb [PSap02]. Hopefully, a combination of the analytical and numerical approaches for some light ions might here improve the situation.

Acknowledgments

The authors want to express their thanks for stimulating discussions with our colleagues Eric-Olivier LeBigot, Paul Indelicato, Peter Mohr, Vladimir Shabaev and Gerhard Soff, as well as to our former and present collaborators Thomas Beier, Martin Gustavsson, Ann-Marie Pendrill, Hans Persson, and Per Sunnergren, who have contributed considerably to the works presented here. The support from the Swedish Research Council and the Alexander von Humboldt Foundation is gratefully acknowledged.

A Evaluation of one and two-photon evolution-operator diagrams

sec:Eval

In this Appendix we shall first evaluate some covariant-evolution-operator diagrams in the standard way. In Appendix B we shall consider *time-ordered* diagrams and evaluate each time-ordering separately. This will lead to a general scheme for diagram evaluation, described in Appendix C, which is utilized in the merging procedure of QED and MBPT in section 8.

A.1 Evaluation of the single-photon exchange

SingPhotEv

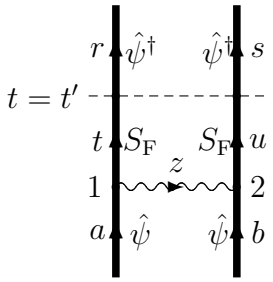

Fig. A.1. Graphical representation of the covariant-evolution operator for single-photon exchange (Fig. 15).

Fig:SingPhotAp

The covariant evolution operator for single-photon exchange, illustrated in Fig. A.1, is (209)

$$\begin{aligned}
&\left\langle rs\middle|\hat{U}^{(2)}_{\rm Cov}(t',-\infty)\middle|ab\right\rangle = -\iint {\rm d}t_1\,{\rm d}t_2 \\
&\times\left\langle rs\middle|{\rm i}S_{\rm F}(x_1',x_1)\,{\rm i}S_{\rm F}(x_2',x_2)\,{\rm i}I(x_2,x_1)\middle|ab\right\rangle {\rm e}^{{\rm i}t'(\varepsilon_r+\varepsilon_s)}\,{\rm e}^{-{\rm i}t_1\varepsilon_a-{\rm i}t_2\varepsilon_b}\,{\rm e}^{-\gamma(|t_1|+|t_2|)} \\
&={\rm i}\iint {\rm d}t_1\,{\rm d}t_2\left\langle rs\middle|\int\frac{{\rm d}z}{2\pi}\int\frac{{\rm d}\omega_1}{2\pi}\frac{|t\rangle\langle t|}{\omega_1-\varepsilon_t+{\rm i}\eta_t}\int\frac{{\rm d}\omega_2}{2\pi}\frac{|u\rangle\langle u|}{\omega_2-\varepsilon_u+{\rm i}\eta_u}\,I(z)\middle|ab\right\rangle \\
&\times{\rm e}^{{\rm i}t'(\varepsilon_r+\varepsilon_s)}\,{\rm e}^{-{\rm i}\omega_1(t'-t_1)}\,{\rm e}^{-{\rm i}\omega_2(t'-t_2)}\,{\rm e}^{-{\rm i}z(t_2-t_1)}\,{\rm e}^{-{\rm i}t_1\varepsilon_a-{\rm i}t_2\varepsilon_b}\,{\rm e}^{-\gamma(|t_1|+|t_2|)}, \qquad \text{(A.1)}
\end{aligned}$$

U2CovA

using the form (192) of the electron propagators and the Fourier transform (169) of the electron-electron interaction. The quantities η_t, η_u are infinitesimally small quantities with the same sign as ε_t and ε_u, respectively, with the purpose of determining the poles of the electron propagator. The time integration over t_1 becomes, using the Δ function (174),

$$\int {\rm d}t_1\,e^{{\rm i}t_1(\omega_1+z-\varepsilon_a)}\,e^{-\gamma|t_1|}=\frac{2\gamma}{(\omega_1+z-\varepsilon_a)^2+\gamma^2}=2\pi\Delta_\gamma(\omega_1+z-\varepsilon_a). \qquad \text{(A.2)}$$

U2Int

The ω_1 integral then becomes

$$\int\frac{{\rm d}\omega_1}{2\pi}\frac{1}{\omega_1-\varepsilon_r+{\rm i}\eta_r}\,\frac{2\gamma}{(\omega_1+z-\varepsilon_a)^2+\gamma^2}\,e^{-{\rm i}t'(\omega_1-\varepsilon_r)},$$

using the fact that only the terms $t = r$ and $u = s$ survive. Here, the poles appear at $\omega_1 = \varepsilon_r - \mathrm{i}\eta_r$ and $\omega_1 = \varepsilon_a - z \pm \mathrm{i}\gamma$. If $\varepsilon_r > 0$ ($\eta_r = \eta$) we may integrate over the *positive* half plane with the pole $\omega_1 = \varepsilon_a - z + \mathrm{i}\gamma$, yielding

$$\frac{1}{q - z + \mathrm{i}\eta + \mathrm{i}\gamma}\, e^{-\mathrm{i}t'(q-z+\mathrm{i}\gamma)}$$

with $q = \varepsilon_a - \varepsilon_r$. Similarly, when $\varepsilon_r < 0$ we may integrate over the *negative* half plane (pole $\omega_1 = \varepsilon_a - z - \mathrm{i}\gamma$), and the integration yields

$$\frac{1}{q - z - \mathrm{i}\eta - \mathrm{i}\gamma}\, e^{-\mathrm{i}t'(q-z-\mathrm{i}\gamma)}.$$

In the integrals here there are *two imaginary parts*, one (η) associated with the electron propagator and one (γ) with the adiabatic damping. The purpose of the former is to indicate the position of the poles of the propagator, while the latter is a parameter that is going to zero in the adiabatic process. It should be noted that these quantities are of *different character* – γ is a *finite quantity*, which is eventually switched off, while η is an infinitesimally small quantity. Therefore, we can omit η, when it appears together with γ, and the results above can be summarized as

$$\frac{1}{q - z + \mathrm{i}\gamma_r}\, e^{-\mathrm{i}t'(q-z+\mathrm{i}\gamma_r)},$$

where $\gamma_r = \gamma\,\mathrm{sgn}(\varepsilon_r)$. In the same way the integrations over t_2 and ω_2 yield

$$\frac{1}{q' + z + \mathrm{i}\gamma_s}\, e^{-\mathrm{i}t'(q'+z+\mathrm{i}\gamma_s)}$$

with $q' = \varepsilon_b - \varepsilon_s$ and $\gamma_s = \gamma\,\mathrm{sgn}(\varepsilon_s)$.

After the integrations above, the expression (A.1) becomes

$$\begin{aligned}\left\langle rs\left|\hat{U}^{(2)}_{\mathrm{Cov}}(t',-\infty)\right|ab\right\rangle &= \mathrm{i}\int\frac{\mathrm{d}z}{2\pi}\,\frac{\left\langle rs\middle|I(z)\middle|ab\right\rangle}{(q-z+\mathrm{i}\gamma_r)(q'+z+\mathrm{i}\gamma_s)}\,\mathrm{e}^{-\mathrm{i}t'(q+q')}\\ &= \mathrm{i}\,\frac{\mathrm{e}^{-\mathrm{i}t'(q+q')}}{q+q'}\int\frac{\mathrm{d}z}{2\pi}\,\langle rs|I(z)|ab\rangle\Big[\frac{1}{q-z+\mathrm{i}\gamma_r}+\frac{1}{q'+z+\mathrm{i}\gamma_s}\Big]. \qquad \text{(A.3)}\end{aligned}$$

U2CovInt

Eventually, all γ:s will go to zero, and they are needed only to determine the position of the poles. Since the factor $(q+q')$ is not involved in any integration, we can leave out the imaginary part of that factor.

The interaction $I(z)$ is in the Feynman gauge given by (77)

$$I(z) = e^2 \alpha_1^\mu \alpha_2^\nu \, D_{\mathrm{F}\nu\mu}(\boldsymbol{x}_2 - \boldsymbol{x}_1, z) = \int_0^\infty \frac{2k \, \mathrm{d}k \, f(k)}{z^2 - k^2 + \mathrm{i}\eta}$$

$$f(k) = -\frac{e^2}{4\pi^2 \, r_{12}} \, (1 - \boldsymbol{\alpha}_1 \cdot \boldsymbol{\alpha}_2) \, \sin(k r_{12}). \tag{A.4}$$

IFeynman

The z integral is here

$$\int \frac{\mathrm{d}z}{2\pi} \left[\frac{1}{q - z + \mathrm{i}\gamma_r} + \frac{1}{q' + z + \mathrm{i}\gamma_s} \right] \frac{1}{z^2 - k^2 + \mathrm{i}\eta}. \tag{A.5}$$

SingPhotzInt

We can rewrite the last denominator as

$$(z - k + \mathrm{i}\eta)(z + k - \mathrm{i}\eta) = z^2 - k^2 + 2k \, \mathrm{i} \, \eta.$$

Since η is an infinitesimally small positive quantity, $2k\eta$ is equivalent to η for positive k.

The first term in (A.5) has poles at $z = q + \mathrm{i}\gamma_r$ and $z = \pm(k - \mathrm{i}\eta)$. When $\gamma_r = \gamma > 0$, there is one pole in the *negative* half-plane, $z = k - \mathrm{i}\gamma$, and the integral becomes

$$-\frac{\mathrm{i}}{2(k - \mathrm{i}\eta)(q - k + \mathrm{i}\eta + \mathrm{i}\gamma)} \, .$$

As before, we can omit the η term in comparison with the γ term, but we keep for the moment the η term in the first factor,

$$-\frac{\mathrm{i}}{(2k - \mathrm{i}\eta)(q - k + \mathrm{i}\gamma)} \, .$$

When $\gamma_r = -\gamma < 0$, there is one pole in the *positive* half-plane, $z = -k + \mathrm{i}\eta$, and the integral becomes similarly

$$-\frac{\mathrm{i}}{(2k - \mathrm{i}\eta)(q + k - \mathrm{i}\gamma)} \, ,$$

and the result can be summarized as

$$-\frac{\mathrm{i}}{(2k - \mathrm{i}\eta)\Big(q - (k - \mathrm{i}\gamma)_r\Big)} \, ,$$

where $(A)_- \equiv (A)\,\mathrm{sgn}(\varepsilon_x)$. Similarly, the integration of the second term in (A.5) yields

SingPhotzInt

$$-\frac{\mathrm{i}}{(2k - \mathrm{i}\eta)\Big(q' - (k - \mathrm{i}\gamma)_s\Big)} \, ,$$

and the complete integral becomes

$$-\frac{\mathrm{i}}{(2k - \mathrm{i}\eta)} \left[\frac{1}{q - (k - \mathrm{i}\gamma)_r} + \frac{1}{q' - (k - \mathrm{i}\gamma)_s} \right].$$

When including the interaction (A.4), there is a factor of $2k$ in the numerator, and then it follows that the pole at $k = 0$ does not contribute. Therefore, *the matrix element of the covariant evolution operator for single photon exchange* becomes

$$\boxed{\left\langle rs\left|\hat{U}^{(2)}_{\rm Cov}(t',-\infty)\right|ab\right\rangle = \left\langle rs\middle|V(q,q')\middle|ab\right\rangle \frac{{\rm e}^{-{\rm i}t'(q+q')}}{q+q'}} \qquad \text{(A.6)}$$

$$\boxed{V(q,q') = \int {\rm d}k\, f(k)\left[\frac{1}{q-(k-{\rm i}\gamma)_r} + \frac{1}{q'-(k-{\rm i}\gamma)_s}\right],} \qquad \text{(A.7)}$$

where $q = \varepsilon_a - \varepsilon_r$ and $q' = \varepsilon_b - \varepsilon_s$. According to the expression (130) for the effective interaction, $V(q,q')$ is the first-order contribution to the effective Hamiltonian,

$$\boxed{\left\langle rs\middle|H^{(1)}_{\rm eff}\middle|ab\right\rangle = \left\langle rs\middle|V(q,q')\middle|ab\right\rangle.} \qquad \text{(A.8)}$$

A.2 Evaluation of the two-photon ladder diagram

(See also (?).)

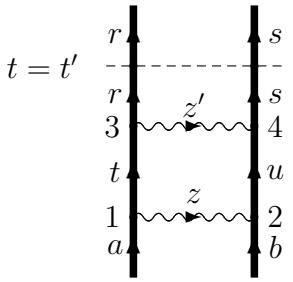

Fig. A.2. Graphical representation of the covariant-evolution operator for the two-photon ladder diagram (Fig. 17).

The matrix element of the two-photon ladder diagram, shown in Fig. A.2, is given in Eq. (220)

$$\begin{aligned}\left\langle rs\left|\hat{U}^{(4)}_{\rm Cov}(t',-\infty)\right|ab\right\rangle &= \left\langle rs\middle|\iint {\rm d}^4x_3\,{\rm d}^4x_4\,{\rm i}S_{\rm F}(x'_3,x_3)\,{\rm i}S_{\rm F}(x'_4,x_4)\,{\rm i}I(x_4,x_3)\right.\\ &\times\left.\iint {\rm d}t_1\,{\rm d}t_2\,{\rm i}S_{\rm F}(x_3,x_1)\,{\rm i}S_{\rm F}(x_4,x_2)\,{\rm i}I(x_2,x_1)\middle|ab\right\rangle\\ &\times{\rm e}^{{\rm i}t'(\varepsilon_r+\varepsilon_s)}\,{\rm e}^{-{\rm i}t_1\varepsilon_a-{\rm i}t_2\varepsilon_b}\,{\rm e}^{-\gamma(|t_1|+|t_2|+|t_3|+|t_4|)},\end{aligned} \qquad \text{(A.9)}$$

which in analogy with the single-photon case can be expressed

$$
\begin{aligned}
&\left\langle rs \left| \hat{U}^{(4)}_{\rm Cov}(t',-\infty) \right| ab \right\rangle = \\
&- \iint \mathrm{d}t_3\, \mathrm{d}t_4 \left\langle rs \right| \int \frac{\mathrm{d}z'}{2\pi} \int \frac{\mathrm{d}\omega_3}{2\pi} \frac{|r\rangle\langle r|}{\omega_3 - \varepsilon_r + \mathrm{i}\eta_r} \int \frac{\mathrm{d}\omega_4}{2\pi} \frac{|s\rangle\langle s|}{\omega_4 - \varepsilon_s + \mathrm{i}\eta_s} I(z') \left| tu \right\rangle \\
&\times \iint \mathrm{d}t_1\, \mathrm{d}t_2 \left\langle tu \right| \int \frac{\mathrm{d}z}{2\pi} \int \frac{\mathrm{d}\omega_1}{2\pi} \frac{|t\rangle\langle t|}{\omega_1 - \varepsilon_t + \mathrm{i}\eta_t} \int \frac{\mathrm{d}\omega_2}{2\pi} \frac{|u\rangle\langle u|}{\omega_2 - \varepsilon_u + \mathrm{i}\eta_u} I(z) \left| ab \right\rangle \\
&\times \mathrm{e}^{\mathrm{i}t'(\varepsilon_r+\varepsilon_s)}\, \mathrm{e}^{-\mathrm{i}\omega_3(t'-t_3)}\, \mathrm{e}^{-\mathrm{i}\omega_4(t'-t_4)}\, \mathrm{e}^{-\mathrm{i}z'(t_4-t_3)} \\
&\times \mathrm{e}^{-\mathrm{i}\omega_1(t_3-t_1)}\, \mathrm{e}^{-\mathrm{i}\omega_2(t_4-t_2)} \mathrm{e}^{-\mathrm{i}z(t_2-t_1)}\, \mathrm{e}^{-\mathrm{i}t_1\varepsilon_a - \mathrm{i}t_2\varepsilon_b} \mathrm{e}^{-\gamma(|t_1|+|t_2|+|t_3|+|t_4|)}. \qquad \text{(A.10)}
\end{aligned}
$$

U4CovA1

The time integrations yield here, using Eq. (174), Delta

$$
\Delta_\gamma(\omega_1 - \omega_3 - z')\, \Delta_\gamma(\omega_2 - \omega_4 + z')\, \Delta_\gamma(\varepsilon_a - z - \omega_1)\, \Delta_\gamma(\varepsilon_b + z - \omega_2)
$$

(leaving out the factors of 2π). If r is a positive-energy state, we integrate ω_3 over the positive half plane with the pole $\omega_3 = \omega_1 - z' + \mathrm{i}\gamma$, which yields

$$
\frac{1}{\omega_1 - z' - \varepsilon_r + \mathrm{i}\gamma + \mathrm{i}\eta}.
$$

The ω_1 integrand now becomes

$$
\int \frac{\mathrm{d}\omega_1}{2\pi} \frac{2\pi\Delta_\gamma(\varepsilon_a - z - \omega_1)}{(\omega_1 - z' - \varepsilon_r + \mathrm{i}\gamma + \mathrm{i}\eta)(\omega_1 - \varepsilon_t + \mathrm{i}\eta_t)}
$$

and the poles appear at $\omega_1 = \varepsilon_t - \mathrm{i}\eta_t$, $\omega_1 = \varepsilon_r + z' - \mathrm{i}\gamma_r$ and $\omega_1 = \varepsilon_a - z \pm \mathrm{i}\gamma$. If also t is a positive-energy state, we integrate over the positive half plane with the pole $\omega_1 = \varepsilon_a - z + \mathrm{i}\gamma$, yielding

$$
\frac{1}{(q - z - z' + 2\mathrm{i}\gamma)(p - z + \mathrm{i}\gamma)}
$$

with $q = \varepsilon_a - \varepsilon_r$ and $p = \varepsilon_a - \varepsilon_t$. Similarly, if both t and r are negative-energy states, we obtain

$$
\frac{1}{(q - z - z' - 2\mathrm{i}\gamma)(p - z - \mathrm{i}\gamma)}.
$$

If we assume that t is a negative-energy state and r still a positive-energy state, then there are two poles in each half plane – in the negative half plane $\omega_1 = \varepsilon_a - z - \mathrm{i}\gamma$ and $\omega_1 = z' + \varepsilon_r - \mathrm{i}\gamma - \mathrm{i}\eta$ – yielding

$$
\begin{aligned}
&\frac{1}{(q - z - z' + \mathrm{i}\eta)(p - z - \mathrm{i}\gamma - \mathrm{i}\eta)} \\
&- \frac{2\mathrm{i}\gamma}{(q - z - z' + 2\mathrm{i}\gamma + \mathrm{i}\eta)(q - z - z' + \mathrm{i}\eta)(q - p - z' + \mathrm{i}\gamma + 2\mathrm{i}\eta)}.
\end{aligned}
$$

Here, we see that it is important to keep the η term, since the γ term vanishes in the first denominator. The last term vanishes as $\gamma \to 0$. The corresponding

result is obtained when the signs of ε_r and ε_t are reversed. Generally, the result of the ω_1 integration can then be expressed (in the limit)

$$\frac{1}{(q-z-z'+\mathrm{i}\gamma_r+\mathrm{i}\gamma_t+\mathrm{i}\eta_r)(p-z+\mathrm{i}\gamma_t+\mathrm{i}\eta_t)},$$

but since the imaginary parts are here only used to indicate the position of the poles, this is equivalent to

$$\frac{1}{(q-z-z'+\mathrm{i}\gamma_r)(p-z+\mathrm{i}\gamma_t)}.$$

The results after the complete ω integrations can now be summarized as follows

$$\begin{aligned}\left\langle rs\left|\hat{U}^{(4)}_{\mathrm{Cov}}(t',-\infty)\right|ab\right\rangle &= -\iint \frac{\mathrm{d}z'}{2\pi}\,\frac{\mathrm{d}z}{2\pi}\,\frac{\left\langle rs\middle|I(z')\middle|tu\right\rangle}{(q-z-z'+\mathrm{i}\gamma_r)(q'+z+z'+\mathrm{i}\gamma_s)}\\ &\times\frac{\left\langle tu\middle|I(z)\middle|ab\right\rangle}{(p-z+\mathrm{i}\gamma_t)(p'+z+\mathrm{i}\gamma_u)}\,\mathrm{e}^{-\mathrm{i}t'(q+q')} \qquad \text{(A.11)}\end{aligned}$$

U4Cov2A

with $q=\varepsilon_a-\varepsilon_r$; $q'=\varepsilon_b-\varepsilon_s$; $p=\varepsilon_a-\varepsilon_t$ and $p'=\varepsilon_b-\varepsilon_u$. As before, we leave out the imaginary part in factors not involved in any integration.

The last two denominators of (A.11) can be written

$$\frac{1}{(p-z+\mathrm{i}\gamma_t)(p'+z+\mathrm{i}\gamma_u)}=\left[\frac{1}{p-z+\mathrm{i}\gamma_t}+\frac{1}{p'+z+\mathrm{i}\gamma_u}\right]\frac{1}{p+p'}$$

and the first two

$$\begin{aligned}&\frac{1}{(q-z-z'+\mathrm{i}\gamma_r)(q'+z+z'+\mathrm{i}\gamma_s)}=\\ &=\left[\frac{1}{q-z-z'+\mathrm{i}\gamma_r}+\frac{1}{q'+z+z'+\mathrm{i}\gamma_s}\right]\frac{1}{q+q'}, \qquad \text{(A.12)}\end{aligned}$$

which gives

$$\begin{aligned}&\left\langle rs\left|\hat{U}^{(4)}_{\mathrm{Cov}}(t',-\infty)\right|ab\right\rangle\\ &=\iint\frac{\mathrm{d}z'}{2\pi}\,\frac{\mathrm{d}z}{2\pi}\,\langle rs|f(k')|tu\rangle\langle tu|f(k)|ab\rangle\,\frac{(A+B+C+D)\,\mathrm{e}^{-\mathrm{i}t'(q+q')}}{(q+q')(p+p')} \qquad \text{(A.13)}\end{aligned}$$

$$
\begin{aligned}
A &= -\iint \frac{\mathrm{d}z'}{2\pi}\,\frac{\mathrm{d}z}{2\pi}\iint \mathrm{d}k'\mathrm{d}k\,\frac{4k\,k'}{(q-z-z'+\mathrm{i}\gamma_r)(p-z+\mathrm{i}\gamma_t)(z'^2-k'^2+\mathrm{i}\eta)(z^2-k^2+\mathrm{i}\eta)}\\
B &= -\iint \frac{\mathrm{d}z'}{2\pi}\,\frac{\mathrm{d}z}{2\pi}\iint \mathrm{d}k'\mathrm{d}k\,\frac{4k\,k'}{(q-z-z'+\mathrm{i}\gamma_r)(p'+z+\mathrm{i}\gamma_u)(z'^2-k'^2+\mathrm{i}\eta)(z^2-k^2+\mathrm{i}\eta)}\\
C &= -\iint \frac{\mathrm{d}z'}{2\pi}\,\frac{\mathrm{d}z}{2\pi}\iint \mathrm{d}k'\mathrm{d}k\,\frac{4k\,k'}{(q'+z+z'+\mathrm{i}\gamma_s)(p-z+\mathrm{i}\gamma_t)(z'^2-k'^2+\mathrm{i}\eta)(z^2-k^2+\mathrm{i}\eta)}\\
D &= -\iint \frac{\mathrm{d}z'}{2\pi}\,\frac{\mathrm{d}z}{2\pi}\iint \mathrm{d}k'\mathrm{d}k\,\frac{4k\,k'}{(q'+z+z'+\mathrm{i}\gamma_s)(p'+z+\mathrm{i}\gamma_u)(z'^2-k'^2+\mathrm{i}\eta)(z^2-k^2+\mathrm{i}\eta)}.
\end{aligned}
\tag{A.14}
$$

ABCD

As a consequence of the generalized factorization theorem (FactTh 121) and the regularity of the reduced evolution operator, the adiabatic-damping parameter γ can be switched off *individually* for each vertex in the evolution-operator method – in contrast to the situation in the S-matrix method, using the Gell-Mann–Low–Sucher method (Sucher 165). The γ's are needed, though, for the pole integrations, and therefore the sign of γ is important (but not its size). Then it is possible to apply a simplified method, where *the time integrations will directly lead to Dirac delta functions*, and the ω integrations will be trivial. It has to be observed, though, as illustrated above, that the γ term might disappear when negative-energy states are involved, and then the η term from the propagator will determine the position of the pole.

We now evaluate the z, z' integrals when t, u (as well as r and s) are *positive-energy* states ($\gamma_t = \gamma_u = \gamma > 0$). Then A has one z pole $z = k - \mathrm{i}\eta$ and one z' pole $z' = k' - \mathrm{i}\eta$ in the negative half planes (c.f. (SingPhotzInt A.5)), yielding

$$
A = \frac{1}{(q-k-k'+\mathrm{i}\gamma)(p-k+\mathrm{i}\gamma)}.
$$

B has two z poles $z = k - \mathrm{i}\eta$ and $z = -p' - \mathrm{i}\gamma$ and one z' pole $z' = k' - \mathrm{i}\eta$ in the negative half planes, which yields similarly

$$
B = \frac{1}{(q-k-k'+\mathrm{i}\gamma)(p'+k+\mathrm{i}\gamma)} + \frac{2k}{(q+p'-k'+\mathrm{i}\gamma)\Big((p'+\mathrm{i}\gamma)^2-k^2\Big)}.
$$

Similarly, C has the poles $z = -k + \mathrm{i}\eta$, $z = p + \mathrm{i}\gamma$ and $z' = -k' + \mathrm{i}\eta$ in the *positive* half plane, and integration yields

$$
C = \frac{1}{(q'-k-k'+\mathrm{i}\gamma)(p+k+\mathrm{i}\gamma)} + \frac{2k}{(q'+p-k'+\mathrm{i}\gamma)\Big((p+\mathrm{i}\gamma)^2-k^2\Big)}.
$$

D has the poles $z = -k + \mathrm{i}\eta$ and $z' = -k' + \mathrm{i}\eta$ in the *positive* half plane, yielding

$$
D = \frac{1}{(q'-k-k'+\mathrm{i}\gamma)(p'-k+\mathrm{i}\gamma)}.
$$

The B term can be rewritten as

$$B = \frac{1}{q + p' - k' + \mathrm{i}\gamma} \left[\frac{1}{q - k - k' + \mathrm{i}\gamma} + \frac{1}{p' - k + \mathrm{i}\gamma} \right]$$

and the C term

$$C = \frac{1}{q' + p - k' + \mathrm{i}\gamma} \left[\frac{1}{q' - k - k' + \mathrm{i}\gamma} + \frac{1}{p - k + \mathrm{i}\gamma} \right],$$

which eliminates an apparent pole in the k integration.

A.3 Evaluation of the screened self-energy diagram

c:ScrSEEvOpA

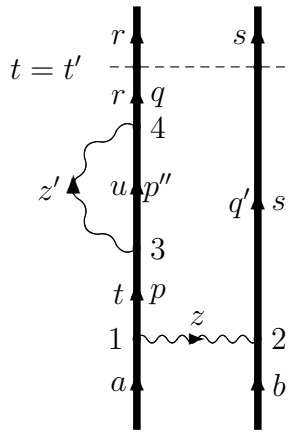

Fig. A.3. The covariant-evolution-operator diagram representing the screened self--energy.

Fig:ScrSEA1

Next, we shall evaluate the covariant evolution-operator diagram for the screened self-energy, given by the expression (237), assuming all states being positive-energy states,

ScrSEEvOp1

$$\left\langle rs \middle| H^{(2)}_{\mathrm{eff}} \middle| ab \right\rangle =$$
$$- \iint \frac{\mathrm{d}z}{2\pi} \frac{\mathrm{d}z'}{2\pi} \frac{\left\langle ru \middle| I(z') \middle| ut \right\rangle \left\langle ts \middle| I(z) \middle| ab \right\rangle}{(p'' - z - z' + \mathrm{i}\gamma)(p - z + \mathrm{i}\gamma)} \left[\frac{1}{q - z + \mathrm{i}\gamma} + \frac{1}{q' + z + \mathrm{i}\gamma} \right]. \quad \text{(A.15)}$$

ScrSEEvOp1A

For the first term in the square brackets we integrate over the negative half plane with the pole $z = k - \mathrm{i}\eta$ from the photon propagator, yielding

$$\mathrm{i} \frac{\left\langle ru \middle| I(z') \middle| ut \right\rangle \left\langle ts \middle| f(k) \middle| ab \right\rangle}{(p'' - k - z' + \mathrm{i}\gamma)(p - k + \mathrm{i}\gamma)(q - k + \mathrm{i}\gamma)}$$

and after integration over z'

$$\frac{\left\langle ru \middle| f(k') \middle| ut \right\rangle \left\langle ts \middle| f(k) \middle| ab \right\rangle}{(p'' - k - k' + \mathrm{i}\gamma)(p - k + \mathrm{i}\gamma)(q - k + \mathrm{i}\gamma)}.$$

The second term has two poles in the negative half plane, $z = k - \mathrm{i}\eta$ and $z = -q' - \mathrm{i}\gamma$, and yields similarly

$$\frac{\Big\langle ru\Big|f(k')\Big|ut\Big\rangle\Big\langle ts\Big|f(k)\Big|ab\Big\rangle}{(p''-k-k'+\mathrm{i}\gamma)(p-k+\mathrm{i}\gamma)(q'+k+\mathrm{i}\gamma)}$$
$$+\frac{\Big\langle ru\Big|f(k')\Big|ut\Big\rangle\Big\langle ts\Big|f(k)\Big|ab\Big\rangle}{(p''+q'-k'+\mathrm{i}\gamma)(p+q'+\mathrm{i}\gamma)}\Big[\frac{1}{q'-k+\mathrm{i}\gamma}-\frac{1}{q'+k+\mathrm{i}\gamma}\Big]. \qquad \text{(A.16)}$$

After some algebra the denominators can be rewritten, eliminating an apparent pole,

$$\frac{1}{(p''+q'-k'+\mathrm{i}\gamma)(p+q')}\Big[\frac{1}{p-k+\mathrm{i}\gamma}+\frac{1}{q'-k+\mathrm{i}\gamma}\Big]$$
$$+\frac{1}{(p''-k-k'+\mathrm{i}\gamma)(p-k+\mathrm{i}\gamma)}\Big[\frac{1}{p''+q'-k'+\mathrm{i}\gamma}+\frac{1}{q-k+\mathrm{i}\gamma}\Big]. \qquad \text{(A.17)}$$

ScrSEEvOp2A

B Evaluation of time-ordered diagrams

sec:timeOrd

In this Appendix we shall consider the evaluation of *time-ordered diagrams*, which, as we shall see, will lead to a general scheme for expressing the covariant-evolution-operator diagrams at arbitrary order. This procedure will form the basis for the model of merging QED with MBPT, discussed in section 8.

MBPT/QED

B.1 Two-photon ladder

As an illustration we consider the two-photon ladder, treated in Appendix A, sec:Eval for which two time-orderings are shown in Fig. B.1. Using the expression (184) Fig:LadderTimeOrd E1Prop2

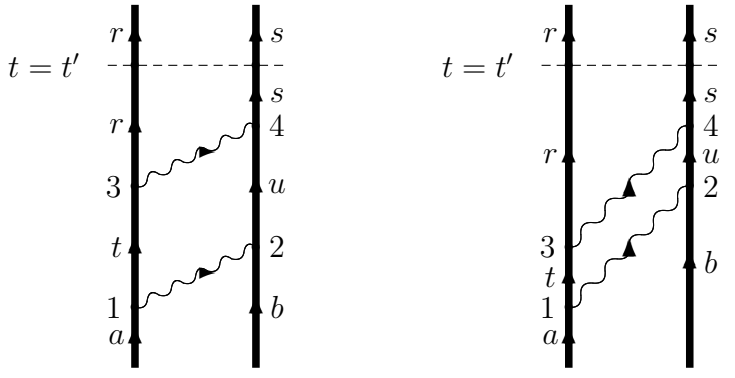

Fig. B.1. Two time-ordered two-photon-ladder diagrams, representing the separable part (left) and nonseparable part (right) of the two-photon ladder diagram.

Fig:LadderTime

of the electron propagators we can write the two-photon ladder (A.9) as

$$\Big\langle rs\,\Big|\hat{U}^{(4)}_{\rm Cov}(t',-\infty)\Big|\,ab\Big\rangle = -\iint \mathrm{d}^4x_3\,\mathrm{d}^4x_4\int\frac{\mathrm{d}z'}{2\pi}\Big[\Theta(t'-t_3)\,\phi^\dagger_{r_+}(\boldsymbol{x}_3)-\Theta(t_3-t')\,\phi^\dagger_{r_-}(\boldsymbol{x}_3)\Big]$$
$$\times\Big[\Theta(t'-t_4)\,\phi^\dagger_{s_+}(\boldsymbol{x}_4)-\Theta(t_4-t')\,\phi^\dagger_{s_-}(\boldsymbol{x}_4)\Big]\,I(\boldsymbol{x}_4,\boldsymbol{x}_3,z')$$
$$\times\iint \mathrm{d}^4x_1\,\mathrm{d}^4x_2\int\frac{\mathrm{d}z}{2\pi}\Big[\Theta(t_3-t_1)\,\phi_{t_+}(\boldsymbol{x}_3)\phi^\dagger_{t_+}(\boldsymbol{x}_1)-\Theta(t_1-t_3)\,\phi^\dagger_{t_-}(\boldsymbol{x}_1)\phi_{t_-}(\boldsymbol{x}_3)\Big]$$
$$\times\Big[\Theta(t_4-t_2)\,\phi_{u_+}(\boldsymbol{x}_4)\phi^\dagger_{u_+}(\boldsymbol{x}_2)-\Theta(t_2-t_4)\,\phi^\dagger_{u_-}(\boldsymbol{x}_2)\phi_{u_+}(\boldsymbol{x}_4)\Big]\,I(\boldsymbol{x}_2,\boldsymbol{x}_1,z)\,\phi_a(\boldsymbol{x}_1)\phi_b(\boldsymbol{x}_2)$$
$$\times\mathrm{e}^{-\mathrm{i}t_3(\varepsilon_t-\varepsilon_r-z')}\mathrm{e}^{-\mathrm{i}t_4(\varepsilon_u-\varepsilon_s+z')}\mathrm{e}^{-\mathrm{i}t_1(\varepsilon_a-\varepsilon_t-z)}\mathrm{e}^{-\mathrm{i}t_2(\varepsilon_b-\varepsilon_u+z)}\,\mathrm{e}^{-\gamma(|t_1|+|t_2|+|t_3|+|t_4|)}. \tag{B.1}$$

For simplicity we introduce the following short-hand notations:

$$\begin{aligned}
&d_1=\varepsilon_a-\varepsilon_t-z=p-z && d_2=\varepsilon_b-\varepsilon_u+z=p'+z\\
&d_3=\varepsilon_t-\varepsilon_r-z'=q-p-z' && d_4=\varepsilon_u-\varepsilon_s+z'=q'-p'+z'\\
&d_{12}=d_1+d_2=p+p' && d_{34}=d_3+d_4=q+q'-p-p'\\
&d_{13}=d_1+d_3=q-z-z' && d_{24}=d_2+d_4=q'+z+z'\\
&d_{123}=d_1+d_2+d_3=q+p'-z' && d_{124}=d_1+d_2+d_4=q'+p+z'\\
&d_{1234}=d_1+d_2+d_3+d_4=q+q',
\end{aligned} \tag{B.2}$$

d

and the notations $d_{1\pm}=d_1\pm\mathrm{i}\gamma$ etc. to indicate the sign of the imaginary part.

We assume first that all states are *positive-energy states*. Then we have the time-ordering $t'>t_3>t_1$ and $t'>t_4>t_2$, and the time integrations yield

$$\begin{aligned}
\int_{-\infty}^{t'}\mathrm{d}t_3\,\mathrm{e}^{-\mathrm{i}t_3d_{3+}}\int_{-\infty}^{t_3}\mathrm{d}t_1\,\mathrm{e}^{-\mathrm{i}t_1d_{1+}} &= -\frac{\mathrm{e}^{-\mathrm{i}t'd_{13+}}}{d_{13+}\,d_{1+}}\\
\int_{-\infty}^{t'}\mathrm{d}t_4\,\mathrm{e}^{-\mathrm{i}t_4d_{4+}}\int_{-\infty}^{t_4}\mathrm{d}t_2\,\mathrm{e}^{-\mathrm{i}t_2d_{2+}} &= -\frac{\mathrm{e}^{-\mathrm{i}t'd_{24}}}{d_{24+}\,d_{2+}}.
\end{aligned} \tag{B.3}$$

43,21

The total time integration then becomes

$$\frac{\mathrm{e}^{-\mathrm{i}t'd_{1234}}}{d_{13+}\,d_{24+}\,d_{1+}\,d_{2+}}=\frac{\mathrm{e}^{-\mathrm{i}t'd_{1234}}}{d_{1234}}\Big(\frac{1}{d_{13+}}+\frac{1}{d_{24+}}\Big)\frac{1}{d_{12+}}\Big(\frac{1}{d_{1+}}+\frac{1}{d_{2+}}\Big) \tag{B.4}$$

43,21A

and with the notations above

$$\frac{\mathrm{e}^{-\mathrm{i}t'(q+q'+4\mathrm{i}\gamma)}}{q+q'+4\mathrm{i}\gamma}\Big(\frac{1}{q-z-z'+2\mathrm{i}\gamma}+\frac{1}{q'+z+z'+2\mathrm{i}\gamma}\Big)\frac{1}{p+p'+2\mathrm{i}\gamma}$$
$$\times\Big(\frac{1}{p-z+\mathrm{i}\gamma}+\frac{1}{p'+z+\mathrm{i}\gamma}\Big), \tag{B.5}$$

43,21B

in agreement with (A.14). Here, also the magnitude of the imaginary parts come out correctly, although we do not need them in our method.

If the intermediate state t is a *negative-energy* state – and r still a positive-energy state – then the time-ordering becomes $t'>t_3<t_1$, and the time

integration over t_1 and t_3 becomes

$$\int_{-\infty}^{t'} \mathrm{d}t_3\, \mathrm{e}^{-\mathrm{i}t_3 d_{3+}} \int_{\infty}^{t_3} \mathrm{d}t_1\, \mathrm{e}^{-\mathrm{i}t_1 d_{1-}} = -\frac{\mathrm{e}^{-\mathrm{i}t' d_{13+}}}{d_{13+}\, d_{1-}}. \tag{B.6}$$

13h

Here, we have an example where the γ contribution cancels, and the + sign is due to the η term, as discussed in Appendix A.2. This leads to the change in (B.5)

TwoPhotonApp

43,21B

$$\frac{1}{p-z+\mathrm{i}\gamma} \Rightarrow \frac{1}{p-z-\mathrm{i}\gamma},$$

in agreement with (A.14).

ABCD

B.1.1 Separable and nonseparable parts

We consider next the *separable* part of the ladder diagram. Assuming first that all states are *positive-energy* states, the separable diagram in Fig. B.1 corresponds to the time-ordering $t' > t_4 > t_3 > t_2 > t_1$, and the time integration yields

Fig:LadderTimeOrd

$$\begin{aligned}&\int_{-\infty}^{t'} \mathrm{d}t_4\, \mathrm{e}^{-\mathrm{i}t_4 d_{4+}} \int_{-\infty}^{t_4} \mathrm{d}t_3\, \mathrm{e}^{-\mathrm{i}t_3 d_{3+}} \int_{-\infty}^{t_3} \mathrm{d}t_2\, \mathrm{e}^{-\mathrm{i}t_2 d_{2+}} \int_{-\infty}^{t_2} \mathrm{d}t_1\, \mathrm{e}^{-\mathrm{i}t_1 d_{1+}} \\ &= \frac{\mathrm{e}^{-\mathrm{i}t' d_{1234+}}}{d_{1234+}\, d_{123+}\, d_{12+}\, d_{1+}}. \end{aligned} \tag{B.7}$$

4321

The remaining time-orderings are obtained by means of the exchanges $1 \leftrightarrow 2$ and $3 \leftrightarrow 4$, which leads to

$$\frac{\mathrm{e}^{-\mathrm{i}t' d_{1234+}}}{d_{1234+}} \left(\frac{1}{d_{123+}} + \frac{1}{d_{124+}}\right) \frac{1}{d_{12+}} \left(\frac{1}{d_{1+}} + \frac{1}{d_{2+}}\right) \tag{B.8}$$

Sep

or

$$\frac{\mathrm{e}^{-\mathrm{i}t'(q+q'+2\mathrm{i}\gamma)}}{q+q'+2\mathrm{i}\gamma} \left(\frac{1}{q+p'-z'+2\mathrm{i}\gamma} + \frac{1}{q'+p+z'+2\mathrm{i}\gamma}\right) \frac{1}{p+p'} \left(\frac{1}{p-z+\mathrm{i}\gamma} + \frac{1}{p'+z+\mathrm{i}\gamma}\right). \tag{B.9}$$

SepA

This leads to the *contribution to the effective interaction due to the separable ladder*, using (130),

EffInt2

$$\left\langle rs\middle|H_{\mathrm{eff}}\middle|ab\right\rangle_{\mathrm{Sep}} = \frac{\left\langle rs\middle|V(q+p',q'+p)\middle|tu\right\rangle \left\langle tu\middle|V(p,p')\middle|ab\right\rangle}{p+p'}, \tag{B.10}$$

U4SepA

where V is given by (A.7).

SingPhotIntA

The *nonseparable* diagram in Fig. B.1 corresponds to the time-ordering $t' > t_4 > t_2 > t_3 > t_1$, and the time integral is obtained from (B.7) by the exchange

Fig:LadderTimeOrd

4321

$3 \leftrightarrow 2$,

$$\frac{\mathrm{e}^{-\mathrm{i}t' d_{1234+}}}{d_{1234+}\, d_{123+}\, d_{13+}\, d_{1+}}. \tag{B.11}$$

4231

Similarly, the opposite time-ordering, $t' > t_3 > t_1 > t_4 > t_2$, yields

$$\frac{\mathrm{e}^{-\mathrm{i}t' d_{1234+}}}{d_{1234+}\, d_{124+}\, d_{24+}\, d_{2+}}. \tag{B.12}$$

3142

The total time integration for the nonseparable part of the ladder diagram then becomes

$$\frac{\mathrm{e}^{-\mathrm{i}t' d_{1234+}}}{d_{1234+}} \left(\frac{1}{d_{123+}\, d_{13+}\, d_{1+}} + \frac{1}{d_{124+}\, d_{24+}\, d_{2+}} \right), \tag{B.13}$$

NonSepA

when all states are positive-energy states.

As a corollary we may add the separable (B.8) and nonseparable (B.13) parts of the ladder diagram,

$$\begin{aligned} &\left(\frac{1}{d_{123+}} + \frac{1}{d_{124+}} \right) \frac{1}{d_{1+}\, d_{2+}} + \frac{1}{d_{123+}\, d_{13+}\, d_{1+}} + \frac{1}{d_{124+}\, d_{24+}\, d_{2+}} \\ &= \frac{1}{d_{13+}\, d_{1+}\, d_{2+}} + \frac{1}{d_{24+}\, d_{1+}\, d_{2+}}, \end{aligned} \tag{B.14}$$

Coll

which agrees with (B.4).

¿From (B.13) the nonseparable contribution to the effective interaction contains

$$\frac{I(z')I(z)}{(q+p'-z')(q-z-z')(p-z)} + \frac{I(z')I(z)}{(q'+p+z')(q'+z+z')(p'+z)}, \tag{B.15}$$

U4NonSepA

and integrations over z and z' yield

$$\frac{f(k')f(k)}{(q+p'-k')(q-k-k')(p-k)} + \frac{f(k')f(k)}{(q'+p+k')(q'+k+k')(p'+k)}. \tag{B.16}$$

U4NonSepA2

C General evaluation procedure

sec:GenProc

C.1 General rules

The diagram evaluation discussed above using time-ordered diagrams can be generalized to higher orders. When the involved states are *positive-energy states*, we find that we can construct the energy denominators in the following way. Inserting a horizontal line above each vertex, the corresponding denominator is given by

- *the orbital excitation energies counted from the bottom*
- *a term* $-z+\mathrm{i}\gamma$ *for each photon cut by the line.*

as illustrated in Fig. C.1. (The direction of the photon line is immaterial, but we have here assumed that it is directed *upwards*, which yields the minus sign of z.)

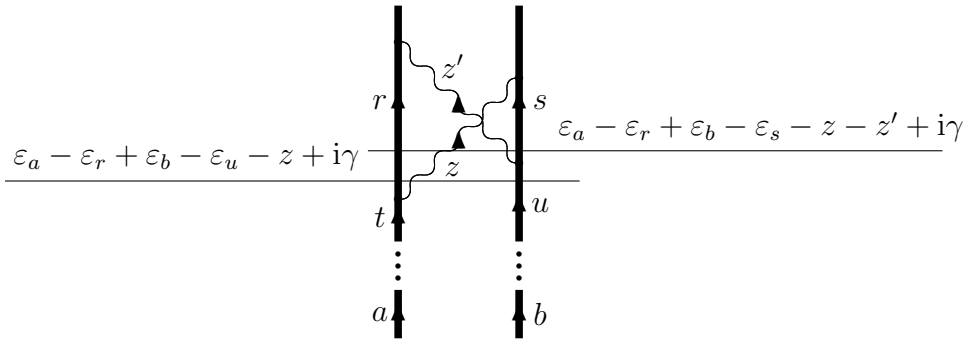

Fig. C.1. Two time-ordered versions of the two-photon-crossed diagram.

If a photon line is cut by only one horizontal line, considering first positive-energy states, then the denominator is of the type

$$\frac{1}{A-z+\mathrm{i}\gamma}\,,$$

and the poles for the z integration are located at $z=A+\mathrm{i}\gamma$ and $z=\pm(k-\mathrm{i}\eta)$ from the photon propagator. We then integrate over the negative half-plane with the pole $z=k$. (As discussed in Appendix A.1 the η term can be omitted in relation to the γ term.) The result of the integration is then obtained by replacing z by k and multiplying by $-\mathrm{i}/2k$, i.e.,

$$\frac{1}{A-z+\mathrm{i}\gamma}\Rightarrow\frac{-\mathrm{i}}{2k(A-k+\mathrm{i}\gamma)}. \tag{C.1}$$

If there are several photon lines cut by several vertical lines, then the denominators are of the type

$$\frac{1}{A-z+\mathrm{i}\gamma}\,\frac{1}{B-z-z'+\mathrm{i}\gamma}\,\cdots$$

Here, each z always appears with the same sign, and we can integrate over the z's as before, yielding

$$\frac{1}{A-z+\mathrm{i}\gamma}\,\frac{1}{B-z-z'+\mathrm{i}\gamma}\,\cdots\Rightarrow\frac{\mathrm{i}}{2k(A-k+\mathrm{i}\gamma)}\,\frac{\mathrm{i}}{2k'(B-k-k'+\mathrm{i}\gamma)}\,\cdots \tag{C.2}$$

The rules given here hold with minor modification also when there are *negative-energy states* involved. The only difference is that certain time integrations are

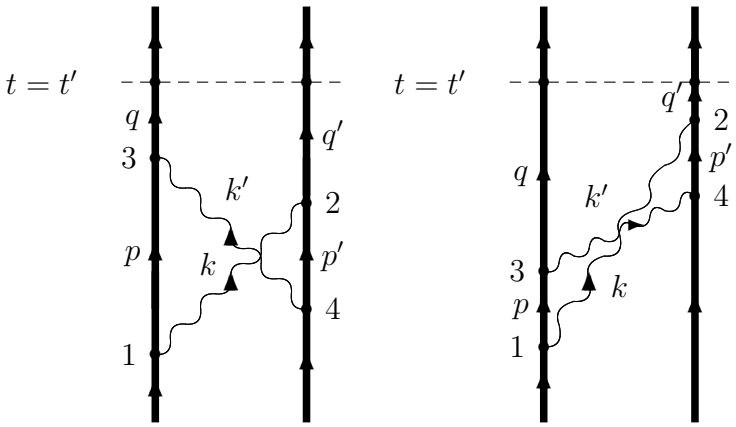

Fig. C.2. Two time-ordered versions of the two-photon-crossed diagram.

Fig:Cross

performed to $t = +\infty$ and the sign of the corresponding imaginary part is reversed.

C.2 Application

C.2.1 Two-photon cross

We shall first apply the rules given above to evaluate the evolution-operator diagram for the two crossed photons, shown in Fig. 17. Two time-ordered variants are shown in Fig. C.2.

Fig:TwoPhot

Fig:Cross

With the time-ordering of the first diagram in the figure, the evaluation yields (for simplicity leaving out the imaginary parts)

$$\frac{1}{q' + p - k'} \frac{1}{p - k + p' - k'} \frac{1}{p - k},$$

evaluating the denominators from the bottom and leaving out the final denominator. Reversing $1 \to 4$, leads to the replacement $p - k \to p' - k'$ in the last factor, and $3 \to 2$ to $q' + p - k' \to q + p' - k$. Adding these effects together, yields

$$\left(\frac{1}{q' + p - k'} + \frac{1}{q + p' - k}\right) \frac{1}{p' - k'} \frac{1}{p - k}.$$

Finally, we can reverse the order of 3 and 4, which leads to the second diagram in the figure. The denominators then become

$$\frac{1}{q + p' - k} \frac{1}{q - k' - k} \frac{1}{p - k}$$

and reversing the direction of the photons yields the final contribution

$$\frac{1}{q' + p - k'} \frac{1}{q' - k - k'} \frac{1}{p' - k'}.$$

This agrees with the result of [?]. BAs02

sec:ScrSE

C.2.2 Screened self-energy

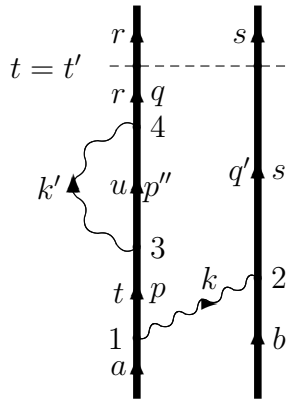

Fig. C.3. Time-ordered diagram representing the one-time covariant-evolution-operator for the screened self-energy. Fig:ScrSEA

Next, we consider the screened self-energy diagram with this general procedure. Starting with the time-ordering shown in Fig. C.3, $t' > t_4 > t_3 > t_2 > t_1$, and using the notations

$$
\begin{aligned}
&d_1 = \varepsilon_a - \varepsilon_t - k = p - k, \quad d_2 = \varepsilon_b - \varepsilon_s + k = q' + k \\
&d_3 = \varepsilon_t - \varepsilon_u - k' = p'' - p - k', \quad d_4 = \varepsilon_u - \varepsilon_r + k' = q - p'' + k', \\
&d_{12} = p + q', \quad d_{13} = p'' - k - k', \quad d_{123} = p'' + q' - k', \quad d_{134} = q - k,
\end{aligned}
$$

the denominators become

$$
\frac{1}{d_{123}\, d_{12}\, d_1} = \frac{1}{(p'' + q' - k')(p + q')(p - k)}.
$$

Reversing 1 and 2 yields

$$
\frac{1}{d_{123}\, d_{12}\, d_2} = \frac{1}{(p'' + q' - k')(p + q')(q' - k)}.
$$

Reversing 2 and 3 of the first expression yields

$$
\frac{1}{d_{123}\, d_{13}\, d_1} = \frac{1}{(p'' + q' - k')(p'' - k - k')(p - k)}
$$

and finally reversing 2 and 4 of the last expression

$$
\frac{1}{d_{134}\, d_{13}\, d_1} = \frac{1}{(q - k)(p'' - k - k')(p - k)}.
$$

This agrees with the previous result (A.17). ScrSEEvOp2A

adiabatic damping (sec. 3.3)
Bethe-Salpeter equation (sec. 8.2)
Block equation (sec. 2.2, eq. 14)
Block equation, linked-diagram form (sec. 2.4, eq. 42)
Block equation, generalized (sec. 2.2, eq. 14)
Breit interaction (sec. 2.6.2)
Brown-Ravenhall disease (sec. 2.6.2)
Brueckner orbitals (sec. 2.5)
CCSD, *coupled cluster singles and doubles approximation* (sec. 2.5.2, eq. 52)
closed diagram (sec. 2.4)
cluster operator (sec. 2.5.1)
complete model space (sec. 2.4)
CCA, *coupled cluster approach* (sec. 2.5.1)
coordinate representation (sec. 4.2)
contraction (sec. 2.3, eq. 38)
counterterm (sec. 3.4)
Coulomb-Breit interaction (sec. 2.6.2)
Coulomb gauge (sec. 2.6.2)
Coulomb-Gaunt interaction (sec. 2.6.2)
Coulomb-Gaunt interaction, retarded (sec. 3.1, eq. 78)
covariant evolution operator (sec. 5)
Δ *function* (sec: 4.1.1)
Dirac-Coulomb Hamiltonian (sec. 2.6.2)
Coulomb-Breit interaction, retarded (sec. 3.1, eq. 79)
Dirac matrices (sec. 2.6.1, 3.1)
discretization (sec. 2.5.3)
disconnected diagram (sec. 2.4)
effective Hamiltonian (sec. 2.1, eq. 13)
effective interaction (sec. 2.2, eq. 15)
electron-field operators (sec. 2.3, eq. 28)
electro-magnetic field operators (sec. 3.1, eq. 69)
extended model space (sec. 2.1)
electron propagator (sec. 4.2)
electron self energy (sec. 5.3, 5.3)
electron self energy, screened (sec. 5.4.1)
factorization theorem (sec. 3.4, eq. 121)
Feynman gauge (sec. 2.6.2)
Fock states (sec. 6.2)
folded diagram (sec. 2.4, eq. 13)
Gell-Mann–Low relation (sec. 3.3)
Gell-Mann–Low relation, generalized (sec. 3.3.2)
Goldstone diagram (sec. 2.4)